UNIVERSITÀ DI SIENA 1240

University of Siena - Department of Medical Biotechnologies

PhD Programme in
Genetics, Oncology and Clinical Medicine (GenOMeC)

XXXVI Cycle (2020-2023)

Coordinator: Prof.ssa Ilaria Meloni

New pharmacological targets for human diseases

Scientific disciplinary sector: MED/03 – Medical Genetics

PhD Candidate

Giovanni Inzalaco

Firma digitale del candidato

09/03/2024 14:40:45
GIOVANNI INZALACO

Tutor

Mario Chiariello, MD, PhD

Istituto di Fisiologia Clinica, Consiglio Nazionale delle Ricerche (IFC-CNR)
Core Research Laboratory, Istituto per lo Studio, la Prevenzione e la Rete Oncologica

Supervisor

Laura Poliseno, PhD

Istituto di Fisiologia Clinica, Consiglio Nazionale delle Ricerche (IFC-CNR)

Core Research Laboratory, Istituto per lo Studio, la Prevenzione e la Rete Oncologica

Academic Year 2022/2023

University of Siena - Department of Medical Biotechnologies

PhD Programme in

Genetics, Oncology and Clinical Medicine (GenOMeC)

XXXVI Cycle (2020-2023)

Final exam date:

March 20th, 2024

EXAMINING BOARD

Mario Chiariello, MD, PhD

Prof. Francesca Carlomagno, MD, PhD

Paola De Candia, PhD

Monia Taranta, PhD

ABSTRACT

INTRODUCTION In the past decade, significant steps have been made in cancer research, particularly in the field of targeted therapy driven by the identification of specific molecular alterations in various tumours. This continuous evolution of knowledge has led to the discovery of new druggable biomarkers, optimizing therapeutic efficiency while minimizing side effects associated with conventional cancer treatments. Notably, breast cancer is the most prevalent cancer, accounted for 12.5% of new cases in 2020. Lifestyle factors, including alcohol consumption, smoking, and obesity, strongly influence its occurrence. The heterogeneous nature of breast cancer poses challenges, with some cases displaying slow growth and good prognosis, while others prove aggressive and unresponsive to conventional therapies. Advances in targeted therapies, such as endocrine therapies and HER2 inhibitors, showcase promising results and exemplify personalized approaches to breast cancer. However, it is necessary to discover novel molecular targets, aiding clinicians in refining therapeutic decisions. Additionally, human behaviours, particularly obesity resulting from excessive calorie intake, plays a pivotal role in tumours onset, with approximately 20% of tumours attributed to obesity. Increasing evidence suggests specific alterations in lipid metabolism in cancer cells, emphasizing the need to explore these pathways for a deeper understanding of cancer development and outcomes. Lipid metabolism is in a constant state of dynamic equilibrium through food intake, de-novo lipogenesis, and consumption of lipids, to satisfy the needs of the body. Therefore, alterations of one or more of these processes or its dysfunctions, such as in the case of the metabolic syndrome and type 2 diabetes mellitus, can damage the liver as it represents the main organ for lipid metabolism.

This thesis is the result of a study carried out for the characterisation of two pharmacological targets and their role in the metabolic pathways respectively in mammarian cancer and non-alcoholic fatty liver disease (NAFLD) leading to liver cancer. I have divided the work in two sections as the activities for the study of each of the molecular target:

1. In the first section I report an already peer-reviewed published work based on the pharmacological inhibition of the DEAD-box RNA helicase 3 X (DDX3X). Specifically, it focuses on the pharmacological inhibition DDX3X as a potential treatment for breast cancer. Inhibition of DDX3X has demonstrated reduced cell proliferation in various tumour tissues, particularly in breast cancer, where its expression correlates with aggressiveness. The study employed an *in-silico* drug discovery approach, identifying FHP01 as a promising molecule through molecular

docking at DDX3X's RNA binding site. Specifically, FHP01 displayed potent antiproliferative effects against different breast cancer cell types *in vitro,* notably against triple-negative breast cancer (TNBC) cells. *In vivo* experiments with MDA MB 231-derived TNBC xenograft models showed a significant reduction in tumour growth. Importantly, FHP01 demonstrated good bioavailability and exhibited no toxicity on normal peripheral blood mononuclear cells *in vitro* and on several mouse tissues *in vivo*. The findings suggest that FHP01 and related compounds hold promise as a novel therapeutic approach with potential efficacy against breast cancer, including the challenging triple-negative subtype, where targeted therapies are limited.

2. In the second section I report recent findings on the involvement of mitogen activated protein kinase 15 (MAPK15) in non-alcoholic fatty liver disease (NAFLD). NAFLD stands out as the predominant cause of chronic liver disease globally, encompassing stages from simple steatosis to non-alcoholic steatohepatitis (NASH), which can advance to cirrhosis and hepatocellular carcinoma (HCC), the primary form of liver cancer. Notably, NASH-induced HCC is considered less sensible to cure compared to HCC resulting from viral factors. The excessive accumulation of fatty acids within hepatocytes is identified as a pivotal event in NAFLD progression. Fatty acid transporters play a crucial role in regulating fatty acid uptake across the plasma membrane. The presented data indicate a correlation between the atypical MAP kinase, MAPK15, and hepatic steatosis. Preliminary findings suggest that MAPK15 influences fatty acid transporters in vitro and in vivo. Reduced or absent expression of MAPK15 in mammalian cells is linked to increased lipid accumulation, leading to hepatic steatosis, adipose tissue accumulation, and insulin resistance – factors that elevate the risk of cancer development. The data presented underscore the need for further investigation into the involvement of MAPK15 in NAFLD development. Further investigation is now needed in order to understand how MAPK15 is involved in the development of NAFLD and, finally, if its expression may represent a marker of the worsening of liver steatosis, opening new possibilities to prevent NASH and liver cancer development.

INDEX

1. New pharmacological targets for human diseases

In the last decade, remarkable progress has been made in cancer research, more so when considering the latest advances in targeted therapy, driven by the discovery of specific molecular alteration that characterise different cancer types and subtypes. Knowledge about cancer targeted therapy is indeed, in continuous upgrade, (Fasola et al., 2023) and promotes the discovery of new druggable biomarkers that allow the optimization of therapeutic efficiency while reducing the unwanted side effects seen with conventional cancer therapy, ultimately extending the life-span of patients (Palumbo et al., 2013).

Breast cancer is the most common cancer overall contributing for the 12.5% of the total number of new cases diagnosed in 2020. (https://www.wcrf.org/cancer-trends/worldwide-cancer-data/ accessed on 11 February 2024). Behind factors risk of age, sex, race, genetic makeup -related occurrences of breast cancer (Kamińska et al., 2015) there is factors conditioned by lifestyle such as excessive alcohol consumption, smoke, and obesity (Sun et al., 2017).

This tumour is highly heterogeneous, some cases manifest excellent prognosis, while others are very aggressive (Eliyatkın et al., 2015). In the last century many subtypes of breast cancer have been discovered and characterised for several features which make them insensitive to conventional therapies (Holliday & Speirs, 2011). However, recently, thanks to the development of targeted therapies, several good results have been achieved, like in the cases of endocrine therapies and human epidermal growth factor receptor 2 inhibitors that nowadays is the "prototype" of targeted therapy for breast cancer (Eliyatkın et al., 2015; Crimini et al., 2021). Therefore, there is an unmet need for the discovery of new molecular targets to assist clinicians in their therapeutic decisions to treat breast cancer (Crimini et al., 2021).

Human behaviour is central to the aetiology and management of cancer outcomes. Nowadays, obesity, as result of excess intake of calories, is known to play an important role in increasing the risk of developing several cancer (Fu et al., 2021), current estimations indicate that 20% of all tumours can be attributed to obesity (Santos & Schulze, 2012), and there is increasing evidence that cancer cells show specific alterations in different aspects of lipid metabolism (Santos & Schulze, 2012). In this contest, it will be more and more important to explore lipid metabolism and its key players, to understand how they can influence cancer development and outcomes.

Lipid metabolism is in a constant state of dynamic equilibrium through food intake, de-novo lipogenesis, and consumption of lipids to satisfy the needs of the body (Patel, 2018). Therefore, alterations of one or more of these processes or its dysfunctions, such as in the case of the metabolic syndrome and type 2 diabetes mellitus, can damage the liver as it represents the main organ for lipid metabolism (Alves-Bezerra & Cohen, 2017; Sheka et al., 2020; Powell et al., 2021; Ding et al., 2017).

While the aetiology of several liver diseases and pathological conditions such as virus-, drug- or drinking abuse-derived hepatitis, result from external factors, non-alcoholic fatty liver disease (NAFLD) is a condition in which fat accumulates in liver causing hepatic steatosis (Chalasani et al., 2018). Moreover, increasing liver inflammation, damage and steatosis may lead to development of non-alcoholic steatohepatitis (NASH), with or without fibrosis (Sheka et al., 2020; Chalasani et al., 2018; Stine et al., 2018). NASH is now considered to become a leading cause of hepato-cellular carcinoma (HCC), the most common type of primary liver cancer. Importantly, preliminary studies suggest that hepatocellular carcinoma caused by NASH hold less chance of cure, when compared to viral-related hepatocellular carcinoma (Pinter et al., 2023). In general, liver cancer is a disease with a poor clinical outcome and represents the 6th most common cancer worldwide (the 5th most common in men and the 9th in women, in 2020) (https://www.wcrf.org/cancer-trends/liver-cancer-statistics/). It is therefore necessary to discover new targets and develop new therapies to prevent the worsening of NAFLD and to improve treatment efficacy against liver cancer by reprogramming its metabolic dysfunctions (Pinter et al., 2023).

This thesis is the result of a study carried out for the characterization of two pharmacological targets and their role in the metabolic pathways respectively in breast cancer and hepatic steatosis. I have divided the work in two sections as the activities for the study of each of the molecular target:

1) In the first section I describe the characterization of a pharmacological inhibitor of the DEAD-box RNA helicase 3 X (DDX3X), an already proven helicase enzyme exerting pro-tumorigenic effects in breast cancer (He et al., 2018). However, the novelty of this work lays in the fact that I investigated the activity of a less characterised binding site domain. Specifically in collaboration with First Health Pharmaceuticals B.V. (FHPBV), that provided us a DDX3X novel inhibitor against its RNA binding domain, we performed *in vivo* and *in vitro* experiments demonstrating that FHP01 demonstrates highly potent

antiproliferative and cytotoxic effects across various breast cancer cell lines when assessed *in vitro*. Furthermore, the molecule, when administered systemically, exhibits robust inhibition of tumour growth in xenograft models *in vivo*. These results have been already published in 2023 (Gherardini et al., 2021).

2) In the second section we reported our recent findings on the involvement of mitogen activated protein kinase 15 (MAPK15) in NAFLD, both *in vitro* through siRNA-downregulation of MAPK15 and *in vivo* in MAPK15 knockout (KO) mice*,* in order to understand how MAPK15 is involved in the development of NAFLD and, finally, if the expression of this atypical MAP kinase may represent a marker of the worsening of liver steatosis, opening new possibilities to prevent NASH and liver cancer development.

2. A new targeted approach against breast cancer, by inhibiting the RNA helicase activity of DDX3X.

Parts of the work described in this chapter have been previously published on the peer-reviewed journal “cancers”, into the special issue “novel personalized therapeutic strategies for breast cancer”.

DOI: *10.3390/CANCERS13194830*

2.1. Abstract

The suppression of DDX3X expression and/or activity has been identified to curtail cell proliferation across diverse tumour types, with its expression frequently aligning with heightened tumour aggressiveness. This positions DDX3X as a compelling candidate for the development of drugs tailored for innovative personalized therapeutic strategies. Commencing with an *in-silico* drug discovery approach, a cohort of molecules was meticulously chosen through molecular docking at the RNA binding site of DDX3X. Notably, among these candidates, FHP01 emerged as the most promising and was subsequently evaluated in preclinical models of breast cancer. Specifically, FHP01 demonstrated remarkable antiproliferative and cytotoxic effects on various breast cancer cell types, including triple-negative breast cancer (TNBC) cells. Intriguingly, FHP01 also exhibited the capability to impede WNT signalling, a pivotal tumorigenic pathway previously associated with DDX3X functions in breast cancer model cell lines. Ultimately, FHP01 induced a significant reduction in the growth of TNBC xenograft models derived from MDA MB 231, as observed *in vivo.* Crucially, FHP01 displayed favourable bioavailability and demonstrated no toxicity on normal peripheral blood mononuclear cells *in vitro*, as well as on various mouse tissues *in vivo*. Taken together, our findings strongly suggest that the utilization of FHP01 and its related compounds holds promise as a novel therapeutic approach with substantial potential against breast cancer, including the triple-negative subtype often linked to unfavourable outcomes due to the scarcity of available targeted therapies.

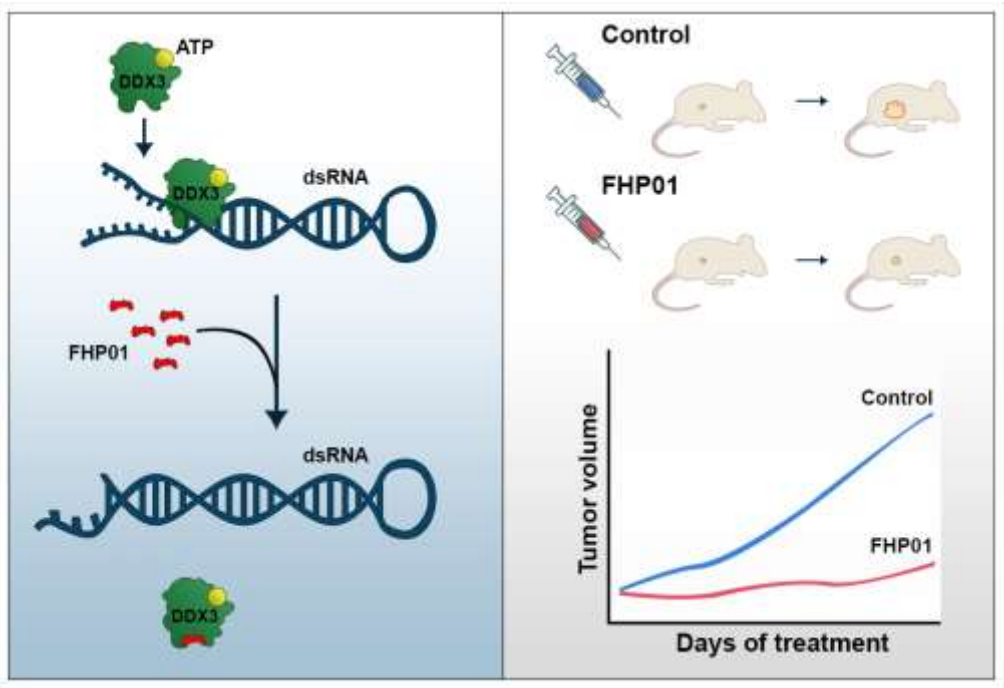

Graphical Abstract

2.2. Introduction

2.2.1. Triple-negative breast cancer

Breast cancer stands as a significant public health challenge, ranking as the most prevalent cancer overall contributing for the 12.5% of the total number of new cases diagnosed in 2020 (https://www.wcrf.org/cancer-trends/worldwide-cancer-data/ accessed on 11 February 2024). The pathological landscape of breast cancer exhibits considerable heterogeneity, with some cases demonstrating a favourable prognosis, while others display heightened aggressiveness. Typically, the expression of estrogen and progesterone receptors (ER and PR, respectively) indicates a more positive prognosis, characterized by reduced aggressiveness and the potential for make use of endocrine therapies such as tamoxifen and aromatase inhibitors. (Eliyatkın et al., 2015). Conversely, human epidermal growth factor receptor 2 (HER2) protein overexpression, while allowing for targeted drug interventions (such as: monoclonal antibody), is typically linked with the presence of more aggressive tumours and an unfavourable prognosis. (Eliyatkın et al., 2015). Within the spectrum of breast cancer subtypes, triple-negative breast cancer (TNBC) stands out, affecting approximately 10 to 20 percent of patients. TNBC is defined by tumours lacking ER and PR, as well as without HER2 overexpression (Eliyatkın et al., 2015). These distinctive features make TNBC insensitive to therapies specifically targeting these proteins (Holliday & Speirs, 2011). While endocrine therapy and HER2 inhibitors remain central to personalized approaches for various breast tumours, ongoing efforts to discover and validate new actionable molecular targets are crucial. These efforts aim to guide clinicians in making therapeutic decisions for a substantial number of breast cancer cases. (Crimini et al., 2021).

2.2.2. DEAD-box helicases 3

The high demand for protein synthesis and mRNA stabilization in cancer cells underscores their dependency on the translational machinery. This intricate process is significantly influenced by DEAD-box helicases, characterized by the D-E-A-D amino acid motif (Asp-Glu-Ala-Asp), which plays a vital role in regulating RNA processing and metabolism through the ATP-dependent unwinding of short double-stranded (ds) RNAs (Crimini et al., 2021). The dysregulation of various members of the DEAD-box protein family has been implicated in biological processes governing cancer development (Fuller-Pace, 2013; Mo et al., 2021; Voss et al., 2017). Situated on the X-chromosome, the DEAD-box RNA helicase 3 X (DDX3X) gene is ubiquitously expressed across various organisms, where it orchestrates diverse physiological events in different tissues. DDX3X is a key player in regulating various facets of RNA metabolism,

encompassing splicing, export, transcription, and translation initiation. Its influence spans numerous cellular processes, from stress regulation to cell proliferation and apoptosis (He et al., 2018). Given its integral role in fundamental mechanisms governing cell proliferation, it is unsurprising to observe aberrant expression and function of DDX3X in human tumours, particularly breast cancer, where it has been consistently implicated in pro-tumorigenic effects (He et al., 2018). Indeed, knockdown of DDX3X in breast cancer cell lines demonstrated reduced proliferation and clonogenicity in vitro, coupled with diminished tumour-forming and metastatic capabilities in vivo (Xie et al., 2015).

Furthermore, DDX3X is frequently overexpressed in breast cancers, with upregulated expression in distant metastases, especially in the brain, where DDX3X protein expression is associated with a worse survival rate (Heerma van Voss et al., 2017a). Recent observations revealed that breast cancer patients with low DDX3X gene expression exhibited significantly better prognosis, highlighting its specific prognostic role in these tumour types (**Figure 1 -** Log-Rank test's p-value < 0.01). Considering this, DDX3X emerges as a promising potential target for pharmacological inhibition in breast cancers therapy. Despite this potential, compounds targeting the ATPase domain of DDX3X have not yet progressed to clinical studies.

Exploiting in silico modelling approaches, a novel class of molecules has recently been identified, demonstrating interaction with the RNA-binding site of DDX3X. This mechanism distinguishes them from conventional DDX3X inhibitors that compete for ATP binding sites. (Brai et al., 2016; Radi et al., 2012)

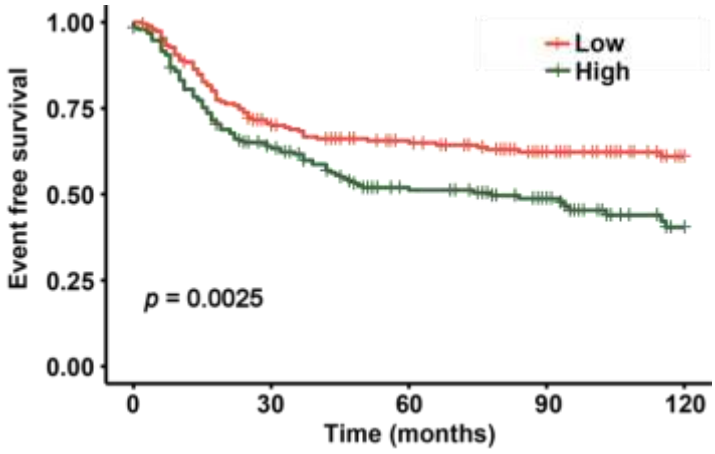

Figure 1. "Kaplan-Meier curves for Event Free Survival of TNBC patients from GSE31519 dataset". To investigate the impact of DDX3X gene expression on the clinical outcome of TNBC patients, we exploited a cohort of 579 cases and event free survival (EFS) follow up data, corresponding to re- lapse-free survival endpoint. Samples are divided in two groups according to the DDX3X median expression level ("Low" stands for < median value; "High" stands for > median value). Log-rank test's p-value is shown.

2.2.3. AIM

In this investigation, our focus was on assessing the potent antiproliferative properties of the FHP01 molecule, as detailed in the patent document (https://patents.google.com/patent/WO2017162834A1/en), against various human breast cancer models. Significantly, FHP01 exhibited robust cytotoxic effects *in vitro* across a diverse range of breast cancer cell lines, encompassing models representative of triple-negative breast cancer (TNBC). This intriguing in vitro activity was notably associated with FHP01's capacity to suppress the WNT/β-catenin signalling axis, a pathway intricately linked to DDX3X-dependent cell proliferation and transformation (Nusse & Clevers, 2017).

Building upon these promising findings and recognizing the favourable pharmacokinetic profile and distribution observed in mouse models, we extended our exploration to evaluate FHP01's efficacy in a well-established *in vivo* model for TNBC. The outcomes were noteworthy, as FHP01 exhibited potent anti-tumour activity without any relevant signs of specific organ toxicity. Additionally, the compound demonstrated “good drug tolerance”, further underlining its potential as a promising candidate for further development in the context of triple-negative breast cancer treatment.

2.3. Materials and Methods

2.3.1. Chemistry

The commercially available reagents were purchased by Sigma-Aldrich and used without further purification. Prior to use solvents (DCM and MeOH) were dried by distillation from magnesium methoxyde or calcium hydride. TLC was carried out using Merck TLC plates silica gel 60 F254. Chromatographic purifications were performed using Waters Acquity UPLC with Single Quadrupole Detector with ESI source, and XBridge

BEH C18 XP column. 1H-NMR spectra were recorded at 300 MHz, on a Mercury 300 NMR spectrometer. Chemical shifts are reported relative to tetramethylsilane at 0.00 ppm. 1H patterns are described using the following abbreviations: s = singlet, d = doublet, t = triplet, q = quartet, quin = quintet, sx = sextet, sept = septet, m = multiplet, br = broad signal, br s = broad singlet.

Mass spectra (MS) data were obtained using an Agilent 6100 LC/MS (G6130B) spectrometer with a 0.4 mL/min flow rate using a binary solvent system of 95:5 methanol/water. UV detection was monitored at 215 nm and 276 nm. Mass spectra were acquired in positive and negative mode scanning over the mass range.

4-butyl-1-(4-nitrophenyl)-1H-1,2,3-triazole (1b). (Purification eluent: DCM/MeOH 95:5). Yield 94%, yellow solid.MS (ESI) m/z 245 [M-H]-, 281 [M+Cl]-.

4-butyl-1-(4-aminophenyl)-1H-1,2,3-triazole (1c) (Purification eluent: DCM/MeOH 95:5). Yield 91%, white solid. MS (ESI) m/z 217 [M+H]+, 240 [M+Na]+.

1-(4-(4-butyl-1H-1,2,3-triazol-1-yl)phenyl)-3-(2-(trifluoromethyl)phenyl)urea (FHP01): (Purification eluent: H2O/ACN 70:30).Yield 40%, white solid. HPLC Purity 99.7% (at 215nm); 1HNMR (400 MHz DMSO-d6):δ 9.60 (s, 1H), 8.47 (s, 1H), 8.16 (s, 1H), 7.95 (d, 1H), 7.79 (d, 2H), 7.74-7.62 (m, 4H), 7.30 (t, 1H), 2.69 (t, 2H), 1.65 (quint, 2H), 1.37 (sx, 2H), 0.92 (t, 3H)ppm. MS (ES+) m/z 404.8 [M+1], (ES-) m/z 402.9 [M-1].

2.3.2. Homology Modelling

For the present computational studies, the closed conformation that binds double stranded RNA is fundamental, and the models of the closed conformation of DDX3X has been prepared by homology modeling using the Swiss-Model web Server (Waterhouse et al., 2018).

The homology model was generated by SWISS-MODEL web interface. The template library (SMTL version 2017-05-03, PDB release 2017-04-28) was searched with Blast (Altschul et al., 1997) and HHBlits (Remmert et al., 2011) for evolutionary related structures matching the

targets sequence. The global and per-residue model quality was assessed using the QMEAN scoring function (Benkert et al., 2011). Finally, for each helicase, the best QMEAN score homology model of closed conformation was selected for further analysis by molecular dynamics simulations.

The homology model for DDX3X was built with ProMod3 (version 1.0.2, OpenStructure, SIB Swiss Institute of Bioinformatics Biozentrum University of Basel, Basel, Switzerland) (Biasini et al., 2013) the protein was modeled as monomer without ligands with a GMQE value of 0.51 (per residue local quality estimation and a QMEAN value of -1.80 (data not shown).

The template structure selected was the ATP dependent RNA helicase vasa, the XRay structure with PDB id 2DB3 (chain B), resolution 2.20 Å, residue range 136-671, coverage of target sequence 63%, with a sequence identity of 51.32%, and sequence similarity score 0.44, identified by BLAST.

2.3.3. Molecular Dynamics Simulations

The selected homology model of DDX3X has been prepared for a series of explicit solvent molecular dynamics simulations. The homology model was refined by adding ATP co-factor and magnesium 2+ ion with coordination water molecules, the protonation state and orientation of histidine, asparagine and glutamine residues have been optimized by PDB2PQR (version 2.1.0, Poissonboltzmann; Washington University in St. Louis, St. Louis, MO, USA); (Dolinsky et al., 2004; Dolinsky et al., 2007). All the missing hydrogen atoms were added according to the AMBER 14 topology parameters using the LEAP module of AMBERTOOLS. ATP was parametrized using the parameters set as described from Meagher, Redman, and Carlson (Meagher et al., 2003). The proteins were solvated in a cubic water-box of TIP3P waters, solvent constituting 10 Å buffer form the protein to the periodic boundary. The system was then neutralized adding the appropriate number of sodium and chloride ions to simulate a concentration of 0.1M. Topology files were parameterized using AMBER14SB forcefield.

All the molecular dynamics simulations were performed with NAMD (version 2.12, Theoretical and Computational Biophysics Group; University Of Illinois at Urbana-Champaign, Urbana, IL, USA) (Phillips et al., 2005). A total of 5000 steps of energy minimization have been carried out to remove artificial contacts, without constraint. The system was then equilibrated for 1 ns with a 2 fs time-step at 1 atm pressure following a two-step equilibration protocol: the first step consists of 0.1 ns simulation where the system was heated form 0°K to 310°K with a Berendsen thermostat simulation; the second step was a 0.9 ns Langevin dynamics simulation at 310°K temperature. Finally, a 20 ns simulation was carried out. The simulations were

performed with GPU accelerated molecular dynamics in an 88 CPUs system with two GPU (NVIDIA GeForce GTX 1080) with an average speed of 0.2 days/ns of simulation. Simulation snapshots have been collected every 10,000 steps resulting in 1000 frames, that represent the conformational sampling of the aminoacids sidechains degree of freedom, the RMSD fluctuation plots of the carbon alpha trace of the protein respect to the average structure, indicate that the helicases modeled was reasonably equilibrated. The molecular dynamics trajectories have been sampled to select a series of 20 frame representative of the flexibility of binding site residues, by clustering and centroid conformation selection. The pairwise RMSD matrix between the frames has been calculated with VMD (Humphrey et al., 1996), by alignment and RMSD calculation between the residues that contribute to the helicase binding site surface. The clustering was performed by hierarchical clustering with average linkage at RMSD 2.0 Å selecting a maximum number of 20 clusters. For each protein the representative structure of each cluster was selected for the ensemble molecular docking procedure (Amaro et al., 2018)to account the flexibility of the binding site.

2.3.4. Ensemble Molecular Docking

The molecular docking experiments were performed combining two different programs SMINA (Trott & Olson, 2010) and RBDOCK (Morley & Afshar, 2004). The molecular docking protocol is based on the docking in parallel with both SMINA and RBDOCK, in the conformation ensemble of DDX3X. The ligand docking poses obtained from the two docking programs were rescored using an external scoring function, RF-SCORE-VS (Wójcikowski et al., 2017), and clustered by hierarchical clustering with average linkage at RMSD 2.5 Å.

Key interaction of FHP01 have been identified using the following parameters: the hydrogen bond donor (HBD) and hydrogen bond acceptor (HBA) interaction are identified when the distance between the heavy atoms is less or equal than 3.6 Å and a maximum angle of 63 degree, the Van der Waals interactions (VdW) are considered present when any of the atoms of the ligand are at a distance between 3 and 4.5 Å from the atom of the protein residues.

2.3.5. Synthesis of FHP01

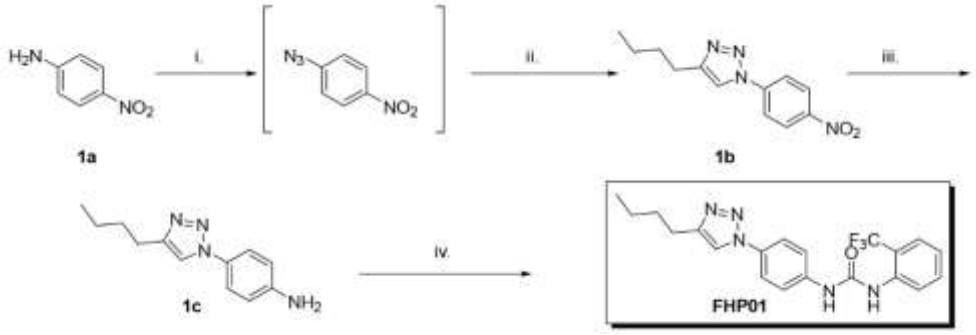

Reagents and conditions: i. a) tBuONO, CH3CN, 0°C, 20 min, b) TMSN3, CH3CN, r.t., 2h; ii. 1-Hexyne CuSO4. 5H2O, Sodium Ascorbate, H2O:tBuOH (1:1 v/v), MW 125°C, 15 min; (94%); iii. Raney nickel, hydrazine, MeOH, r.t. (91%); iv. 1-isocyanato-2-(trifluoromethyl)benzene, DCM, 5h, r.t. (40%).

The synthesis procedure followed to obtain FHP01 is shown in Scheme 1. The intermediate 1-azido-4-nitrobenzene was obtained from 4-nitroaniline (1a), by reaction with tBuONO in acetonitrile in ice bath for 20 min, then ice bath was removed and TMSN3 was added and reacted at room temperature for 2 hours. The 1-azido-4-nitrobenzene was reacted with 1-Hexyne in presence of CuSO4 pentahydrate and sodium Ascorbate in H2O/tBuOH (1:1 v/v) in microwave at 125 °C for 15 min, leading to obtain the 4-butyl-1(4-nitrophenyl)-1H-1,2,3-triazole (1b). The intermediate 1c was obtained by reduction with Raney nickel and hydrazine hydrate, refluxing in methanol for 3 hours. The final compound FHP01 was afforded by reaction with 1-isocyanato-2-(trifluoromethyl)benzene in DCM for 5 hours at room temperature. FHP01 was purified by reverse phase chromatography (Water/Acetonitrile), obtaining 400 mg as white solid with purity of 99.7% (at 215 nm) and 99.6% (at 276 nm).

2.3.6. Helicase activity Assay

293T cells (3×10^5) were initially plated in 6-well plates and, following a 24-hour incubation period, transfected with 1 µg of HA-DDX3 (Addgene plasmid #44975) (Lee et al., 2008) using the Lipofectamine reagent (Thermo Fischer Scientific, Waltham, MA, USA). After 36 hours, cells were harvested and lysed in NP-40 Lysis Buffer (20 mM HEPES pH = 7.5, 10 mM EGTA pH = 8, 40 mM β-glycerolphosphate, 1% NP40, 2.5 mM $MgCl_2$, 2 mM Orthovanadate, 2 mM NaF, 1 mM DTT, and 1X protease inhibitors mixture). Subsequently, 2 mg of proteins were subjected to immunoprecipitation using anti-HA antibodies (Covance, Princeton, NJ, USA) in NP40 lysis buffer. The immunoprecipitated samples underwent two washes with lysis buffer and one wash

in helicase reaction buffer (50 mM Tris HCl pH = 8, 1 mM DTT, 5% glycerol, 10 mM $MgCl_2$). The beads were then resuspended in helicase reaction buffer.

To assess DDX3X helicase activity, we measured the unwinding of an 18/36mer double-stranded (ds) RNA oligonucleotide:

- r36mer 5'-ACCAGCUUUGUUCCUUGGGUUCUUGGGAGCAGCAGG-3' and
- r18mer_FAM [6FAM] -5'-CCCAAGAACCCAAGGAAC-3' (Garbelli et al., 2011).

The 36mer oligonucleotide sequence is designed to be complementary to the 18mer. To prevent reannealing of the probed RNA following unwinding, we used an RNA oligonucleotide homologous to the 18mer (without FAM modification) as a competitor. Annealing reactions were conducted in 50 mM Tris HCl pH = 8, 10 mM $MgCl_2$, 0.2 µM of r18mer, and 0.2 µM of r36mer. To assess the efficiency of competition, a sample with a final concentration of 20 nM of dsRNA plus 100 nM of the competitor was heated at 90 °C for 1 min.

Subsequently, the helicase reactions were carried out in a final volume of 100 µL of helicase reaction buffer with 4 mM ATP, 30 µL of beads used for immunoprecipitating HA-DDX3X, 20 nM of 18/36mer dsRNA, and 100 nM of the competitor at 37 °C for 1 hour. The reactions were quenched by adding 10 µL of a stopping solution (60 mM EDTA pH = 8, 40% glycerol, 0.6% SDS, 1% Orange G). The resulting samples were loaded onto a 15% polyacrylamide TBE gel containing 1% SDS in 1× TBE buffer with 0.1% SDS and run at 4 °C for 1.5 hours. Visualization of the unwinding reaction products, r18mer_FAM, and the dsRNA was performed using an Image-Quant Las4000 (GE Healthcare, Chicago, IL, USA) with a Cy3 detection filter and Green Epi light. Quantification of the ssRNA was carried out using the ImageJ software (National Institutes of Health, Bethesda, MD, USA).

2.3.7. Cell Culture and Media

Breast cancer cells were purchased from ATCC, and all cells were maintained in the appropriate medium at 37 °C under a 5% CO_2/air atmosphere. Specifically, SKBR3 cells were cultured in RPMI 1640 with 10% FBS, 250 mg glucose, 1 mM sodium pyruvate, 2 mM L-glutamine, and 100 units/mL penicillin–streptomycin; MDA MB 231, T47D, MCF7, and 293T cells were cultured in Dulbecco's Modified Eagle's Medium (DMEM), 10% fetal bovine serum (FBS), 2 mM L-glutamine, 100 units per mL penicillin–streptomycin; MCF10A in DMEM/F12, 5% Horse serum, 20 ng/mL EGF, 0.5 µg/mL Hydrocortisone, 100 ng/mL Cholera Toxin, 10 µg /mL Insulin, 2 mM L-glutamine, 100 units per mL penicillin–streptomycin; MDA MB 468 in RPMI 1640, 10% FBS, 2 mM L-glutamine, 100 units per mL penicillin– streptomycin. Peripheral blood mononuclear cells (PBMCs) were cultured in RPMI 1640 supplemented with 10% heat-

inactivated fetal bovine serum, 100 U/mL penicillin, 100 µg/mL streptomycin, interleukin-2 20 U/mL, and HEPES 12.5 mM.

2.3.8. Assessment of Cell Viability in Breast Cancer Cells

Cells were plated at a density of 3–5 × 10^4 cells per well in 12-well plates and maintained at 37 °C in 5% CO_2 atmosphere. After 24 h, cells were treated with various concentrations of the specified drugs ranging from 0 to 100 µM (0, 0.1, 1, 10, 50, 100 µM). Following 72 h of incubation, cells were washed with PBS and subsequently harvested. The cell number for each sample was determined using a Z2 Coulter Counter (Beckman Coulter, Brea, CA, USA), in triplicate. The data on cell viability were graphically represented using GraphPad Prism 9.0 software (GraphPad Software, San Diego, CA, USA) to generate dose–response curves and to calculate IC50 values.

2.3.9. Assessment of Cell Viability in PBMC

Two days prior to the assay, phytohemagglutinin-A (PHA) at a concentration of 2 µg/mL was added to the PBMC culture. Cells were plated at 13 × 10^4 cells per well in triplicate and maintained at 37 °C in 5% CO_2. After 24 h, cells were exposed to 10 µM and 50 µM concentrations of the specified drugs. Following a 72h incubation period, cells were washed with PBS and harvested. The cell number for each sample was determined using a Z2 Coulter Counter (Beckman Coulter, Brea, CA, USA), in triplicate. The data on cell viability were graphically represented using GraphPad Prism 9.0 software (GraphPad Software, San Diego, CA, USA) 100% viability corresponding to vehicle DMSO-treated PBMCs.

2.3.10. Western Blots and Antibodies

Cells (1 × 10^5) were initially plated in 6-well plates. Following a 24-hour incubation, cells were subjected to treatments with DMSO (vehicle) or FHP01 for the specified durations. Post-treatment, cells were washed with cold PBS, and total protein extracts were obtained by adding RIPA buffer. (50 mM Tris-HCl pH 8.0, 150 mM NaCl, 0.5% Sodium deoxycholate, 0.1% SDS, 1% NP-40, 2 mM Orthovanadate, 2mM Sodium fluoride, 1mM Dithiothreitol and 1× protease inhibitors). Following mechanical detachment using cell scrapers, total lysates were gathered in tubes, subjected to vortexing, and then incubated for 15 minutes on ice. Tumours from mice were collected and disrupted by bead homogenization in Lysing Matrix D tubes using a FastPrep-24 5G homogenizer (MP Biomedicals, Solon, OH, USA) adding *w:v* of "RIPA buffer". Next, samples were centrifuged for 10 min at 16,000 g, and supernatants were collected. Quantification of total protein extracts was performed using the Bradford assay. Subsequently,

20-25 µg protein samples were mixed at 1X of Laemmli Loading Buffer 5X (containing 250 mM Tris-HCl pH 6.8, 10% SDS, 50% glycerol, bromophenol blue), heated at 95°C for 5 minutes, and stored at -20°C until utilized for Western blot.

For Western blot analysis, the protein sample were loaded onto 8% polyacrylamide gels and separated by SDS-PAGE for 1,5 hours, and transfer onto an Immobilon-P PVDF membrane for 1,5 hours (Millipore, IPVH00010), subsequentially blocked in 5% low fat milk and probed overnight with appropriate antibodies: anti-phospho β-catenin (#9561, Cell Signaling, Danvers, MA, USA), anti-β-catenin (#c19220, BD Biosciences, Franklin Lakes, NJ, USA), anti-ERK2 (#sc-154, Santa Cruz, Dallas, TX, USA), anti-DDX3 (#2635, Cell Signaling, Danvers), and revealed by enhanced chemiluminescence detection (ECL Plus; GE Healthcare, RPN2132). Densitometric analysis of western blots was performed with the free software NIH Image J (National Institutes of Health).

2.3.11. Luciferase Activity Assay in Response to FHP01 Treatment

MDA MB 231 cells were seeded at 3×10^4 cells/well density in 12-well plates, in triplicate, and transfected with 250 ng of the M50 Super 8× TOPFlash reporter vector (Addgene Plasmid #12456) (Veeman et al., 2003) and 1 µg of expression vectors inducing the WNT pathway (Wnt1-V5, Addgene plasmid #43807, and Wnt3A-V5, Addgene plasmid #43810) (MacDonald et al., 2014). Eight hours post-transfection, cells underwent treatment with either FHP01 or DMSO for specified durations before lysing in Passive Lysis Buffer (Promega, Madison, WI, USA). Luciferase activity in cellular lysates was assessed on a Glomax 20/20 luminometer (Promega) using the Luciferase Assay System (Promega). The results were normalized with GFP expression, following transfection with the GFP coding vector (1 µg). The displayed data are representative outcomes from three independent experiments (n = 3), and error bars represent the Standard Error of the Mean. Each sample underwent readings in triplicate at a minimum.

2.3.12. Pharmacokinetic Studies in Animal

These investigations were conducted at the GVKBioscience Pvt. LTD Contract Research and Development Organization (CRDO). The animals were housed in cages with clean bedding, and adult Swiss Albino male mice (weight = 20–35 g) were maintained in accordance with GVKBioscience Pvt. LTD Test Facility SOPs and under the supervision of the laboratory animal veterinarian to ensure their well-being. The mice were provided with certified rodent diet, and water was available ad libitum. Regular water analyses were performed, and the results were archived at the Test Facility. The animal room's environmental controls were configured to

maintain a temperature of 22 to 25 °C, humidity between 40–70%, and a 12-hour light/12-hour dark cycle. The mice were administered intravenously with 1 mg/kg of FHP01, intraperitoneally with 10 mg/kg of the compound, or orally through a gastric gavage needle with 50 mg/kg of the compound.

Next, mice were anesthetized using gaseous anaesthesia and blood samples were collected at each time point, from 3 mice of respective group. After collection of blood samples at each time point, the blood samples were stored on ice, prior to centrifugation. Blood samples were centrifuged at 1540rcf, 4 °C for 10 min to separate plasma. Plasma was transferred to pre-labeled micro-centrifuge tubes and promptly frozen at −80°C until analysis. Samples were characterized by the test item, group, animal number, and collection time point. A bioanalytical method tailored for the purpose was developed to analyse the plasma samples. Prior to processing the sample batch, a series of nine standards was run and utilized to construct the calibration curve. QC samples were meticulously prepared at a minimum of three concentrations: LQC (not exceeding 5 times the lowest standard concentration), HQC (not falling below 75% of the highest standard concentration), and MQC (situated between the low and high concentrations). A minimum of 6 QC samples, comprising three concentrations each in duplicate, were analysed. Both before and after processing the sample batch, a single set of QC samples (LQC, MQC, and HQC) underwent analysis. To analyse drug distribution in the brain and liver, whole-body perfusion was executed on a specific group of animals using chilled saline, followed by decapitation for tissue retrieval. The mice's chests were exposed, the abdominal aorta was clamped, and both jugular veins were incised. Intra-cardial perfusion was carried out through an insertion in the left ventricle. Subsequently, mouse brains and livers were promptly collected, washed, dried, weighed, and frozen at −80 °C until homogenization. The entire procedure received approval from the Institutional Animal Ethics Committee (IAEC).

2.3.13. Cancer Model Animal Study

Animal experiments adhered to the current Italian legislation, and the animal protocol underwent review and approval by the Italian Ministero Della Salute (authorization n. 886/2020-PR). The study aimed to examine the impact of a newly synthesized molecule with DDX3X inhibitor activity, administered intraperitoneally at a concentration of 45 mg/kg, on the tumour growth of xenograft MDA MB 231 human breast cancer cells. In this context, "n" refers to the number of tumours expressed on both flanks of the animals. The sample size was determined using the g-power calculator, considering a predicted large (2-fold increase) effect size, alpha set at 0.05, and a confidence interval of 95%. The experimental unit number was set at 10,

corresponding to 5 animals. The study utilized a total of 10 animals, specifically six-week-old athymic nude mice obtained from Charles River Laboratories. In our animal facilities, five animals were housed in each cage, undergoing a 5-day acclimatization period in individually ventilated cages. The animals were provided with lab diet ad libitum, and water was consistently accessible, maintaining standard specific pathogen-free conditions with a 12-hour light/dark cycle. An initial observational analysis was conducted at the commencement of the experimental procedure to ensure the well-being of the animals. (**Figure 7**).

For the establishment of xenograft tumours, MDA MB 231 cells were cultured in the previously described media. On the experimental day, cells (2.8×10^6) were suspended in 150µL PBS mixed with Matrigel (1:1) and injected subcutaneously on both sides of the flank region of nude mice. The tumour volume, determined manually using callipers, was calculated using the modified ellipsoidal formula: Tumour volume = $1/2(\text{length} \times \text{width}^2)$, where the greatest longitudinal diameter (length) and the greatest transverse diameter (width) were measured.

Group allocation and treatments were initiated when tumours reached a mean size of 24.82 ± 2.56mm^3. Animals were assigned to two groups using a minimization strategy based on tumour size. The treatment group received 100 µL of a 45mg/kg FHP01 suspended in a vehicle (10% DMSO, 5% Tween 80, 85% H_2O) via i.p. injection three times per week for 4 weeks. The control group received 100µL of the vehicle. One control animal reached humane endpoint criteria and was sacrificed, not included in the analysis. The FHP01 treatment group exhibited an outlier that was not considered in the analysis. Upon concluding the experiment, animals were euthanized following FELASA protocol, and relevant internal organs were collected for postmortem histology.

For the final statistics, the number of tumours analysed was 8 in the control group (one animal died for unknown reasons as certified by the AWB designed veterinary) and 9 for the treated group (the volume of one tumour was considered outlier). Results were reported as tumour volume increase, normalizing the value of each measurement to the baseline value of each sample and expressed as mean ± SEM. Two-way RM ANOVA was used to describe the significant effect of treatment versus time, considered significant when $p < 0.05$.

2.3.14. Survival Analysis

Gene expression and clinical data were obtained from GEO database under accession number [GSE31519], (https://www.ncbi.nlm.nih.gov/geo/query/acc.cgi?acc=GSE31519 accessed on 21 August 2020). Our analysis focused on the specific expression of DDX3X probes in relation to Event-Free Survival. Following the segmentation of patients based on the median

expression level of four DDX3X probes, survival analysis was conducted using R software (Version R-4.0.1, R Foundation for Statistical Computing, Vienna, Austria) (Rody et al., 2011). Kaplan–Meier survival curves were constructed, visualized, and compared using the "survival" and "surviminer" CRAN packages, through the Log-rank test.

2.3.15. Histology Sampling

Upon euthanasia, internal organ samples were collected. The spleen, kidney, lung, and brain from each subject were subjected to formalin fixation and paraffin embedding. To assess for signs of toxicity and alterations in morphology, 4-µm-thick sections underwent H&E staining.

2.3.16. Statistical Analysis

The results for each analysis are presented as the mean ± SEM. Statistical comparisons at specific time points were conducted using the t-test. To assess the impact of the two treatments *in vivo*, a Two-way RM ANOVA was employed. All p-values were derived from two-sided statistical analyses, and significance was defined as $p < 0.05$.

2.4. Results

2.4.1. Potent Cytotoxic Effects of FHP01 Treatment on Triple-Negative Breast Cancer Cells

FHP01, depicted in **Figure 2a**, serves as a potent inhibitor of DDX3X helicase activity, evident in its in vitro enzymatic activity with an IC50 of 0.3 µM (https://patents.google.com/patent/WO2017162834A1/en). This compound belongs to a class of molecules discovered and optimized through an *in-silico* drug design approach, employing 3D-pharmacophore screening and molecular docking calculations to identify compounds targeting the RNA binding site of DDX3X (Brai et al., 2016), (https://patents.google.com/patent/WO2017162834A1/en). To validate the binding mode of FHP01, we conducted homology modelling of DDX3X and molecular dynamic simulations (**Figure 2b, Table 1**). Considering DDX3X's complexity and potential influence from various post-translational modifications (Gustafson & Wessel, 2010), which may not be accurately modelled by bacterially overexpressed proteins, we further confirmed FHP01's ability to inhibit DDX3X helicase activity using human protein immunoprecipitated from 293T cells transfected with HA-tagged DDX3X in a "qualitative *in vitro* helicase assay". Notably, FHP01 exhibited comparable activity to RK33, a lead compound inhibitor for DDX3X (**Figure 3a, 3b**) (Bol et al., 2015).

Motivated by the pivotal role of DDX3X in breast cancer (Xie et al., 2015; Botlagunta et al., 2008), we decided to assess FHP01's efficacy *in vitro* by determining its IC50 values in cell lines representing principal molecular subtypes of breast cancer. These include MCF7 and T47D (ER+/PR+ subtype), SKBR3 (HER2+ subtype), MDA-MB-468 and MDA-MB-231 (TNBC subtype), along with immortalized MCF10A cells serving as non-tumorigenic mammary epithelial control cells (**Table 2**) (Holliday & Speirs, 2011). Specifically, in a 72-hour cytotoxicity assay, FHP01 exhibited higher efficacy in TNBC cells (IC50 = 3.058 and 3.21µM in MDA-MB-468 and MDA-MB-231, respectively), intermediate in ER+/PR+ (IC50 = 12.43 and 10.62µM in MCF7 and T47D cells, respectively), and HER2+ (IC50 = 13.46µM in SKBR3) cells. Notably, FHP01's efficacy was lower in control MCF10A cells (IC50 = 28.71µM) (**Figure 4a**). Significantly, FHP01's efficacy in breast cancer cellular in vitro models paralleled that of RK33 (**Figure 4b**) and was not strictly correlated to DDX3X expression (**Figure 4c**), aligning with the findings for RK33 itself (Heerma van Voss et al., 2017a). Crucially, our data phenocopied the reported effects of DDX3X knockdown in breast tumour cells (Xie et al., 2015), underscoring the high potential of this gene as a specific target for breast cancer therapy. As a control for FHP01's specificity in affecting cancer cell survival, no discernible effect of the drug was observed on normal peripheral blood mononuclear cells (PBMC) up to a concentration of 50 µM (**Figure 4d**).

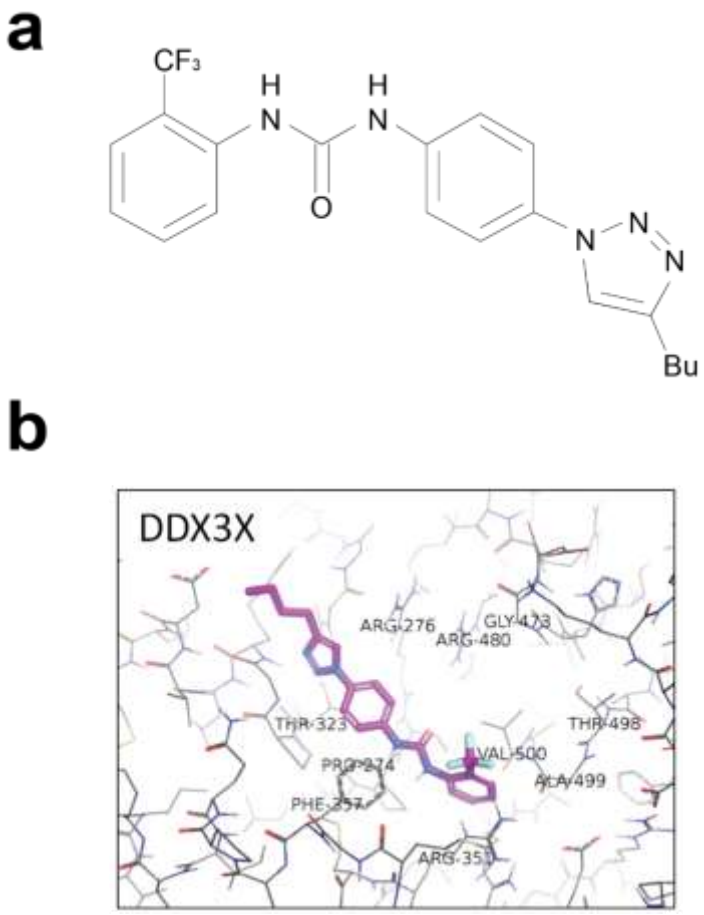

Figure 2. (**a**) The chemical structure of the FHP01 compound. (**b**) Docking Poses of FHP01 in DDX3X RNA Binding Site. The DEAD box helicases consist of two main RecA-like domains that can change their reciprocal position upon the binding of an ATP/ADP co-factor and/or double strand RNA. The reciprocal positions of the two domains are usually indicated as “open” and “closed” conformations. The closed conformation is identified with the binding of double stranded RNA and ATP/ADP, while the open conformation with the binding of only ATP/ADP. Most of the available X-Ray structures of the human DEAD box helicases were obtained in the open conformation. To independently validate the binding mode of FHP01 against the previous published data for this compound series (Eliyatkın et al., 2015) we performed a homology modelling of DDX3X and a molecular dynamic simulation with the objective to collect a set of protein conformations suitable for an ensemble docking procedure. The application of our molecular docking protocol on multi conformation DDX3X ensemble docking model *allows us* to guess a concrete hypothesis about the binding mode of FHP01 in the RNA binding site.

Table 1. The best score binding pose obtained (RFScore of 7.33) showed a set of key interaction with the RNA binding site (Holliday & Speirs, 2011) that agree with the binding mode proposed by Brai et al. for the compound series which FHP01 belongs (Eliyatkın et al., 2015).

Interaction type - index	Residue interacting part	Binding site residues index
HBD-1	Sidechain	Arg 276
HBD-2	Sidechain	Arg 480
HBD-3	Sidechain	Thr 498
VdW/HBA-4	Backbone	Pro 274
VdW-5	Sidechain	Phe 357
VdW-6	Sidechain	Val 500
VdW-7	Sidechain	Gly 473
HBA/HBD-8	Sidechain	Thr 323
HBD-9	Sidechain	Arg 351
HBA/D/VdW-10	Sidechain	Ala499

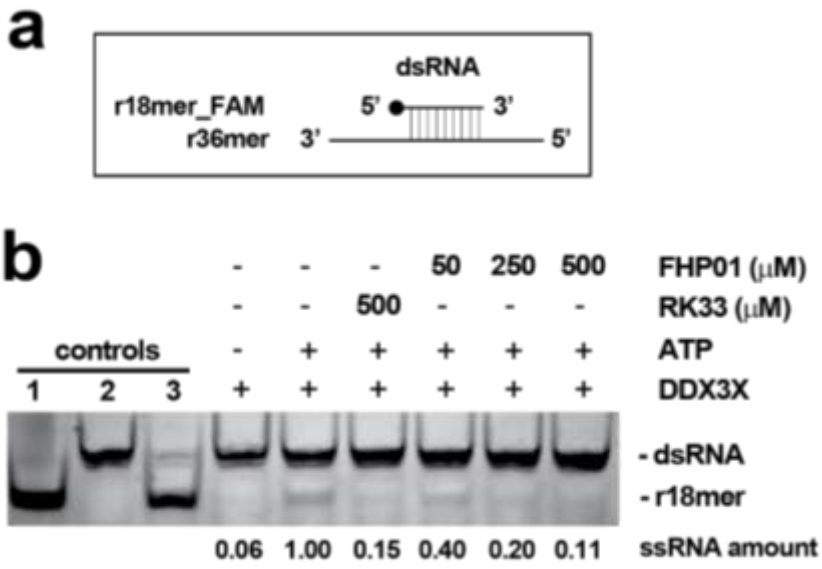

Figure 3 FHP01 helicase activity assay. (**a**) The assay evaluates the helicase activity of immunoprecipitated HA-DDX3X by assessing its capability to unwind a previously annealed double-stranded RNA (dsRNA) composed of a fluorescein amidites (FAM)-modified r18mer and a complementary r36mer. (**b**) Following the unwinding reaction, the resultant products were separated on a polyacrylamide gel to distinguish them from the dsRNA. Unwinding reactions were conducted in the presence of the vehicle (+ATP) or varying amounts of the RK33 and FHP01 DDX3X inhibitors. A complete reaction without ATP (−ATP) was included to establish the background level of activity in this assay. Additional controls, such as the FAM-conjugated r18mer (1), the dsRNA (2), and a dsRNA annealed in excess of an r18mer unconjugated to FAM (competitor) (3), were also loaded onto the gel. The quantification of the r18-mer_FAM product from the unwinding reaction was performed using ImageJ software. The results displayed represent a single experiment from a set of three (n = 3), showcasing the outcomes of a representative helicase assay.

Table 2 Distinct Molecular Profiles of Human Breast Cancer-Derived Cell Lines. The presence or absence of these receptors plays a pivotal role in characterizing the individual cell lines. Abbreviations: ER, estrogen receptor; HER2, human epidermal growth factor receptor 2; PR, progesterone receptor.

Cell line	ERα	PR	HER2	Other characteristics
MCF-10A	-	-	-	Immortalized and non-tumorigenic cell line
MCF-7	+	+	-	Model for endocrine responsive breast cancer
T47D	+	+	-	Model for endocrine responsive breast cancer
SK-BR-3	-	-	+	Model for HER2 positive breast cancer
MDA-MB-468	-	-	-	Model for triple negative breast cancer
MDA-MB-231	-	-	-	Model for triple negative breast cancer

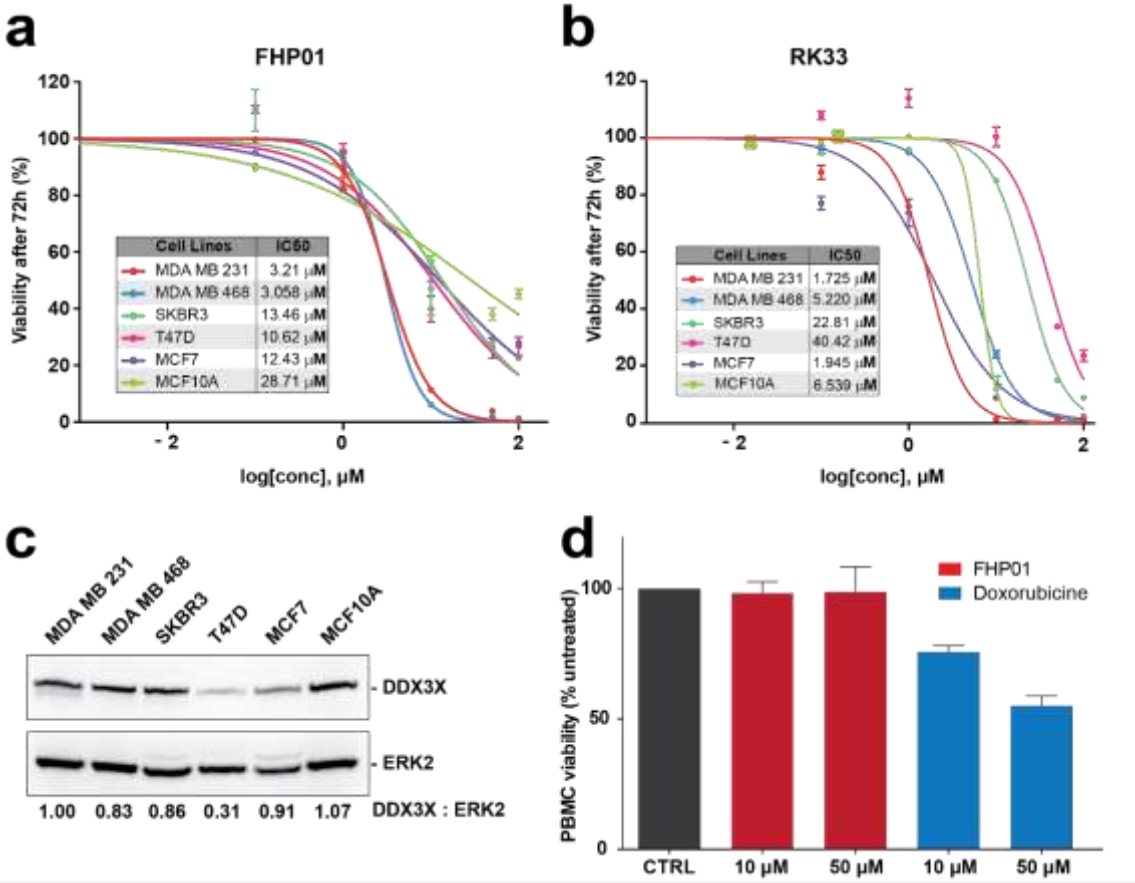

Figure 4. Evaluation of Cytotoxicity Across Human Breast-Derived Cell Lines. (**a**) IC50 Assessment: Following a 72-hour treatment with FHP01 at varying concentrations (0, 0.1, 1, 10, 50, 100 µM), cytotoxicity was evaluated in MDA-MB-231, MDA-MB-468, SKBR3, T47D, MCF7 breast cancer cells, and control MCF-10A immortalized cells. The results, obtained through cell counting using a Z2 Coulter counter, represent averages from triplicate samples in a typical experiment (n=3). (**b**) RK33 Molecule Comparison: Similar to panel (a), this section presents the IC50 evaluation after 72-hour treatment with the RK33 molecule across the mentioned cell lines. (**c**) Western blot analysis assessed DDX3X expression in different breast cancer cell lines, with anti-ERK2 immunoblot normalization for total lysates protein levels. Representative images from three independent experiments (n = 3) are displayed, and densitometric analysis of DDX3X, normalized by ERK2 protein levels, was conducted using NIH ImageJ.; (**d**) Cell viability of peripheral blood mononuclear cells (PBMCs) was measured following a 72-hour treatment with indicated concentrations of FHP01 and Doxorubicin (utilized as a positive control).

2.4.2. Suppression of WNT Signalling in Triple-Negative Breast Cancer Cells by FHP01

Ever since the initial discovery of DDX3X's role as a regulator of WNT- βcatenin signalling in mammalian cells and developmental processes in Xenopus and Caenorhabditis elegans (Cruciat et al., 2013), numerous studies have underscored the involvement of the DDX3X-WNT β-catenin axis in various human tumours (Bol et al., 2015; Chen et al., 2015a; He et al., 2016). A pivotal aspect in this regulatory mechanism is the dependency of DDX3X's control over β-catenin expression on its RNA helicase activity (Chen et al., 2015b).

Motivated by these findings, we decided to use the activation of the WNT-β-catenin pathway as an alternative, even if indirect readout to establish FHP01's impact on DDX3X, specifically its ability to downregulate WNT pathway activation downstream of this RNA helicase. Our approach commenced with a time-dependent Western blot analysis of MDA MB 231 cells treated with FHP01 for 48 to 72 hours, revealing a progressive reduction in β-catenin protein levels (**Figure 5a**). This temporal alteration in β-catenin levels mirrors observations linked to the downregulation of WNT signalling upon DDX3X knockdown (Chen et al., 2015b; He et al., 2016).

To further confirm these findings in a functional assay specifically targeting the WNT pathway, we employed a T cell factor/lymphoid enhancer factor (TCF/LEF) luciferase reporter assay. TCF/LEF transcription factors are recognized as major end-point mediators of WNT signalling across metazoans. In this assay, we observed a robust inhibition of WNT1- and WNT3A-dependent TCF/LEF transcriptional activity (MacDonald et al., 2014) when cells were treated with FHP01 (**Figure 5b**). These results provide additional support to the established efficacy of DDX3X inhibition, emphasizing the capability of FHP01 in downregulating the activation of the WNT pathway. This comprehensive investigation unravels the intricate interplay between FHP01, DDX3X, and the WNT-β-catenin signalling axis, offering valuable insights into the potential therapeutic implications of targeting this regulatory network in the context of WNT-driven malignancies.

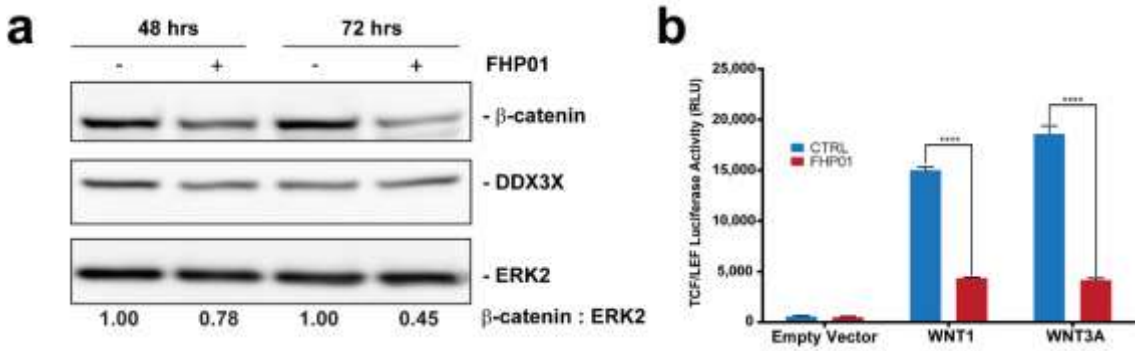

Figure 5. FHP01-Mediated Inhibition of WNT Signaling. (**a**) To elucidate the impact of FHP01 on WNT signaling, MDA-MB-231 cells were subjected to incubation with either the vehicle or the FHP01 DDX3X inhibitor (6μM) for specified durations. Immunoblotting analysis was subsequently performed to assess alterations in β-catenin and DDX3X protein levels. Anti-ERK2 immunoblot served as a normalization control for total lysates protein levels. Representative images from three independent experiments are presented (n = 3). Intensitometric analysis of β-catenin, normalized by ERK2 protein levels, was conducted using NIH ImageJ. (**b**) To further probe the inhibitory effects of FHP01 on WNT signaling, a TCF/LEF luciferase reporter vector was employed after transfection with plasmids encoding the soluble ligands WNT1 and WNT3A. Following 48 hours of treatment with 6μM FHP01, the activation of the TCF/LEF luciferase reporter was quantified in relative light units (RLU). Significantly, statistical analysis revealed a profound inhibition (**** $p < 0.0001$), underscoring the robust impact of FHP01 on WNT signaling activation.

2.4.3. Robust In Vivo Antitumor Efficacy of FHP01 in Triple-Negative Breast Cancer Mouse Model

Considering the promising in vitro implications of DDX3X inhibition in breast cancer, especially in the aggressive TNBC subtype, we engaged an in-depth exploration of FHP01's therapeutic potential in vivo, utilizing a TNBC mouse model. To optimize acute administration, we tested multiple routes—intravenous (i.v.), intraperitoneal (i.p.), and per os (p.o.)—ensuring sufficient drug bioavailability. Addressing concerns from previous studies highlighting inefficiencies of other DDX3X inhibitors due to poor delivery and rapid clearance (Xie et al., 2015) we observed that all tested administration routes achieved substantial plasma concentrations, exerting significant antiproliferative effects on tumour cells in vivo (**Figure 6a**).

While intravenous injection displayed a rapid decline in plasma concentration, both intraperitoneal and per oral administrations exhibited sustained high plasma concentrations resembling the in vitro IC50 for several hours (**Figure 6a**). Notably, impressive levels of FHP01 distribution into the brain at 8 hours after intraperitoneal injection indicated robust bioavailability, even in challenging-to-reach tissues beyond the blood-brain barrier, advocating for intraperitoneal administration in subsequent in vivo experiments. Crucially, FHP01 tissue concentration demonstrated a rapid decline below the quantitation level at 24 hours, mitigating concerns of undesired organ accumulation (**Table 3**).

For in vivo antitumor efficacy assessment, we employed a well-established TNBC preclinical model using athymic nude mice with subcutaneous MDA-MB-231 human cell-derived tumour xenografts. Two weeks post-tumour grafting, animals were randomized into FHP01 treatment (45 mg/kg, i.p., 3 times a week) or control groups. FHP01 treatment significantly suppressed tumour growth compared to controls, with no observed body weight loss or adverse effects (**Figure 6b and 7**).

Post-treatment, histological analysis of liver, spleen, brain, and kidney revealed no treatment-related toxicity after 4 weeks of i.p. FHP01 administration (**Figure 6c**). Remarkably, despite robust biodistribution and significant antitumor effects, no signs of toxicity were observed in vital organs. The analysis of DDX3X and β-catenin expression in tumours reaffirmed FHP01's specific action on DDX3X in vivo, showcasing a substantial reduction in DDX3X and a decreasing tendency in β-catenin levels (**Figure 8**). These findings substantiate the remarkable biocompatibility, good tolerance, and specific antitumor effects of FHP01, laying a robust foundation for potential translational applications in human TNBC therapy.

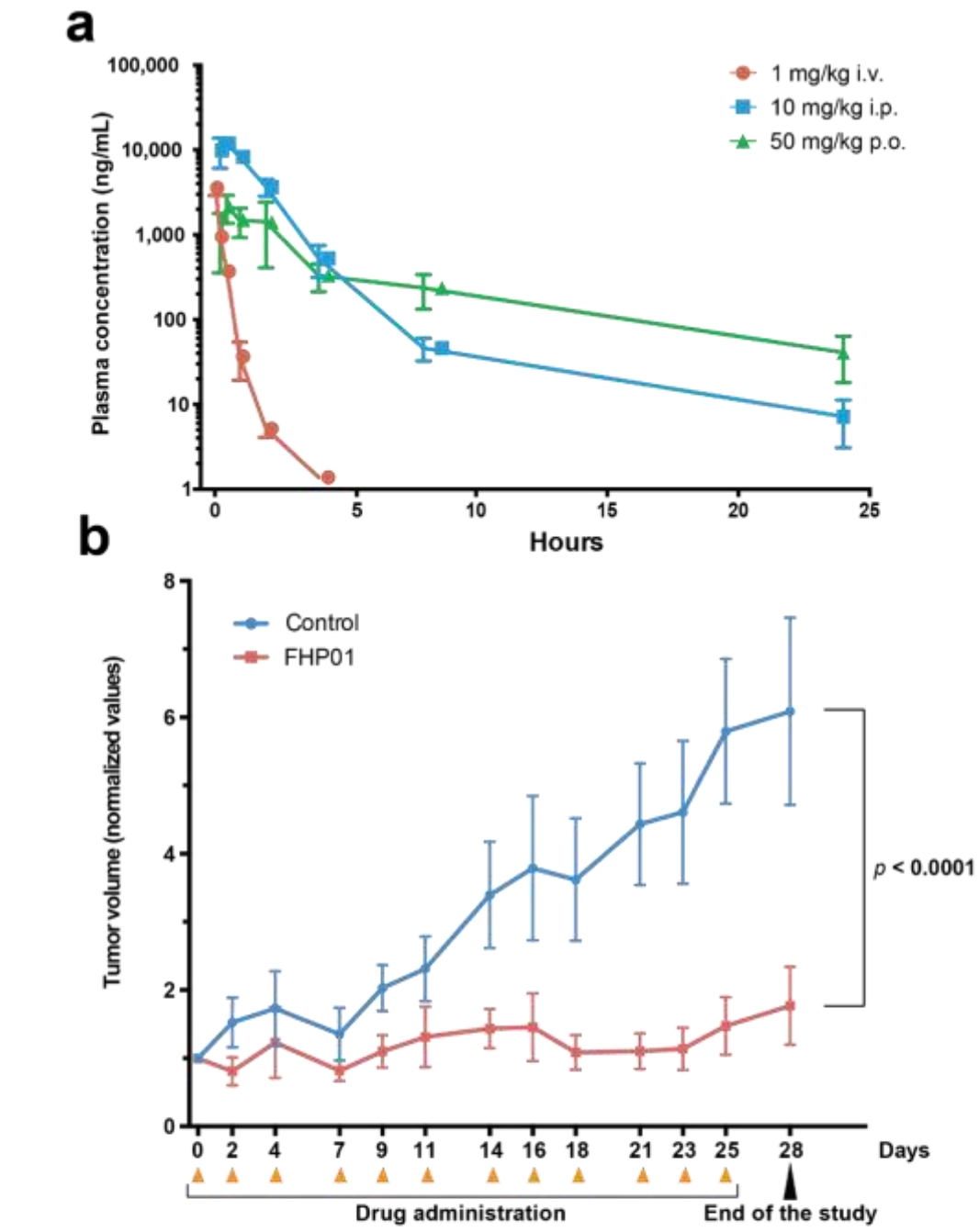
a
100,000
10,000
1,000
100
10
1
Plasma concentration (ng/mL)
1 mg/kg i.v.
10 mg/kg i.p.
50 mg/kg p.o.
0
5
10
15
20
25
Hours
b
8
6
4
2
0
Tumor volume (normalized values)
Control
FHP01
p < 0.0001
0 2 4 7 9 11 14 16 18 21 23 25 28
Days
Drug administration
End of the study
c
Brain
Liver
Kidney
Spleen
Vehicle
FHP01
A
B
C
D
E
F
G
H

Figure 6. Suppression of MDA-MB-231 Tumour Xenograft Growth in Nude Mice through FHP01 Treatment. (**a**) Pharmacokinetic profiling of FHP01 plasma concentrations after intra-venous (i.v.), intra-peritoneal (i.p.) and per os (p.o.) administration. Mean (±SD) plasma concentration vs. time profile of FHP01 following administration at 1.0 mg/kg, 10 mg/kg and 50 mg/kg to Swiss Albino mice. (**b**) Athymic nude mice were bilaterally injected with MDA-MB-231 cells. Upon achieving an average tumour volume of approximately 25.42 ± 2.02 mm3, animals underwent treatment with a 45 mg/kg FHP01 suspension via intraperitoneal injection, administered three times per week for a duration of 4 weeks. The tumour volumes of control (blue, n = 8) and FHP01-treated (red, n = 9) nude mice exhibited a significant divergence, with data normalized to the baseline value of each sample and expressed as mean ± SEM. Statistical comparisons were conducted using two-way RM ANOVA. (**c**) Representative images of histological investigation after 4 weeks, with three injections per week of FHP01 (45 mg/kg) via intraperitoneal route. Qualitative analysis indicated the absence of evident signs of toxicity in the brain (A,B), liver (C,D), kidney (E,F), and spleen (G,H) of both control (A,C,E,G) and treated (B,D,F,H) animals. Scale bars are equivalent to 100 µm. This comprehensive approach provides valuable insights into the response to FHP01 treatment and potential organ-related toxic effects in the context of the experimental model.

Table 3. FHP01 tissue concentration after i.p. administration. Drug levels in the brain and in the liver (expressed in ng/g) were normalized against the levels in plasma, (expressed in ng/mL). BLQ indicates that the ratio was not calculated, as the values were Below the Limits of Quantification in all the tissues.

Time points	Brain / Plasma	Liver / Plasma
4h	0.50 ± 0.24	3.75 ± 1.06
8h	3.14 ± 0.74	6.32 ± 2.23
24h	BLQ	BLQ

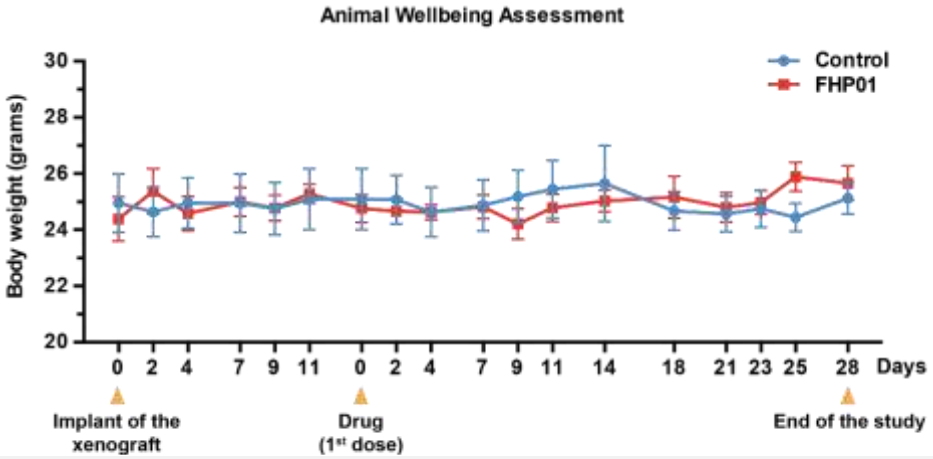

Figure 7. Assessment of animal wellbeing. During the experiment animal weight did not change significantly. Animal were monitored from their arrival and weighted three times per week. No major signs of discomfort were noted in any of the animals to the end of the procedures. One animal from the control group was sacrificed as the tumor was exceeding the volume limit (accordingly with the humane end point score declared in the animal welfare body guidelines) and taken out from the account. Values are expressed as mean ± SEM in grams (Two Way Anova RM).

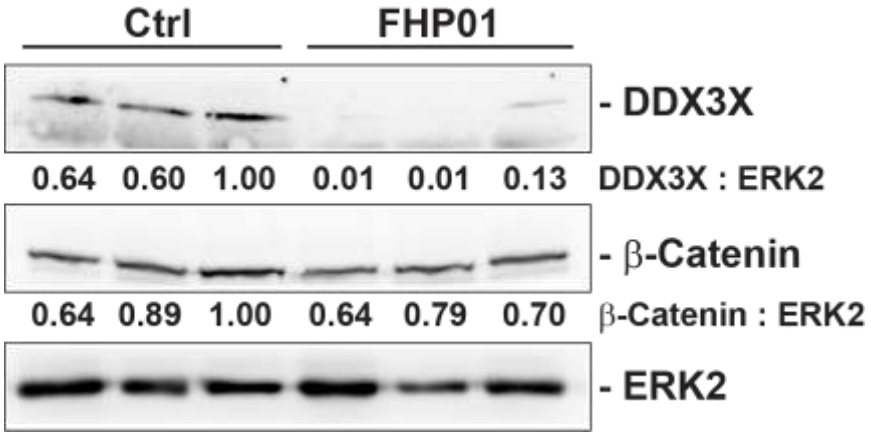

Figure 8. FHP01-Mediated Modulation of DDX3X and WNT signaling in xenograft tumor samples. After 4-week treatment, tumors MDA-MB-231-derived were subsequently harvested, and representative samples were analyzed by Western blotting to evaluate DDX3X and β-catenin protein levels. Anti-ERK2 immunoblot served as a normalization control for total lysates protein levels. Intensitometric analysis, conducted through NIH ImageJ, was performed to evaluate the protein levels of DDX3X and β-catenin, with normalization based on ERK2 protein levels. This analysis unveils the molecular changes induced by FHP01 treatment in tumor tissues, shedding light on its regulatory role in DDX3X and WNT signaling pathways.

2.5. Discussion

In summary, our findings unequivocally establish the potent in vivo anticancer efficacy of the FHP01 compound as a standalone agent in a TNBC tumour model, providing robust support for considering DDX3X helicase inhibitors in breast cancer therapy. However, the multifaceted role of DDX3X, displaying context-dependent pro- or anti-proliferative effects in different cancer types, including breast cancer, necessitates cautious consideration in the development of DDX3X inhibitors for human cancer therapy, as highlighted by varying responses observed in distinct cancer contexts (Mo et al., 2021; He et al., 2018).

Moreover, the identification of DDX3X mutations in certain cancer types, such as medulloblastomas, head and neck squamous cell carcinomas (HNSCC), and haematological malignancies, further complicates the therapeutic landscape. (Heerma van Voss et al., 2017b). Specifically, in medulloblastomas and natural killer/T cell lymphoma (NKTCL), DDX3X stands out as one of the most frequently mutated genes (Jiang et al., 2015; Kool et al., 2014). The effects of these mutations on DDX3X functions remain debated, posing challenges in determining whether inhibition or stimulation of DDX3X activity is essential for targeting these specific tumours (Jiang et al., 2015; Kool et al., 2014; Patmore et al., 2020),

In the pursuit of anticancer and antiviral effects, various DDX3X inhibitors have been identified and studied over the past decade (He et al., 2018; Kukhanova et al., 2020). Targeting the ATPase domain directly or occupying the RNA-binding site are two main mechanisms exploited for inhibition. While ATP-binding site inhibitors demonstrate efficient cytotoxicity in vitro, their single-agent efficacy in vivo is often limited. Current inhibitors predominantly target the ATP-binding site, raising concerns about non-specific binding and potential toxic effects. (He et al., 2018; Kukhanova et al., 2020). Conversely, inhibitors that selectively target the helicase activity of DDX3X offer a more specific approach, with lower toxicity observed in in vivo models (Brai et al., 2016). Consequently, we hypothesized that these types of drugs could represent good candidates to inhibit breast cancer cells' proliferation with a novel targeted approach. Our investigation introduces FHP01 as a novel and selective DDX3X inhibitor, demonstrating significant antiproliferative effects against various human breast cancer cells, particularly TNBC cells. This breakthrough is crucial for TNBC, characterized by unfavourable outcomes and a pressing need for new therapeutic targets (Holliday & Speirs, 2011). Remarkably, our in vivo studies with FHP01 as a single agent in TNBC mouse models exhibit exceptional efficacy coupled with low toxicity, underscoring the considerable potential of this class of molecules as a more effective therapeutic strategy for combating this highly aggressive form of cancer. This evidence

positions FHP01 and related compounds as promising candidates for advancing breast cancer treatment, opening avenues for further exploration and development in the pursuit of improved therapeutic outcomes.

2.6. Conclusions

In the current landscape of personalized medicine, the request of novel molecular targets remains crucial for advancing therapeutic strategies. Among these, DDX3X emerges as a promising candidate, showcasing significant potential for targeted pharmacological interventions in breast cancer due to its pro-tumorigenic role. This study unveils FHP01 as a fascinating agent, demonstrating remarkable antiproliferative and cytotoxic efficacy across diverse breast cancer cell types. Moreover, its robust inhibitory impact on tumour growth in xenograft models substantiates the notion that targeted suppression of DDX3X helicase activity holds substantial promise for breast cancer patients. Collectively, these findings not only underscore the therapeutic potential of FHP01 but also suggest its potential positive impact on the prognosis of this complex disease. This not only reinforces the potential clinical utility of FHP01 but also underscores the importance of exploring more selective DDX3X inhibitors for breast cancer treatment.

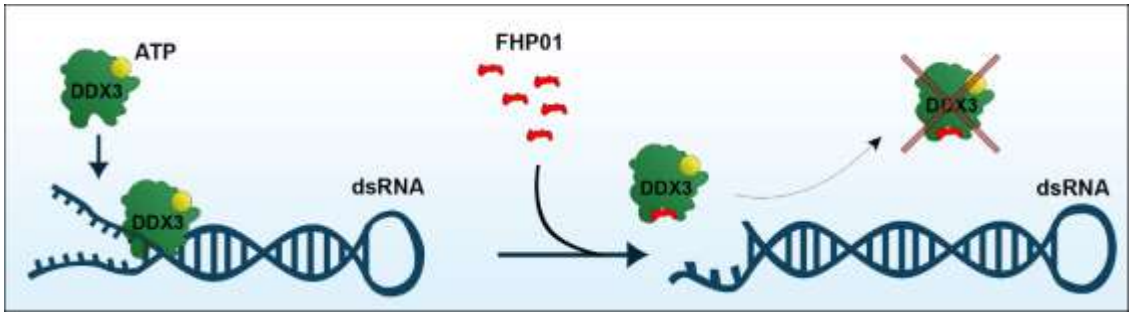

FHP01, the DDX3 inhibitor, is exclusively licensed to First Health Pharmaceuticals B.V. (FHPBV), who supplied it for the conducted studies.

This work is published in the peer-reviewed journal *"Cancers"*, into the Special Issue *"Novel Personalized Therapeutic Strategies for Breast Cancer"* **DOI:** 10.3390/cancers13194830.

3. Altered lipid metabolism in a MAPK15 knockout mouse model.

3.1. Abstract

Non-alcoholic fatty liver disease is the most common cause of chronic liver disease worldwide. NAFLD stages range from simple steatosis to non-alcoholic steatohepatitis which can progress to cirrhosis and hepatocellular carcinoma. One of the crucial events involved in NAFLD progression is the excessive accumulation of fatty acids inside the hepatocytes. CD36 is a membrane glycoprotein involved in regulating the uptake of fatty acids across the plasma membrane. Fatty acids uptake into the cell may be regulated by altering the expression of CD36, or by relocating this protein to the plasma membrane. Here, I report preliminary data correlating the expression of the atypical MAP kinase family member MAPK15 to hepatic steatosis. Specifically, our data suggest that MAPK15 controls CD36 expression and membrane localization *in vitro* and *in vivo* and reduced/absent expression of this MAP kinase in mammalian cells increases accumulation of lipids and leads mice to hepatic steatosis, accumulation of adipose tissue and insulin resistance.

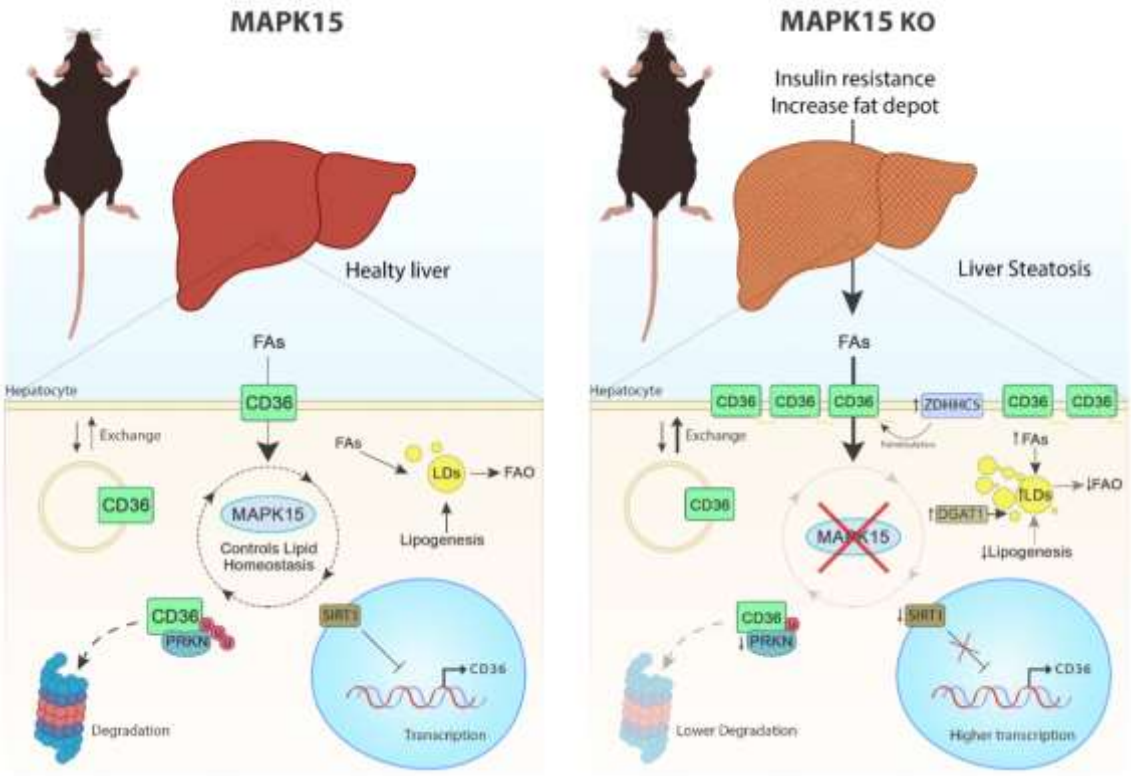

Graphical Abstract

3.2. Introduction

3.2.1. Non-alcoholic fatty liver disease

Non-alcoholic fatty liver disease (NAFLD) has become the most common liver diseases worldwide (Younossi et al., 2016) and is a leading cause of cirrhosis and hepatocellular carcinoma (Wong et al., 2014). NAFLD is a spectrum of liver conditions associated with the increasing prevalence of obesity and other disfunctions such as the metabolic syndrome and type 2 diabetes mellitus (Sheka et al., 2020; Powell et al., 2021; Ding et al., 2017). The main characteristics for defining NAFLD can be summarized in the evidence of hepatic steatosis, which is due to accumulation of triglyceride (TG) in hepatocytes, and in the absence of secondary causes of fatty liver, such as excessive alcohol consumption, use of a steatogenic drugs, or inborn errors of metabolism (Chalasani et al., 2018). Non-alcoholic steatohepatitis (NASH) is the inflammatory subtype of NAFLD, which is characterized by ≥5% hepatic steatosis and inflammation with hepatocyte "ballooning", with or without fibrosis. The progression of NASH is associated with cirrhosis and frequent development of hepatocellular carcinoma (Sheka et al., 2020; Chalasani et al., 2018; Stine et al., 2018). NASH is set to become a leading cause for hepatocellular carcinoma, indeed preliminary data from preclinical studies suggest that the efficacy of the therapies may be lower in hepatocellular carcinoma caused by NASH as compared to viral-related hepatocellular carcinoma (Pinter et al., 2023).

Obesity is an important cofactor for NAFLD/NASH as excess intake of calories causes the growth of subcutaneous adipose depots and, subsequentially, visceral ectopic fat increase. (Britton & Fox, 2011). In these conditions, there is the formation of proinflammatory compartments, due to macrophages infiltration, promoting insulin resistance (Lefere & Tacke, 2019). This, in turn, results in accumulation of fatty acids (FAs) into the liver and increased de-novo lipogenesis, overloading the hepatic homeostasis. The lipid imbalance leads to the formation of lipotoxic lipids species, generating reactive oxygen species (ROS) and oxidative stress, further increasing inflammation and fibrogenesis, ultimately leading to liver degeneration and fibrosis (**Figure1**) (Friedman et al., 2018; Sanyal, 2019).

Although consistent progresses have been made during the past 40 years regarding the natural history of these disease, the complexity of molecular processes behind its pathogenesis has not been untangled yet, and additional research is therefore necessary in order to identify new targets, to improve patient outcomes and biomarkers for earlier diagnosis and more efficacious targeted therapies.

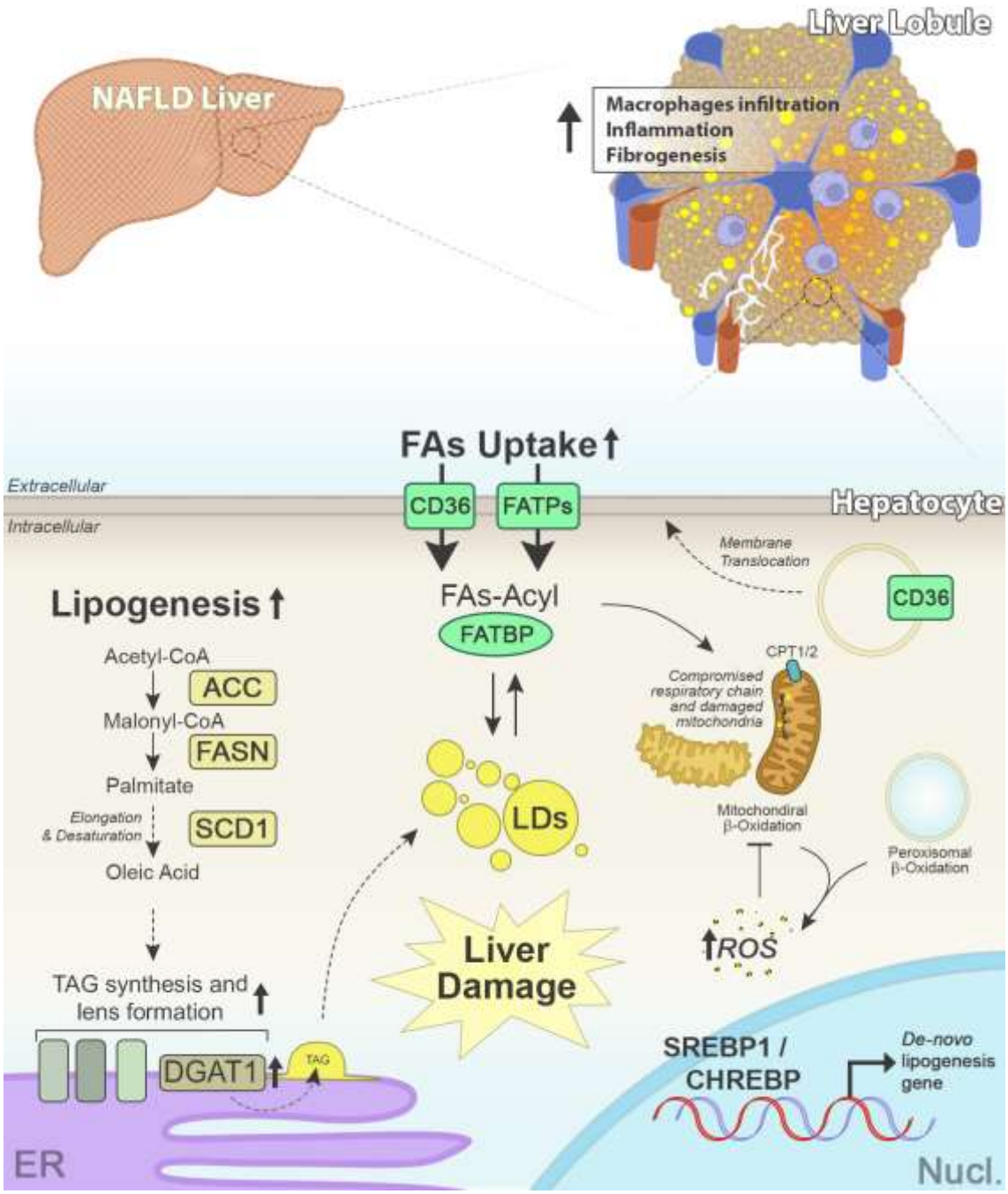

Figure 1. Resume of hepatic lipid metabolism in NAFLD. FATPs mediates increased uptake of circulating lipids in NAFLD. Enhanced de novo lipogenesis is a key feature of NAFLD, contributing significantly to the accumulation of LDs. Although data related to the regulation of FAO are conflicting, mitochondrial dysfunction is an important feature of NAFLD resulting in increased generation of ROS and peroxisome-mediated oxidation. This further promotes oxidative stress, inducing damage to mitochondrial membranes, compromising cellular respiration and metabolism, and impairing liver function by direct and indirect cellular damage. The result is an escalating vicious circle, driven by chronic dyslipidaemia and hepatic lipid overload, leading to impaired liver metabolism and inflammation with macrophages infiltration, ultimately promoting irreversible liver damage, and fibrogenesis. (Yoon et al., 2021)

3.2.2. Lipid metabolism

Lipid metabolism is in a constant state of dynamic equilibrium through food intake, de-novo lipogenesis, release from adipose tissue, and the consumption of lipids to satisfy the needs of the body (such as energy production, signalling, vesicles, etc) (Patel, 2018). Disruption of the contributions of any of these pathways to lipid homeostasis such as increased FAs uptake, enhanced de-novo lipogenesis, or reduced FAs β-oxidation (FAO), are frequent primary causes of excessive storage of these lipids and important human diseases (Ding et al., 2017).

While short chain FAs spread through cell membrane, long chain and very long chain fatty acids need specific transporters. Fatty acid transport proteins (FATPs) are a family of six integral transmembrane proteins that enhance the uptake of FAs into cells, (Houten & Wanders, 2010). FATPs have enzymatic activity and FAs are rapidly converted to acyl-CoAs after translocation across the plasma membrane (Gimeno et al., 2003). Besides FATPs, other transporter plasma membrane fatty acid-binding protein (FABP), and fatty acid translocase (FAT, CD36) are involved in the uptake of fatty acids (Houten & Wanders, 2010).

The primary pathway for the degradation of fatty acids occurs through the mitochondrial FAO, a key metabolic pathway for energy homoeostasis in organs such as the liver, heart, and skeletal muscle (Bartlett & Eaton, 2004). Under starving condition, most tissues, except the brain, can use FAs directly to generate energy (Houten & Wanders, 2010).

While FAs greater than 22 carbons (very long chain fatty acids - VLCFAs) cannot be translocated inside the mitochondria and are metabolized in the peroxisomes (Patel, 2018), long chain FAs (LCFAs) need specific transporters to pass from cytosol to mitochondrial matrix, i.e. Carnitine palmitoyltransferase CPT1 and CPT2, which are localized on the outer and inner mitochondrial membranes respectively (Longo et al., 2016). Specifically, CPT1 perform the first step in the transport, catalysing the binding of a carnitine to acyl-CoAs, and producing acylcarnitine. There are two isoforms of CPT1: the CPT1a isoform is expressed in liver, brain, kidney, lung, and spleen. Conversely, CPT1b is the muscle isoform but is expressed also in testis. Once the acylcarnitine pass through the mitochondrial outer membrane, CPT2, located at the mitochondrial inner membrane, reconverts the acylcarnitines into their CoA esters, which can undergo FAO (Houten & Wanders, 2010; Bartlett & Eaton, 2004; Longo et al., 2016).

FAO is characterized by several enzymatic reactions that, through FAs chain shortening, produce acetyl-CoA. The acetyl-CoA, produced by mitochondrial FAO, has different fates, depending on the tissue and on the energy homeostasis of the organism: e.g., in liver, the acetyl-CoA is used to form ketone bodies, that serve, depending on body energy status, as an additional energy source mostly exported to other tissues, while acetyl-CoA in other tissue such as the

heart and the skeletal muscle, enters the Krebs cycle and is used for ATP synthesis and protein acetylation (Bartlett & Eaton, 2004; Szrok-Jurga et al., 2023a).

Also in this case, alterations of these mechanisms resulting in a reduction of cellular FAO can cause several specific disorders (FAODs) (Guerra et al., 2022), which are able to cause accumulation of FAs and their carnitine derivatives inside the cells, ultimately causing dangerous metabolic diseases (Sheka et al., 2020; Szrok-Jurga et al., 2023b).

Excess dietary intake of carbohydrate and amino acids can be converted in triacylglycerol by a process known as lipogenesis (Voet et al., 2006). In mammalians, FAs synthesis occurs mainly in the liver and adipose tissue, as well as into the mammary glands during lactation (Voet et al., 2006). The two lipogenic master regulators are Sterol Regulatory Element Binding Transcription Factor 1 (SREBP-1c) and Carbohydrate Response Element Binding Protein (ChREBP – also known as MLX Interacting Protein Like) (Postic & Girard, 2008; Strable & Ntambi, 2010). Upon activation, SREBP-1c binds DNA and activate lipogenesis by activating the promoters of different lipogenic genes, such as Acetyl-CoA Carboxylase 1 (ACC1), fatty acid synthase (FASN), Stearoyl-CoA Desaturase-1 (SCD1) (Ponugoti et al., 2010). The acetyl CoA, obtained from the breakdown of both carbohydrates (by glycolysis) and lipids (by β-oxidation) (Wilson & Walker, 2006), is first converted to malonyl-CoA by ACC, then elongated from FASN to generate palmitic acid which can be loaded into the mitochondria to undergo FAO or further used by Elongase to produce longer FAs which can be stored in lipid droplets (LDs) (Patel, 2018). Subsequent desaturation of palmitic acid by SCD1 produces the monounsaturated FAs (MUFA) oleic acid (Koundouros & Poulogiannis, 2020).

ChREBP is another key transcription factor involved in de-novo lipogenesis and acts synergistically with SREBP-1c (Ding et al., 2017). In the nucleus, ChREBP association with Max-Like protein (MLX) binds to the carbohydrate response element, regulating glycolytic genes (e.g. liver pyruvate kinase - LPK) and lipogenic genes (such as ACC1, FASN and SCD1) (Ding et al., 2017).

Diacylglycerol O-acyltransferase 1 (DGAT1) and DGAT2 are enzymes that catalyse the last step in cellular triglycerides (TG) synthesis by using diacylglycerol and fatty acyl-CoA as substrates (Chen & Farese, 2005a). TG synthesized by TG synthesis chain are then also stored through DGAT in cytosolic LDs, and these reactions take place primarily in the endoplasmic reticulum (Chen & Farese, 2005a). Interestingly, a specific role for DGAT1 in esterification of exogenous fatty acids has been reported, involving this enzyme in the development of steatosis due to exogenous FAs (but not endogenous FA synthesis), as demonstrated by DGAT1-dependent worsening of liver steatosis in mice undergoing high-fat diet (Villanueva et al.,

2009a). Indeed, DGAT1 expression is increased in humans with NAFLD obesity and hepatic steatosis (Kohjima et al., 2007; Villanueva et al., 2009b).

LDs are the organelles used by cells to store neutral lipids in most organisms, from yeast to mammals (Olzmann & Carvalho, 2019). The number, size and FAs composition of LDs differ reflecting the metabolic states of the cells. Despite their heterogenicity, LDs have in common the characteristic of being surrounded by a phospholipid and protein monolayer that have their polar head groups oriented towards the cytosol whereas their acyl chains contact the hydrophobic neutral lipid core mostly composed of triacylglycerol and sterol esters (Tauchi-Sato et al., 2002). LDs are formed from the membrane of endoplasmic reticulum (ER) and originates from the expansion of the neutral lipid lens between the double layer membrane of ER, resulting in lipid droplet budding (Olzmann & Carvalho, 2019). Next, LDs expand in three ways: a) droplet–droplet fusion, b) through transfer of triacylglycerol to LDs via ER membrane or, c) through triacylglycerol synthesis directly on the lipid droplet surface. (Olzmann & Carvalho, 2019). A recent study observed nutrient-regulated LDs binding with regions of ER, Golgi, mitochondria, lysosomes and peroxisomes, regions in which organelles exchange lipids, metabolites, and ions. (Prinz, 2014). During periods of starvation or cell proliferation/growth, which requires phospholipid for membrane expansion, FAs are mobilized from LDs either by lipolysis or by lipophagy (Olzmann & Carvalho, 2019). Another role of LDs is in the protection against lipotoxicity by sequestering FAs, (Greenberg et al., 2011; Krahmer et al., 2013a) because of their nature that can directly disrupt membrane integrity or can form cytotoxic lipid species (such as ceramide, acylcarnitine and diacylglycerol) (Greenberg & Coleman…, 2011). Accordingly, when FAs storage in LDs is impaired or the storage capacity of LDs is at full capacity, this can result in diseases related to lipotoxicity, such as type 2 diabetes and NAFLD (Greenberg & Coleman…, 2011; Krahmer et al., 2013b).

In summary, excessive FAs accumulation in in LDs, as a result of excessive dietary intake, altered FAO or enhanced uptake, and biosynthesis, when occurring chronically may result in liver steatosis and obesity (Ding et al., 2017).

Among the mammalian sirtuins, Sirtuin 1 (SIRT 1) is a NAD+ dependent deacetylase that plays several roles in regulating hepatic homeostasis by deacetylating different transcriptional regulators, ultimately opposing the progression of both non-alcoholic and alcoholic fatty liver diseases (Chaudhary & Pfluger, 2009; Nassir & Ibdah, 2016; Xu et al., 2010a). Studies also already revealed that SIRT1-mediated deacetylation of SREBP-1 down-regulates its transcriptional activity and promotes its instability by increasing its ubiquitination and proteasomal degradation, ultimately resulting in decreased lipogenesis (Ponugoti et al., 2010).

Increased ChREBP acetylation, which upregulates its transcriptional activity, is also associated to hepatic steatosis and increased expression of target lipogenic genes (Ding et al., 2017). These data suggest an important role for SIRT1 in controlling lipid metabolism and its associated human diseases, as also supported by data showing low SIRT1 expression in livers of NAFLD mice model, and a protective function of its overexpression from developing NAFLD in this model (Colak et al., 2014; Colak et al., 2011). Accordingly, liver steatosis was observed in liver specific SIRT1 knockout mice, which exhibited increased ChREBP expression (Wang et al., 2010).

SIRT1 also deacetylates the co-activator Peroxisome Proliferator-Activated Receptor Gamma Coactivator 1-Alpha (PGC-1α), thereby enhancing FAO by increasing Peroxisome Proliferator Activated Receptor Alpha (PPARα) transcriptional activity in liver (Ding et al., 2017). Indeed, liver specific knockout of SIRT1 impairs PPARα activity, resulting in impaired FAO and development of hepatic steatosis and inflammation in mice (Purushotham et al., 2009). Accordingly, SIRT1 overexpression increases FAO ameliorating high fat induced hepatic steatosis (Purushotham et al., 2009). Growing evidence links inflammation to liver injury and the rising of hepatic steatosis to NASH, which is characterized by presence of macrophages infiltration and high levels of pro-inflammatory cytokines (Ding et al., 2017). More evidence links SIRT1 to negative regulation of inflammation associated to fatty liver diseases, mainly through deacetylation of nuclear factor kappa B (NF-κB) which inhibits its transcriptional activity (Ding et al., 2017). Importantly, SIRT1 upregulation has been also reported to attenuate the high fat diet (HFD)-induced liver injury through inhibition of NF-κB and fatty acid translocase (CD36/FAT) (Niu et al., 2018). Indeed, it is reported that liver-specific knockout of SIRT1 could significantly increase liver inflammation and macrophage infiltration (Ding et al., 2017; Niu et al., 2018).

3.2.3. Mitogen Activated Protein Kinase 15 (MAPK15)

The mitogen activated protein kinase 15 (MAPK15; also known as ERK8 or ERK7) protein, is an atypical MAP kinase (Deniz et al., 2023) implicated in several cellular processes, such as cell proliferation (Iavarone et al., 2006; Xu et al., 2010b; Colecchia et al., 2015; Jin et al., 2015; Rossi et al., 2016), genomic integrity (Groehler & Lannigan, 2010; Cerone et al., 2011; Rossi et al., 2016), secretion (Zacharogianni et al., 2011; Hasygar & Hietakangas, 2014), autophagy and mitophagy (Colecchia et al., 2012a; Colecchia et al., 2015; Zhang et al., 2021; Franci et al., 2022), oxidative stress, ageing and cellular senescence (Franci et al., 2022) (**Figure 2**).

MAPK15, through genome-wide association studies, has been already associated to obesity (Li et al., 2012) (https://www.ebi.ac.uk/gwas/genes/MAPK15). However, the role of MAPK15 in

lipid metabolism in mammalian has not been addressed. A recent study suggests an involvement of MAPK15 in controlling nutrient homeostasis and lipid storage, ultimately promoting survival on fasting conditions in Drosophila larvae (Hasygar et al., 2021). Specifically, Hasygar and colleagues showed that MAPK15 depletion promotes lipid storage and adiposity because of its control on chromatin binding protein PWP1 and transcription factor Sugarbabe in the Drosophila fat body (a liver- and adipose-like tissue that stores fat and serves as a detoxifying and immune responsive organ) (Hasygar et al., 2021; Musselman et al., 2013). Among these processes, it is important to understand how MAPK15 is involved in lipid homeostasis in mammals and its potential role in NAFLD.

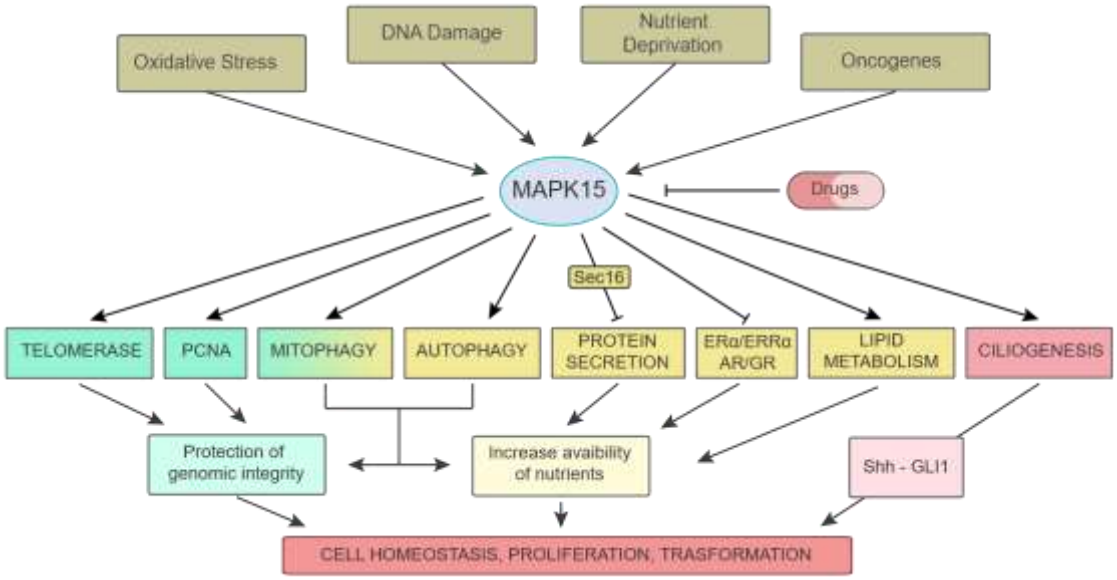

Figure 2. Resume of MAPK15 role in cellular function

3.2.5. CD36

CD36, is an intramembrane multifunctional glycoprotein, that act as a scavenger receptor for a wide range of both protein (such as fibronectin, collagen, etc.) and lipid ligands [such as oxidized low-density lipoprotein (oxLDL), long-chain fatty acids, etc.], inducing activation of intracellular signalling and internalization of the receptor-ligand complexes (Hames et al., 2014). Indeed, it is now well established that, despite having very short intracytoplasmic domains, CD36 can serve as a signalling molecule through the activation of the Src-family non-receptor protein tyrosine kinases Fyn, Lyn, and Yes (Huang et al., 1991; Githaka et al., 2016; Thorne et al., 2006) and consequent activation of mitogen-activated protein (MAP) kinases such as p38 kinases (Jiménez et al., 2000) and the c-JUN N-terminal kinase (JNK) pathway, ultimately enhancing inflammatory paracrine loop between adipocytes and macrophages (Kennedy et al., 2011). CD36

is also involved in FA metabolism, which induces the activation of monophosphate-activated protein kinase (AMPK) through differential association with Fyn-LKB1 pathway (Samovski et al., 2015). Specifically, FA-induced activation of CD36 ultimately results in AMPK activation, which enhances FAO, contributing to maintain FA homeostasis (Samovski et al., 2015).

Palmitoylation is a posttranslational modification that bind a palmitate to a cysteine residue of different proteins, ultimately favouring specific membrane localization (Rocks et al., 2010). Interestingly, Wang et al. reported that CD36 palmitoylation is mediated by ZDHHC4 and ZDHHC5 and is required to localize it on plasma membrane, overall promoting FA uptake (Wang et al., 2019). Indeed, recent studies have reported increased localization of CD36 in hepatocyte plasma membranes in patients with NASH, compared to healthy liver controls. Moreover, increased palmitoylation of CD36 was observed in NASH mice model while inhibition of CD36 palmitoylation was able to protect mice from developing this condition (Zhao et al., 2018). All these findings make CD36 a promising molecular target to affect pathogenesis and possibly treat NASH.

3.2.4. PARKIN (PRKN)

The Parkin gene encodes a 465 amino acid protein functioning as an E3 ubiquitin ligase and, together with E1-activating and E2-conjuganting enzymes, catalysing the binding of a ubiquitin's glycine residue to a lysine residue of a target proteins. While, usually, K48-linked poly-ubiquitin chains are related to a signal of proteasomal degradation, PRKN can also mediate mono-ubiquitination of proteins (Moore, 2006; Moore et al., 2008).

Interestingly, Parkin has been also reported to control lipid uptake through CD36, by increasing CD36 localization to the plasma membrane in basal condition, due to mono-ubiquitination which increases stabilization of the protein (Kim et al., 2011). Indeed, while WT mice, upon high fat diet treatment, showed lipid accumulation into the liver and insulin resistance, accompanied by increased protein levels of CD36 and Parkin, Parkin-deficient (KO) mice were more resistant to these metabolic changes (Kim et al., 2011). Moreover, rescued Parkin expression restored CD36 level and lipid accumulation (Kim et al., 2011). Accordingly, immunoprecipitation experiments suggested an interaction of Parkin and CD36 (Abumrad & Moore, 2011) allowing to propose a model of CD36 stabilization in the plasma membrane through PRKN-medited monoubiquitination, while during FAs stimuli exposition, PRKN promote CD36 polyubiquitination and proteasomal degradation (Kim et al., 2011; Abumrad & Moore, 2011).

3.2.6. AIM

Here, we decided to study the involvement of MAPK15 in NAFLD, both *in vivo* MAPK15 KO mice model and *in vitro*. Specifically, we want to characterize a role for MAPK15 in lipid metabolism, particularly at the level of the liver, and potential roles for this MAP kinase in obesity and NAFLD. This will possibly allow to use its levels for early diagnosis or as a marker of risk in developing liver steatosis. Indeed, based on the evidence of an overweight phenotype in MAPK15 KO mice and of an increased accumulation of lipids in liver cells, we decided to investigate the role of MAPK15 in the principal pathways of lipid metabolism: Lipid Uptake, Lipid Biosynthesis and Lipid Oxidation.

3.3. Materials and Methods

3.3.1. Cell Culture

All Cells were purchased from ATCC and were cultured in the adequate medium at 37 °C in an atmosphere of 5% CO2/air. Specifically, HEPG2 cells were maintained in Earle's Salts Modified Eagle's Medium (EMEM - Euroclone S.p.A. ECB3054D), supplemented with 10% heat-inactivated fetal bovine serum (FBS - Euroclone S.p.A. ECS0180L), 2 mM L-glutamine (Euroclone S.p.A. ECB3000D), 1x Non-Essential Amino Acids (Sigma-Aldrich M7145-100ml), 1 mM sodium pyruvate (Euroclone S.p.A. ECM0542D).

3.3.2. Reagents and antibodies

Lipofectamine® RNAiMAX (Life Technologies, Invitrogen, #13778075) reagent was used specifically for the delivery of siRNA.

The following primary antibodies were used for western blots, confocal microscopy and immunohistochemistry experiments: anti-MAPK15 (Invitrogen, PA5-75930), anti-HA (Covance, MMS-101R) anti-MAPK1 (Santa Cruz Biotechnology, sc-154), anti-CD36 (Novus, NB400-144), Anti DGAT1 (Santa Cruz Biotechnology, sc-271934). anti-FAS (Cell Signalling Technology, 4233), anti-CPT (Cell Signalling Technology, 12252), anti-SCD1 (Cell Signalling Technology, 2794),

The following secondary antibodies were used for western blot experiments: Goat Anti-Mouse IgG HRP- Conjugate (Jackson ImmunoResearch Europe Ltd, #115-036-003) and Goat Anti-Rabbit IgG HRP- Conjugate (Jackson ImmunoResearch Europe Ltd, #111-036-003).

3.3.3. Western blots

Cells were washed with cold PBS and total protein extracts obtained by adding RIPA buffer (50 mM Tris-HCl pH 8.0, 150 mM NaCl, 0.5% Sodium deoxycholate, 0.1% SDS, 1% NP-40, 2 mM Orthovanadate, 2mM Sodium fluoride, 1mM Dithiothreitol and 1× protease inhibitors). Following mechanical detachment using cell scrapers, total lysates were gathered in tubes, subjected to vortexing, and then incubated for 15 minutes on ice. Liver from mice were collected and total lysates were obtained as described before (Gherardini et al., 2021) briefly 50mg of each sample were disrupted by bead homogenization in Lysing Matrix D tubes using a FastPrep-24 5G homogenizer (MP Biomedicals, Solon, OH, USA) filled with 500ul of RIPA Lysis buffer (1:10 - w:v). Next, samples were centrifuged for 10 min at 16,000 g, and supernatants were collected, representing total cell lysates.

Total proteins were quantified by Bradford assay. Laemmli Loading Buffer 5X (250 mM Tris-HCl pH 6.8, 10% SDS, 50% glycerol, bromophenol blue) was added to the same amount of protein samples was at final concentration of 1X, which were then heated for 5 min at 95°C. Lysates were loaded 8% acrylamides gel and resolved by SDS-PAGE, transferred to Immobilon-P PVDF membrane (Millipore, IPVH00010), probed with the indicated primary antibody overnight, and revealed by enhanced chemiluminescence detection (ECL Plus; GE Healthcare, RPN2132). Densitometric analysis of western blots was performed with NIH Image J (National Institutes of Health).

3.3.4. LDs and CD36 quantification

1×10^4 cells were seeded in 12-well cell culture plates and transfected with each siRNA as described. Next, cells were washed with PBS, fixed 4% PFA for 20 min, permeabilized with 1X Digitonin solution for 20 min and then blocked for 30 min with 1% BSA in PBS. Cells were then incubated with appropriate primary antibodies for 30 min, washed three times with PBS, and then incubated with Alexa Fluor 488-conjugated (Invitrogen, A21202) secondary antibodies. LDs were stained using 3.6 µM of BODIPY 493/503 (Cayman Chemical, #25892). Nuclei were stained with 6 µM 4',6-diamidino-2-phenylindole (DAPI) in PBS for 10 min. Coverslips were mounted in fluorescence mounting medium (Dako, S3023) and stored at 4°C. After 24 h samples were visualized on a TSC SP5 confocal microscope (Leica, 5100000750) installed on an inverted LEICA DMI 6000CS (10741320) microscope using an oil immersion PlanApo 40× 1.25 NA. Images were acquired using the LAS AF acquisition software (Leica) and quantitation were performed through unbiased analysis using the Quantitation Module of Volocity software (PerkinElmer Life Science).

Were indicated samples were acquired on a FACS Canto II flow cytometer (BD Biosciences). Data were analysed with FlowJo software. All analyses were performed in triplicate.

3.3.5. Cell Knock-down of endogenous MAPK15

MAPK15-specific siRNA (5'-TTGCTTGGAGGCTACTCCCAA-3') and control non-silencing siRNA (Scramble, 5'-AATTCTCCGAACGTGTCACGT-3') were obtained from Qiagen. All siRNAs were transfected at a final concentration of 50 nM using Lipofectamine® RNAiMAX for HepG2 cells as manufacturer protocols. Samples were collected 72 hrs after transfection.

3.3.6. Samples preparation, LC-MS/MS and bioinformatics analysis

Cell lysis was conducted using RIPA buffer, followed by reduction with Dithiothreitol (DTT) (Merck Group) and subsequent alkylation with iodoacetamide (IAA) (Merck Group). To the cell lysates, 8 M urea (UA) was introduced. Protein quantification was performed using the BCA assay, following the manufacturer's instructions. Approximately 30–70 µg of extracted proteins were processed, with trypsin being added and incubated overnight at 37°C.

Proteomics analyses were conducted through a large-scale, high-throughput format using Liquid Chromatography Tandem Mass Spectrometry (LC-MS/MS) with a Q-Exactive HF-X mass spectrometer coupled with a Nano UPLC RLSC Ultimate 3000 (Thermo Scientific), in triplicate for each sample. Peptide separation was carried out at 37°C on a PepMap RSLC C18 column (75 µm × 15 mm, 2 µm, 100 Å, Thermo Scientific) at a flow rate of 0.300 µl/min. The mobile phases A and B were 0.1% formic acid in water and 0.1% formic acid in 80% acetonitrile and 20% water, respectively. The gradient initiated with 5% of B and increased to 90% over 106 min. Employing Data Dependent Analysis (DDA), the "top twelve" most-abundant ions were selected for MS/MS analysis. Protein identification utilized Proteome Discoverer 2.5 (Thermo Scientific) and the Sequest algorithm. To assess technical triplicate reproducibility, mass spectrometry measurements underwent quality control filtering. Label-Free Quantification (LFQ) intensity calculations were performed for each triplicate, considering only proteins derived from the common overlap. All analyses were conducted with a False Discovery Rate (FDR) < 0.001.

Proteome Discoverer 2.5 analysis provided LFQ intensities of proteins, which were imported and logarithmically transformed with a base of two. Moreover, volcano plots were used to show a summary distribution of differentially expressed proteins between samples. The volcano plot is an easy-to-interpret scatter plot that arranges values along dimensions of biological and statistical ($\log_{10}$ p-value) significance. The proteins located on the upper left region and the upper right region with False discovery rate (FDR<0.01) are differentially expressed.

3.3.7. Analysis of gene expression

Total RNA was purified using QIAzol LysisReagent (Qiagen). Reverse transcription was performed with the QuantiTect Reverse Transcription Kit (Qiagen). Total DNA was purified using QIAamp DNA Mini Kit and loaded 10 ng of purified DNA on each RT-PCR reaction. RT-PCR was performed with Luna Universal qPCR Master Mix on a Rotor-Gene 6000 RT-PCR system (Corbett Life Science). The following primer pairs were used:

RT-qPCR primers list		
Human Gene		**Sequence (5'-3')**
MAPK15	Fwd	TGGCCAGCGTACAACAGGT
	Rev	CAGTCCCGTAGGCTTGGGAGTA
CPT1a	Fwd	GCAGCGTTCTTTGTGACGTT
	Rev	AGGAGTGTTCAGCGTTGAGG
DGAT1	Fwd	ACTACCGTGGCATCCTGAAC
	Rev	TGCAGCCACAGCAAAGACAT
SCD1	Fwd	CAGAGGAGGTACTACAAACC
	Rev	ATAAGGACGATATCCGAAGAG
FASN	Fwd	AGCTGCCAGAGTCGGAGAAC
	Rev	TGTAGCCCACGAGTGTCTCG
CD36	Fwd	CATTGGTGATGAGAAGGCAAAC
	Rev	CACCACACCAACACTGAGTAA
Actin	Fwd	TGCGTGACATTAAGGAGAAG
	Rev	GCTCGTAGCTCTTCTCCA

Mouse Gene		**Sequence (5'-3')**
ERK7	Fwd	5'-GCC CGG ACG CAA TCG CTC AA
	Rev	5'-GGG CTA CGC GGA GGT TTG GG
HPRT	Fwd	AGAATGTCTTGATTGTGGGAAGA
	Rev	ACCTTGACCATCTTTGGATTA
CD36	Fwd	GGAGTGGTGATGTTTGTTGCTT
	Rev	ACACACCACCATTTCTTCTCCTA

3.3.8. Statistical Analysis

Significance (p-value) was assessed, where indicated, by either pairwise Student's t-test, general linear mixed model, Two-way ANOVA, Mann-Whitney test, Kruskal-Wallis test using GraphPad Prism8 software. Asterisks were attributed as follows: *$p < 0.05$, **$p < 0.01$, ***$p < 0.001$.

3.3.9. Compliance with Ethical Standards

All experimental procedures complied with the European Communities Council directives (2010/63/EU) and national regulations (D.L. 26/2014) and were performed in accordance with National Institutes of Health (NIH) recommendations. The present study was approved by the Animal Welfare Board (AWB) of the Fondazione Toscana Life Sciences (FTLS) and by the Italian Ministry of Health (authorization number 175/2021-03-03 and 175/2023-02-17).

3.3.10. Study Design and Animals

Animal experiments adhered to the current Italian legislation, and the animal protocol underwent review and approval by the Italian Ministero Della Salute. Wild Type mice, C57BL/6J, were purchased from Jackson Laboratories (Bar Harbor, ME) via Charles River (Calco, LC, Italy),

MAPK15 KO mice were purchased from Taconic Biosciences, Inc. with a statement of non-suffering phenotype. At 7 weeks of age and were housed in 4 mice per cage under standard conditions (12-hour light cycle, ambient temperature of 20-23°C) and free access to food and water. After 7 days of acclimation, the animals were marked for identification. Body weight and food consumption were monitored 2–3 times per week, over a 16-week period; mice were weighted to the nearest 0.1 gram using an electronic balance, immediately after food was replenished (Ali & Kravitz, 2018). Food pellets were weighted twice per week and the amount of food left in the cages was subtracted from the initially recorded amount. Any large piece of uneaten food found in the cage were also subtracted from the original value and recorded again to maintain maximum precision. Pellets smaller than approximately 5 mm were removed (Ali & Kravitz, 2018). According to NIH-MMPCs guidelines, we calculated the body weight change from the initial body weight measurements to analyse the overall effect of diet on body weight (Ellacott et al., 2010). Furthermore, was monitored the Body Condition Score (BCS) at relevant time points (every 8 weeks) over a 16-week period, since variations in food intake and body weight can occur in different context like obesity or accelerated growth (Cowley et al., 2019). Food intake of mice was analysed as the amount of food consumed /die/ mouse, with a caloric value of 3.15 kcal/g for Standard Diet (STD). To evaluate changes in metabolism according to food intake, was monitored weekly the food efficiency ratio (FER) as the (total weight gain / total food intake) × 100.

3.3.11. Histology and immunohistochemistry sample preparation

Mice livers were divided into pieces: a piece was fixed in 10% formalin for 24 hours, then dehydrated through a series of increasing concentrations of ethanol, clarified in xylene and embedded in paraffin using an automatic embedding machine; while the other one was cryo-preserved and OCT-embedded. All the samples where sectioned in order to obtain 7 micrometres sections, using a Leica rotary microtome for the paraffin-embedded samples and a MICROM cryostat for OCT-embedded ones. OCT-embedded liver sections were formalin-fixed for 2 minutes and stained with Oil- Red O staining in order to identify LDs in hepatocytes. Each slide was incubated for 15 minutes in Oil Red O/isopropanol solution 0.3%. Subsequently, slides were rinsed in isopropanol 60% and in distilled water and counterstained with Carazzi's haematoxylin. Paraffin-embedded livers were used to perform an immunohistochemistry with a CD36 antibody. Sections were de-waxed by two 10 minutes washes in xylene and rehydrated by decreasing concentrations of ethanol and distilled water for 5 minutes each. After that heat induced - epitope retrieval (HIER) was performed at 98° C for 10 minutes in Citrate pH6 buffer. Slides were then incubated with the primary antibody overnight at 4°C, and then incubated with

the appropriate alkaline phosphatase conjugated secondary antibody for 45 minutes. After 90 minutes of incubation with the substrate (kit Vector Blue SK-5300), the reaction was stopped by rinsing slides in distilled water and section were counterstained with Carazzi's haematoxylin. The sections were observed with the Nikon Eclipse E600 optical microscope. Images were acquired with the Nikon DS-U1 camera and analysed using the NIS Element software.

3.3.12. Biochemical analysis

Whole blood was collected at 8 weeks of age and at 16 weeks of age (after 8 weeks of STD) by maxillary facial vein puncture in K3-EDTA vials (100 µl/mouse) under 3 % isoflurane + 2lt/min oxygen anaesthesia (40-60 seconds), to measure non-fasted glucose, cholesterol, and triglycerides (Multicare IN, Biochemical System International). At 24 weeks of age, mice were fasted 3 hours and blood were collected prior to euthanasia under 3% isoflurane + 2lt/min oxygen anaesthesia by cardiac puncture (40-60 seconds) (Carper et al., 2020). Blood samples were centrifuged at 3500 rcf for 15 min to obtain sera, which were immediately frozen (-20° C). Serum alanine aminotransferase (ALT), aspartate transaminase (AST), cholesterol, triglycerides, glucose, urea and creatinine results were provided by the laboratories of a research organization (IZSLT, Rome, Italy; Galileo Research, Pisa, Italy) accredited by the Italian Ministry of Health to carry out studies on rodents for research purposes. In addition, fasted- serum insulin was determined using Ultrasensitive mouse insulin ELISA kit (Mercodia, 10-1249-01). Insulin sensitivity was assessed by using homeostasis model assessment-2 (HOMA2) index using online-based calculator on the Diabetes Trials Unit of the University of Oxford website (https://www.dtu.ox.ac.uk/homacalculator/) providing values for insulin resistance (HOMA-IR), steady-state β-cell function (HOMA-%B), and insulin sensitivity (HOMA-%S).

3.3.13. Ultrasound imaging

Ultrasound images at 8, 16 and 24 weeks of age were acquired and analysed by an experienced veterinary operator, using a high-frequency ultrasound unit (VisualSonics 2100, Toronto, Ontario, Canada) equipped with MS550 Blue Transducer probe (central frequency 40 MHz; focal length 6 mm; depth of penetration 5 -15 mm; 30–40 µm axial and 70–90 µm lateral resolution), and using the Vevo Lab software (version 3.0.0). Mice were not fasted before imaging, to minimize animal discomfort and avoid fasting-induced changes in body weight, metabolism, hepatic enzymes, cardiovascular parameters (Constantinides et al., 2011) During imaging sessions, mice were kept under inhalant anaesthesia (induction chamber with 4% isoflurane plus 2 Lt/min oxygen; maintenance with nose cone using 1.5-1.8% isoflurane) on a heated platform. Such isoflurane concentrations produce stable body temperature, mean arterial pressure (MAP) and heart rate (HR) values in C57BL/6 mice, comparable to those observed in awake animals

(Constantinides et al., 2011) Body temperature was monitored using a rectal probe and kept in a physiological interval by an infrared lamp. Liver images were acquired by two-dimensional (B-mode) imaging through the ventral body wall in transversal and longitudinal planes, and subsequently analysed offline. To be consistent between animals and images, we stored optimized acquisition settings on the instrument. All B mode ultrasound images were acquired under the same data capture settings (frequency = 40 MHz, frame rate = 16 images/s, gain = 30 dB, depth = 11 mm, width = 13.00 mm, dynamic range = 60 dB, sensitivity = high) for each mouse. The time-gain compensation was set to adjust the tissue echogenicity as constant as possible regardless of the depth, and the transmit power was set at 100%. The liver parenchyma was examined for echogenicity, echostructure, presence or absence of nodules, and border definition. The detection and grading of hepatic steatosis by visual inspection and parametric evaluation of liver were performed according to previously validated protocols in humans and already applied to mouse models as marker for steatosis. (Mancini et al., 2009; Pagliuca et al., 2016; Lessa et al., 2010) After the imaging sessions, mice were allowed to recover completely in a heated cage and monitored for signs of pain or discomfort.

3.4. Results

3.4.1. Deletion of MAPK15 in mice promotes NAFLD.

In order to explore the role of MAPK15 in lipid homeostasis, we used MAPK15 knockout (KO) mice with a C57Bl/6J genetic background, feed with a standard diet (STD) for 16 weeks (from 8 to 24 weeks of age) (**Figure 3A**). KO animals were viable and fertile, with no obvious morphological defects. Importantly, while the study was performed both on male and female mice, we herein describe only male data, as female mice have not significative differences between the two genotypes, possibly because of cytokines and hormone sex-related factors already described to affect mammalian responses of different sexes to high fat diets and development of obesity and related diseases (Smiriglia et al., 2023; Riazi et al., 2022; DiStefano, 2020)

Twenty-four weeks old MAPK15 KO male mice showed mean body weight (g) higher than age-matched WT mice aged from 8 to 24 weeks (**Figure 3A**), although the body weight changes rate between the two genotypes is similar (**Figure 3B**), these evidences that there are not alteration in the general growth of mice, but that they may have some alteration in metabolism leading KO mice to gain weight.

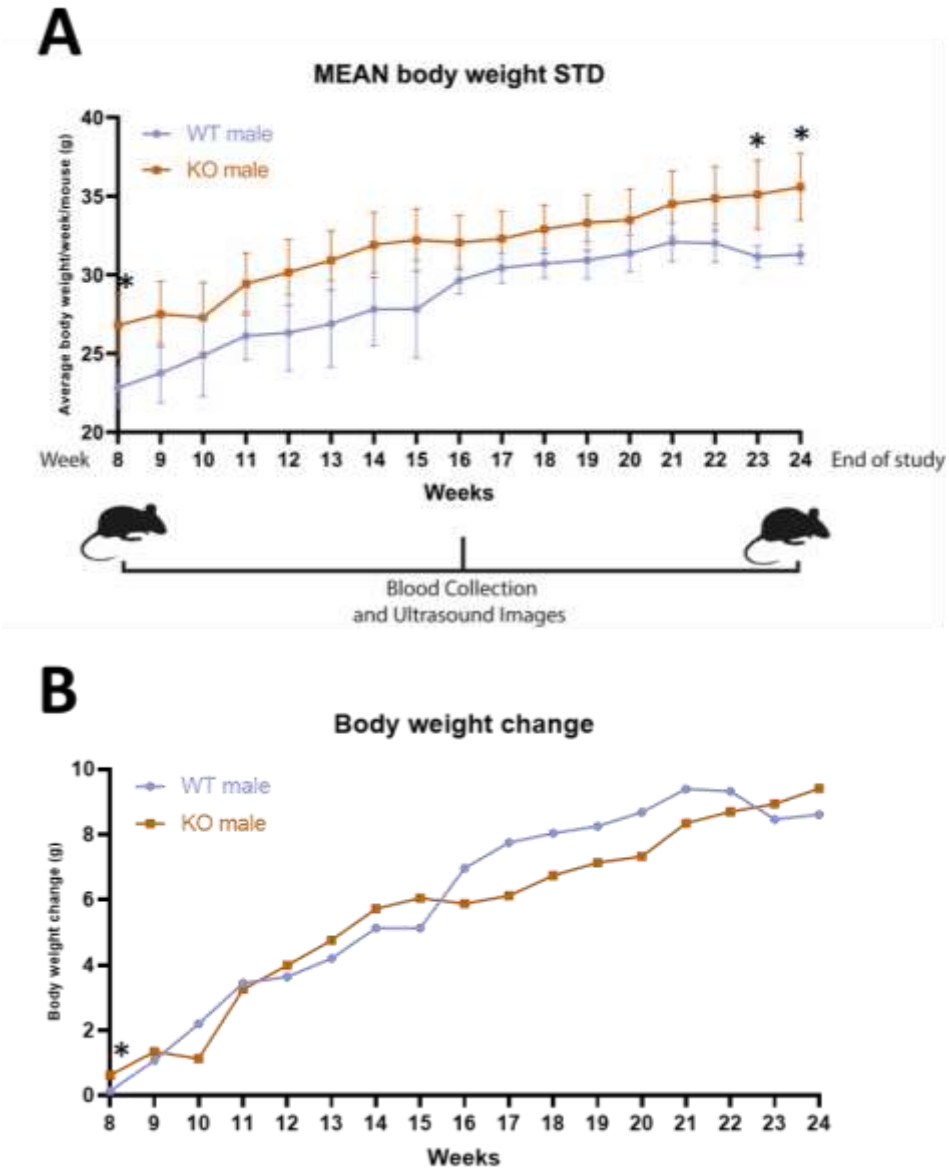

Figure 3. MAPK15 knockout mice, in C57Bl/6J genetic background, were feed with a standard diet for 16 weeks and weighed every week. **(A)** Average body weight per week (grams) KO males had significantly higher body weight than WT ones at week 8, 23 and 24 (Two-way ANOVA repeated measures-Linear Mixed model-genotype as main factor and time as within factor; Šidák's multiple comparison tests *p ≤ 0.05). Blood samples and ultrasound images were collected at week 8, 16 and 24. **(B)** Average weight change per week (g) from baseline was significantly different between WT and KO mice only at week 8.

Indeed, on visual examination, MAPK15 KO male mice also showed accumulation of more abundant subcutaneous and abdominal visceral fat depot compared to WT, overall exhibiting an “overweight” phenotype (**Figure 4A**). Importantly, abdominal ultrasound analysis of mice evidenced decreased echogenicity of KO mice livers, probably due increased accumulation of lipids in liver cells (**Figure 4B**).

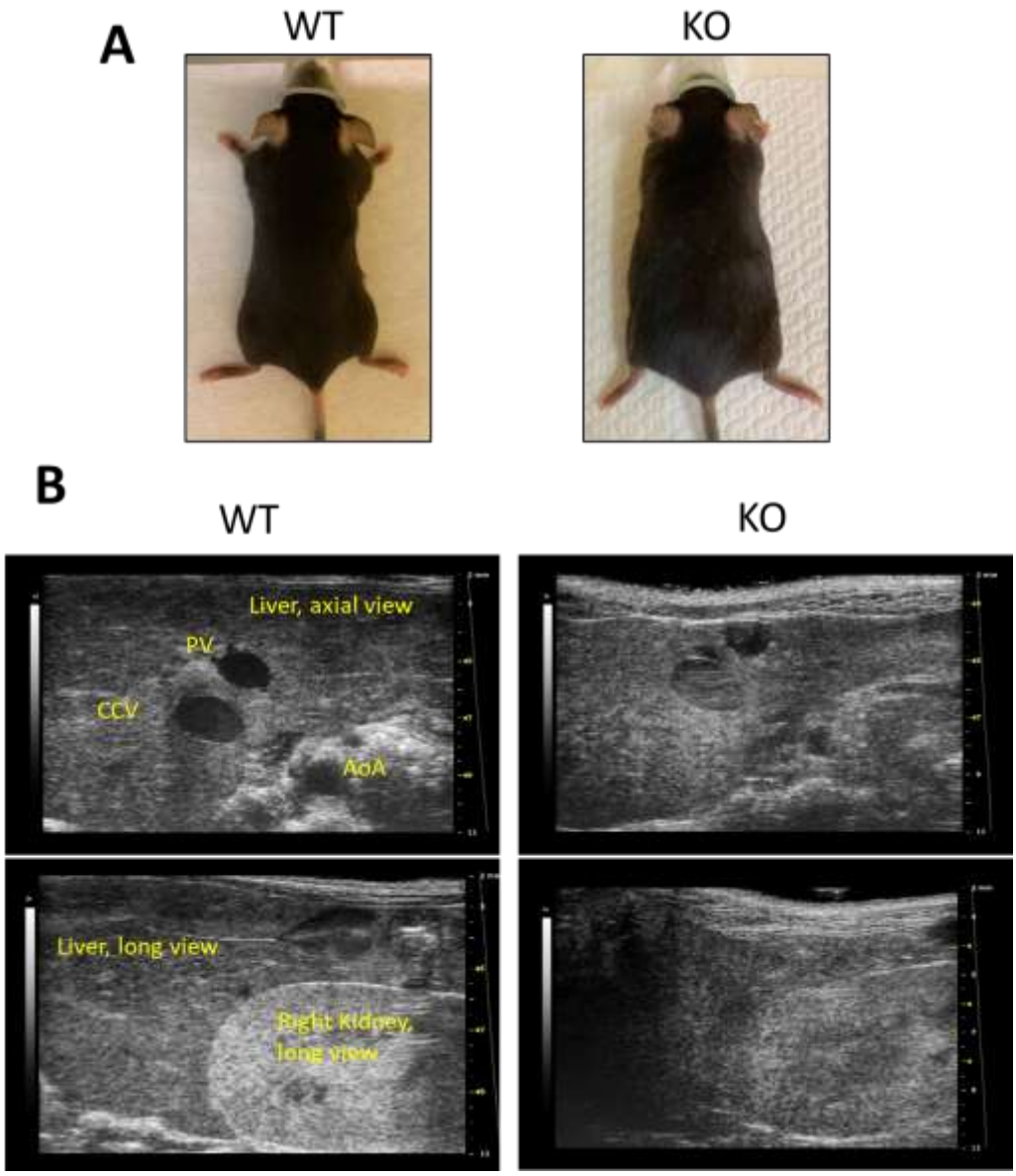

Figure 4. Visual Examination. **(A)** Visual Examination of body condition shows that MAPK15 KO mice have overweight phenotypes compared to WT (representative images). **(B)** Representative ultrasound acquisition in mice fed with standard diet at 24 weeks of age: KO mice are showing qualitative changes of liver echogenicity exhibited an increasing trend of quantitative indexes: liver-to-kidney ratio and liver-to-portal vein ratio (representative images).

Before the sacrifice, to evaluate the general physiological condition, mice were starved for 3 hours, then intracardiac blood samples were collected and serum analysed. Twenty-four weeks old MAPK15 KO male mice showed fasted serum values of glucose and insulin significantly higher than age-matched WT group (**Figure 5, Table 1**). Nonetheless, the application of homeostasis model assessment of β-cell function (HOMA $_{\beta\text{-cell}}$), an index of insulin secretory function derived from fasting plasma glucose and insulin concentrations used to predicts diabetes development (Matthews et al., 1985), shows a comparable β-cell function estimate value (HOMA %B) between genotypes, suggesting no β-cell intrinsic deficiency (**Figure 5, Table 1**). Nonetheless, we observed a significantly lower insulin sensitivity (HOMA %S) and higher insulin resistance (HOMA IR) than WT, at week 24, explaining the observed alterations of metabolic conditions (**Figure 5, Table 1**). Ultimately, MAPK15 KO males showed fasted serum value of cholesterol and creatinine significantly higher than age-matched WT group (**Table 2**).

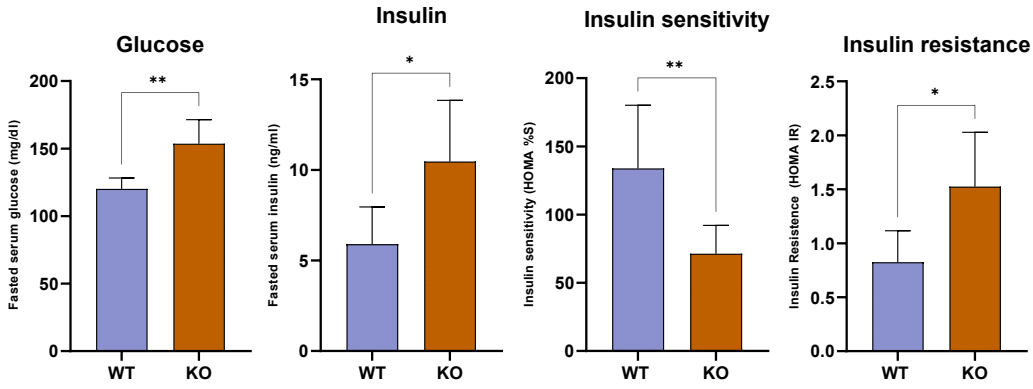

Figure 5. Graphical representation of glucose and insulin related analysis and HOMA β-cell estimation tool results from Table 1. Value of glucose and insulin are significantly higher in MAPK15 KO mice serum, the relative insulin sensitivity is significantly lower in KO compared to WT, conversely and insulin resistance have opposite trend (One way ANOVA –Mann Whitney nonparametric test: *p < 0.05; **p < 0.01).

Table 1. Serum glucose and insulin related analysis and HOMA β-cell estimation tool results. (One way ANOVA –Mann Whitney nonparametric test: *p < 0.05; **p < 0.01).

Fasted serum insulin related values					
Genotype/ parameter	GLU (mg/dL)	Insuline (ng/ml)	β-cell function estimate (HOMA %B)	Insulin Sensitivity (HOMA %S)	Insulin Resistance (HOMA IR)
Male WT	120.2 ± 8.01**	0.23 ± 0.08*	44.36 ± 9.48 ns	133.90 ± 46.22**	0.82± 0.29*
Male KO	153.57 ± 17.89**	0.41 ± 0.13*	41.82 ± 7.79 ns	71.28 ± 20.85**	1.52± 0.50*

Table 2. Serum analysis of lipid metabolism, liver and renal function. MAPK15 KO mice showed fasted serum value of cholesterol and creatinine significantly higher than age-matched WT (One way ANOVA –Mann Whitney nonparametric test: * $p \leq 0.05$) - (COL - Cholesterol; TRIGL - Triglyceride; AZ – Azotemia; CREA - creatinine).

Fasted serum values				
Genotye/ Parameter	**CHOL (mg/dL)**	**TRIGL (mg/dL)**	**AZ (mg/dL)**	**CREA (mg/dL)**
Male WT	64.5 ± 13.75*	52.33 ± 17.44 ns	55.16± 14.85 ns	0.23± 0.07*
Male KO	95.14 ± 28.85*	70.14 ± 27.35 ns	69.71± 57.84 ns	0.36± 0.12*

The post-mortem necroscopy, on the macroscopic visual examination of mice internal organs, these observations were confirmed, showing more subcutaneous and abdominal visceral fat and a slightly paler appearance of the livers on MAPK15 KO male mice, which is usually correlated to increased accumulation of lipids (**Figure 6A**). Indeed, histological analysis of mice livers using oil red staining confirmed increased lipid accumulation in KO livers, as compared to WT organs (**Figure 6B**).

Altogether, our results therefore demonstrate increased propensity of MAPK15 KO male mice in developing hepatic steatosis.

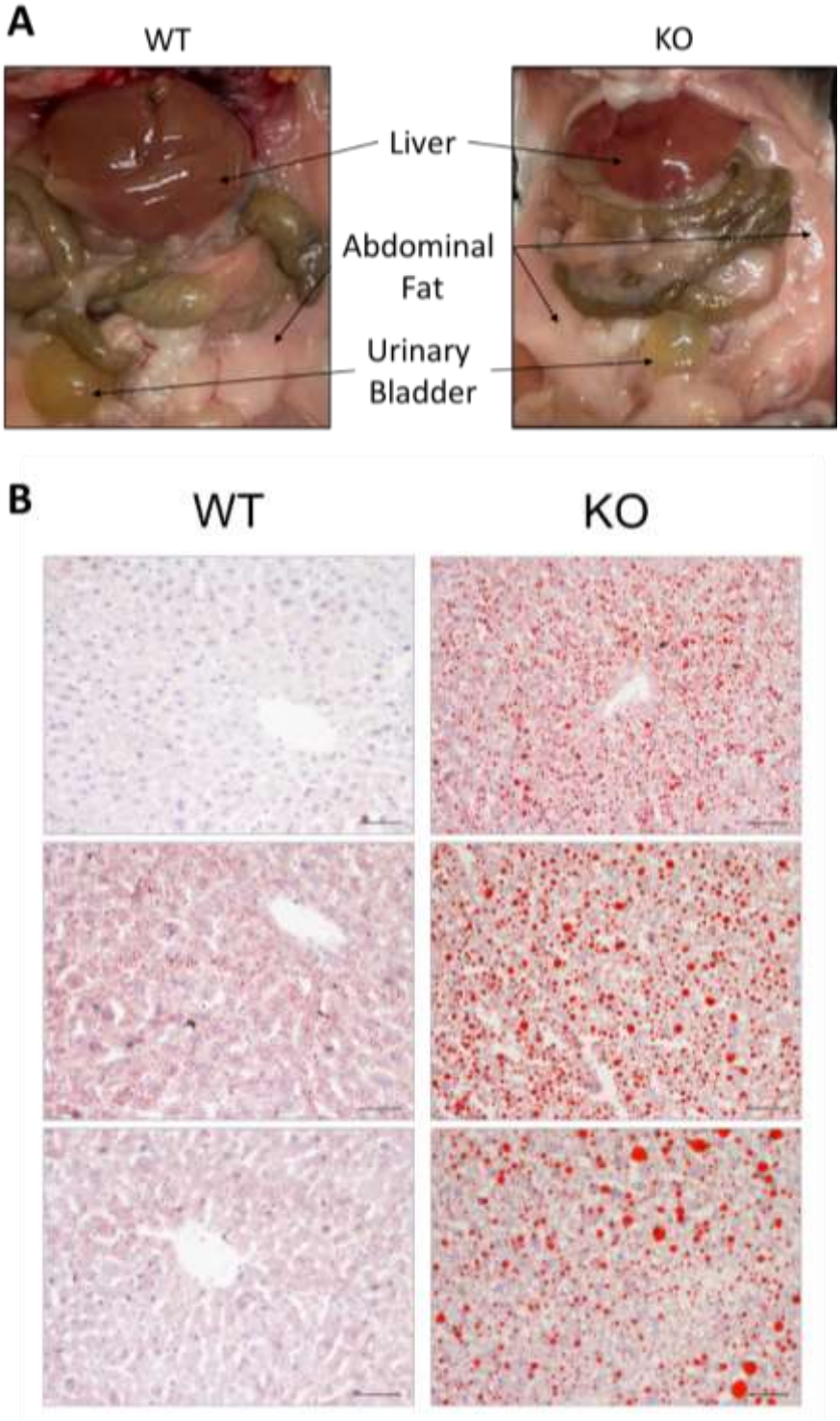

Figure 6. Post-mortem examination of mice organs. **(A)** visceral MAPK15 KO male mice show accumulation of more abundant abdominal visceral fat depot compared to WT and a paler appearance of the livers; **(B)** histological samples of liver of three mice per genotypes stained using oil red, showing increased lipid accumulation in KO livers. Representative images of 3 independent mice livers per genotype (Scalebar 50μm).

3.4.2. MAPK15 control lipids homeostasis in vitro.

To investigate the molecular details behind MAPK15-dependent control of mammalian lipid metabolism, we next decided to use HepG2, a cell line derived from a liver hepatocellular carcinoma (also referred as an hepatoblastoma cell line) (López-Terrada et al., 2009), as a model of liver cell. As LDs are the most important site for storage of lipids at the cellular level and are particularly important in hepatic cells as energy storage during starvation periods, cell growth and vesicles (Olzmann & Carvalho, 2019), we first evaluated their cellular content, by using the BODIPY 493/503 probe, in HepG2 liver cells transiently transfected with a specific siRNAs to downregulate MAPK15. In line with data obtained in mice, also HepG2 cells showed a significant increase in the number and dimensions of LDs in siMAPK15 transfected cells, by confocal microscopy analysis (**Figure 7A-B**). The same result was also confirmed by LDs mean fluorescence intensity quantification through FACS analysis (**Figure 7C**).

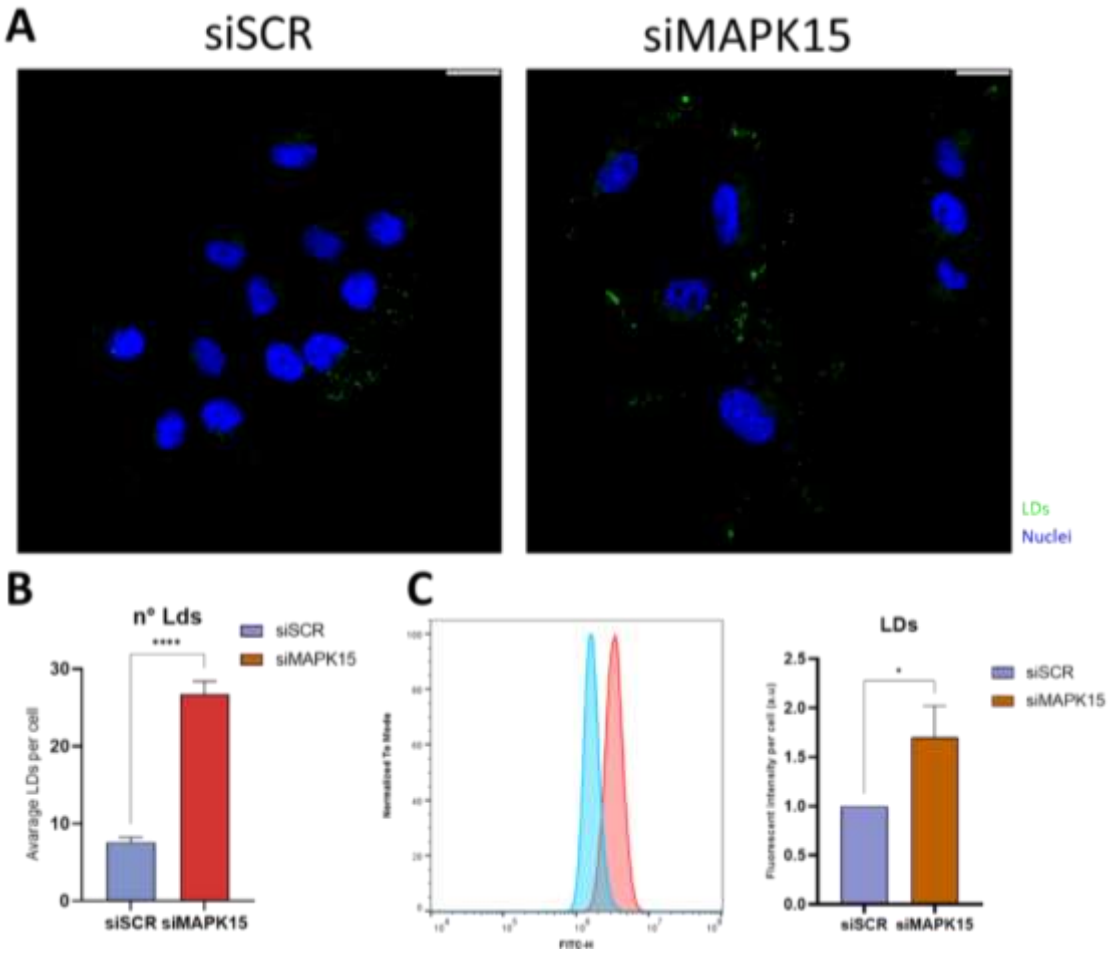

Figure 7. LDs accumulation in MAPK15 downregulated HepG2 cell. **(A)** Representative immunofluorescent acquisition of LDs: LDs was stained with BODIPY 493/503 probe (Scalebar 10μm); **(B)** quantification was carried out with the Quantitation Module of Volocity software (PerkinElmer Life Science); **(C)** FACS mean fluorescence intensity quantification of LDs using BODIPY 493/503. (Student's t-test: ****p < 0.0001; *p < 0.05).

Increasing of cellular FAs is the starting point for excessive cellular accumulation of lipids (Olzmann & Carvalho, 2019). As previously reported, intracellular FAs increase because of chronic excess intake of calories, alterations in ex-novo lipid biosynthesis, increased lipid uptake, impaired Fatty Acid Oxidation (FAO), or increased autophagy flux that consequentially can cause LDs accumulation (Fader Kaiser et al., 2021; Olzmann & Carvalho, 2019). In our case, as autophagy is impaired in MAPK15 depleted cells because of its role in the control of the autophagic machinery (Colecchia et al., 2012b), we excluded that this pathway could be involved in the increase of LDs amount.

Next, we evaluated the contribution of lipid biosynthesis to the metabolism on MAPK15 depleted cells by performing western blot analysis of two important proteins involved in the biosynthetic pathway, FASN and SCD1, in HepG2 cells downregulated for MAPK15 expression by a siRNA approach. Data show that these proteins are significantly downregulated in siMAPK15 HepG2 cell both at protein and mRNA levels (**Figure 8A-B**). Moreover, supporting these data, proteomics analysis of MAPK15 knockdown in human bronchial epithelial derived cell (16HBE14o), performed in collaboration with the Mass Spectrometry Unit of Toscana Life Science, confirmed the downregulation of these two proteins (**Figure 9A-B**).

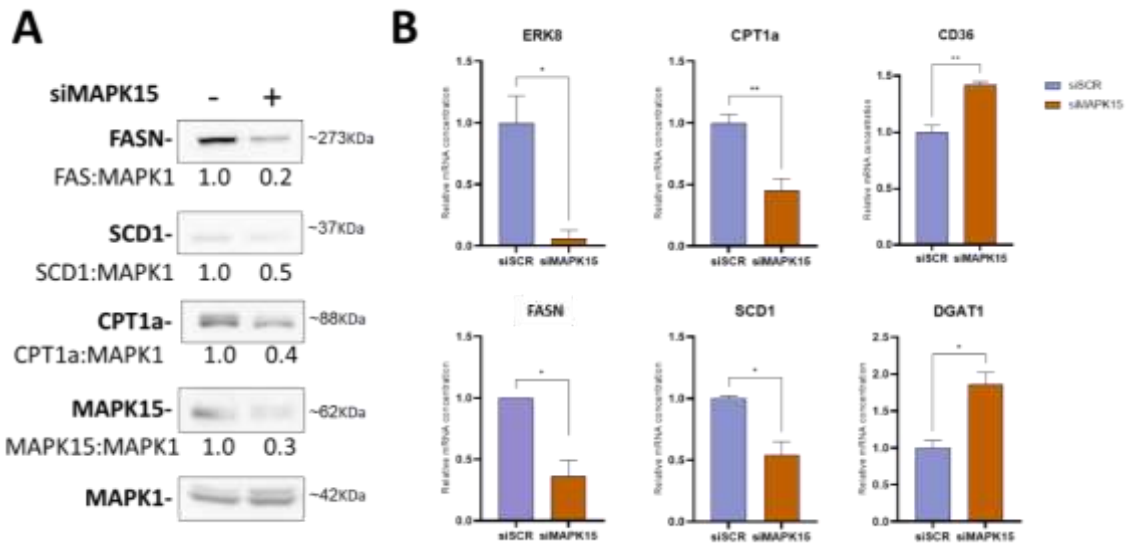

Figure 8. Lipogenesis pathway proteins evaluation. **(A)** Western blot of MAPK15 downregulated HepG2 cells show a downregulated trend of SCD and FASN related to lipogenesis, as well as CPT1A the bottleneck of FAO, suggesting a reduction of FAO and Biogenesis pathways. **(B)** Relative mRNA level of indicated genes. (Student's t-test: *$p < 0.05$; **$p < 0.01$)

Regarding the potential contribution of FAO to the observed increase of LDs in MAPK15 depleted cells, we next analysed the protein level of CPT1a, a mitochondrial lipid transporter considered a bottleneck determining FAO rates (De Oliveira & Liesa, 2020), and observed a significant reduction of CPT1a protein level, suggesting a role for MAPK15 in determining cellular FAO, possibly increasing LDs accumulation because of diminished utilization in cells with reduced MAPK15 expression (**Figure 8A**).

Ultimately, we evaluated the potential contribution of an increased level of cellular lipid uptake to LDs accumulation in MAPK15 depleted cells. Among the different known lipid transporters, growing evidence suggest that CD36 could be a potential biomarker for NAFLD (Rada et al., 2020) due to changes in its levels and membrane localization (Rada et al., 2020)

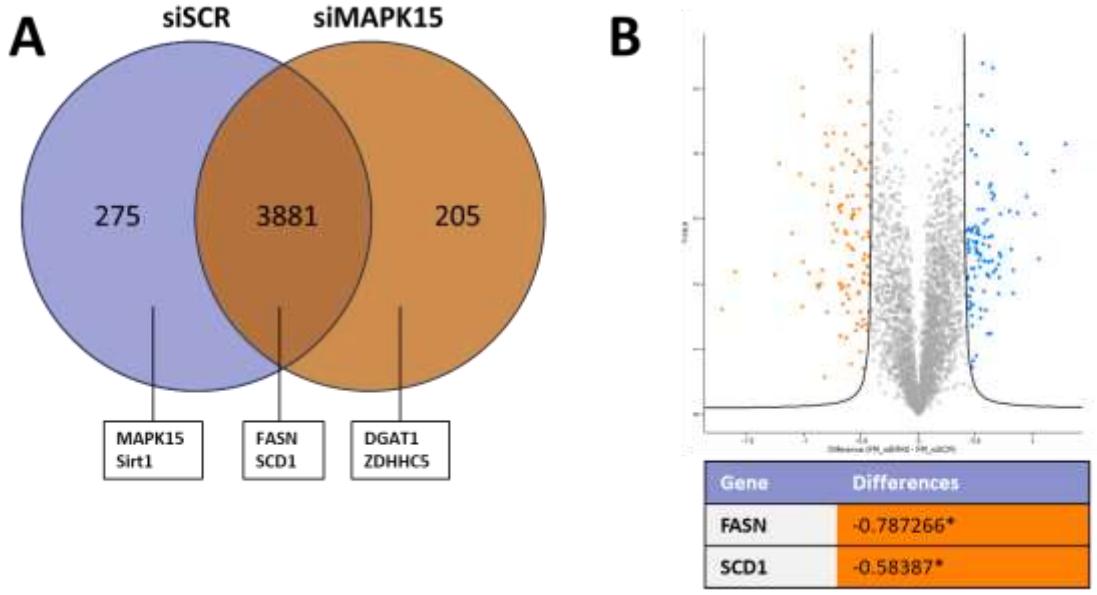

Figure 9. Proteomics analysis. **(A)** Venn diagram showing samples overlap. DGAT1, ZDHHC5 are detectable only in siMAPK15; **(B)** Volcano Plot representing upregulated (in orange) and downregulated (in blue) proteins, in the comparison between control (siSCR) and siMAPK15 cells. FASN and SCD1 are downregulated in siMAPK15 samples (*$p < 0.05$).

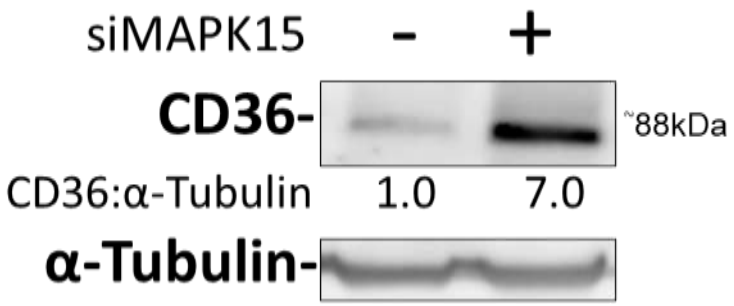

Figure 10. CD36 protein level western blot evaluation**.**

Interestingly, both CD36 mRNA (**Figure 8B**) and protein levels (**Figure 10**) were increased in siMAPK15 transfected HepG2 cells, compared to control siSCR, suggesting a role for this protein in determining cellular lipid content in MAPK15 downregulated cells. As also CD36 plasma membrane localization has been recognized as a key factor in determining the rate of lipid internalization, we evaluated CD36 plasma membrane localization by performing immunofluorescence and cytofluorimetric analysis to detect endogenous CD36. Our experiments, indeed, showed increased membrane localization of CD36 in siMAPK15 samples as compared to control siSCR samples (**Figure 11A-B and 11C**). Overall, our data therefore support the possibility that reduced MAPK15 expression may be able to cause increased LDs amounts because of increased levels and membrane localization of CD36, with consequent increase of FA uptake.

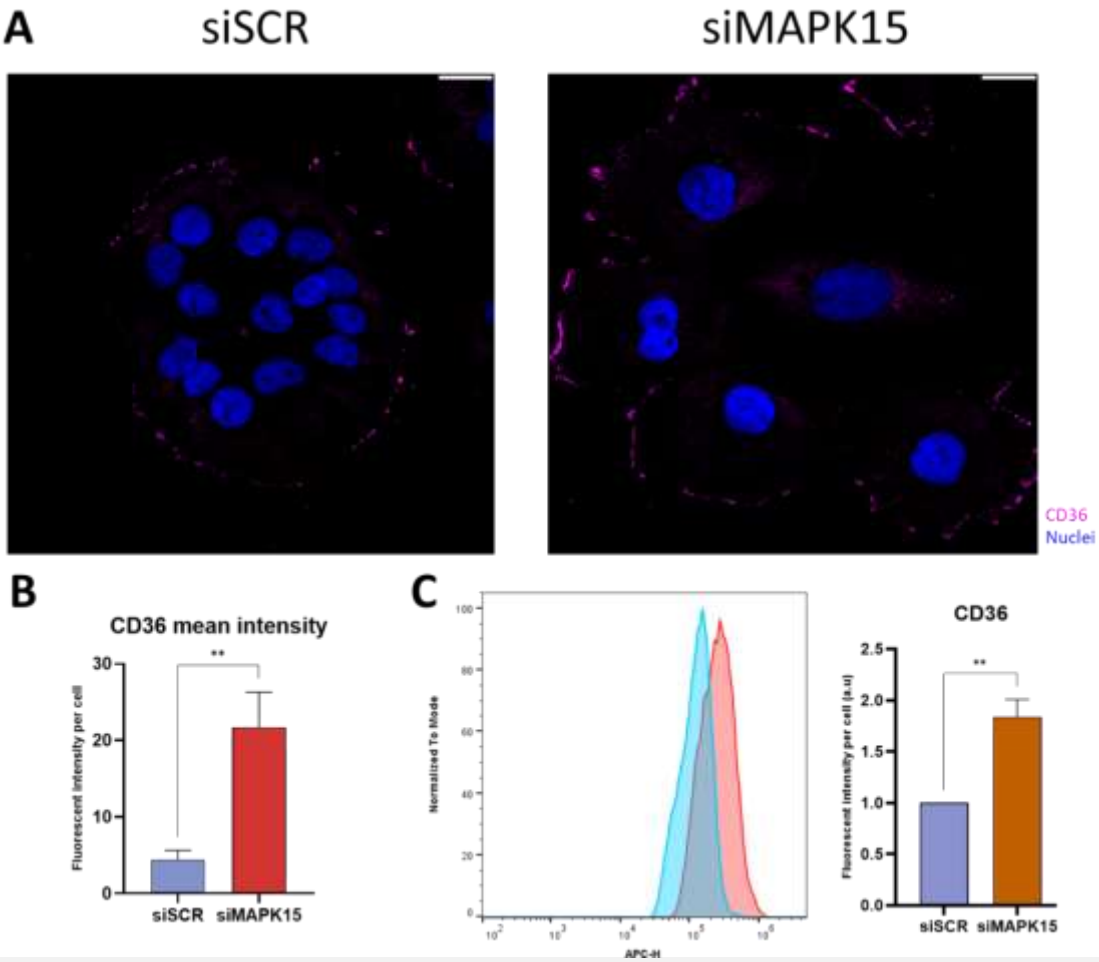

Figure 11. Evaluation of CD36 localization. **(A)** Representative immunofluorescences images of CD36 localized on cytoplasmic membrane. **(B)** Membrane CD36 fluorescence quantification **(C)** FACS analysis and fluorescent quantification of outer membrane CD36 localization. (Student's t-test: **p < 0.01) (Scalebar 10μm)

As previously described, DGAT1 is the protein involved in the last step of LDs formation (Chen & Farese, 2005b; Teixeira et al., 2023). In the context of higher LDs cell content caused by the reduction of MAPK15 expression and increased FAs uptake mediated by CD36, we supposed a possible involvement of DGAT1 (which preferentially utilizes exogenous FAs) (Villanueva et al., 2009b), in this process. Data on MAPK15 depleted cells showed an increased level of DGAT1 protein by western blot (**Figure 12**) and transcriptional upregulation by RT-qPCR (**Figure 8B**) confirmed even in the proteomic analysis (**Figure 9A**).

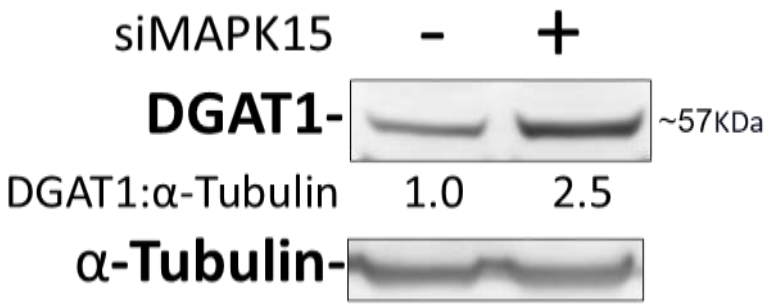

Figure 12. DGAT1 protein level western blot evaluation

Based on these data, we decided to next investigate whether changes in CD36 expression and cellular localization could be responsible also for observed lipid accumulation in the liver of MAPK15 KO mice. Interestingly, livers from MAPK15 KO mice showed increased amounts of CD36 protein and relative mRNA as compared to WT mice (**Figure 13A- 13B**). Moreover, based on a previous proteomic analysis, we also observed that ZDHHC5, the protein involved in palmitoylation and membrane localization of CD36, is overexpressed in siMAPK15 samples (**Figure 9 and 13A**), suggesting a potential mechanism to explain the increased CD36 plasma membrane localization, a possibility that is currently under investigation. Histological analysis of mice livers shows strong localization of CD36 on hepatocyte plasma-membranes in the areas facing the sinusoids, which was not evident in livers from WT mice (**Figure 14**).

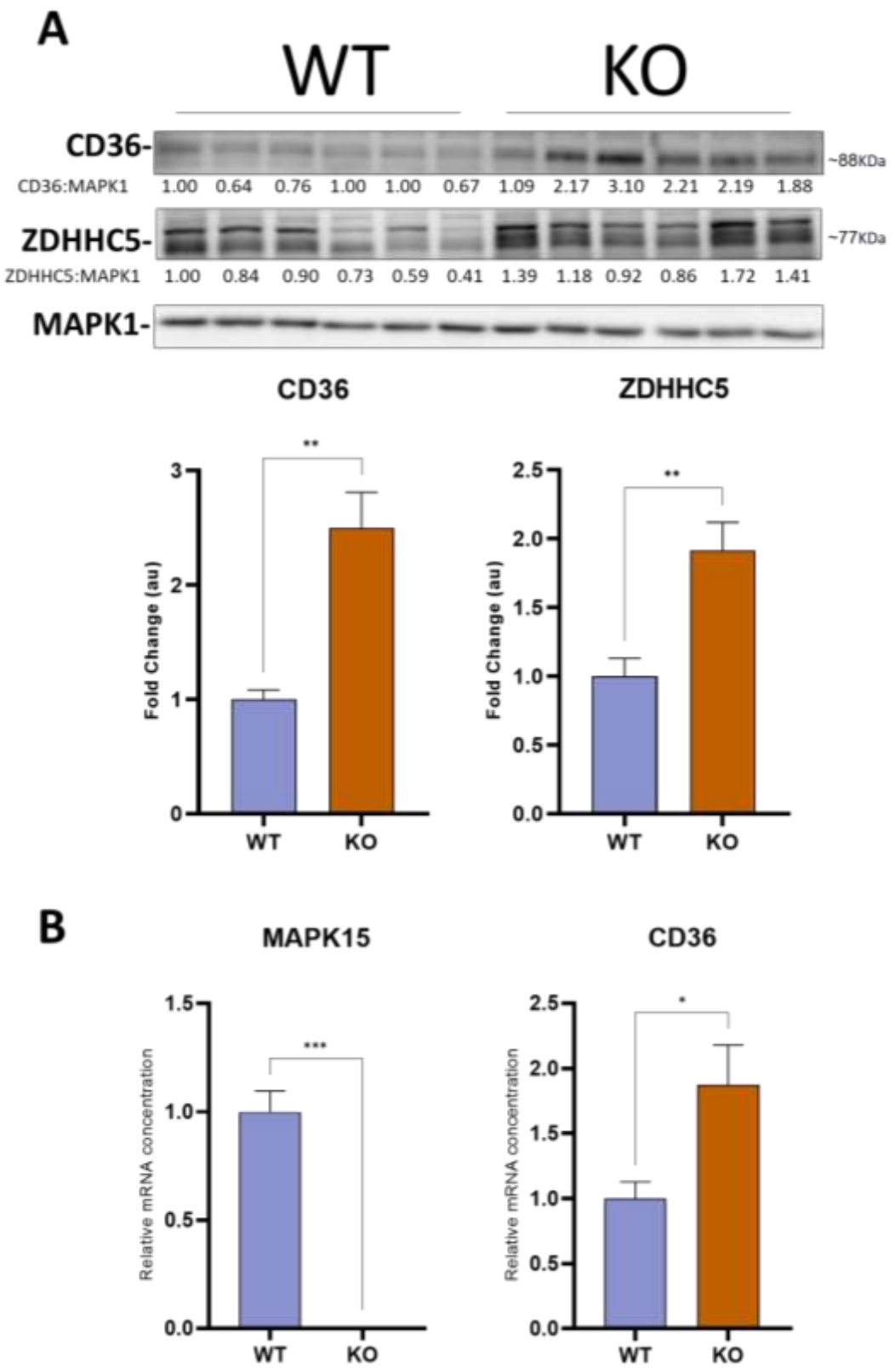

Figure 13. (A) CD36 and ZDHHC5 proteins levels. Western blot evaluation of total protein extract of mice liver (Student's t-test: *p < 0.05, **p < 0.01); **(B)** RT-qPCR results on average mRNA level of MAPK15 and CD36 in mice liver (Student's t-test: *p < 0.05 ***p < 0.001).

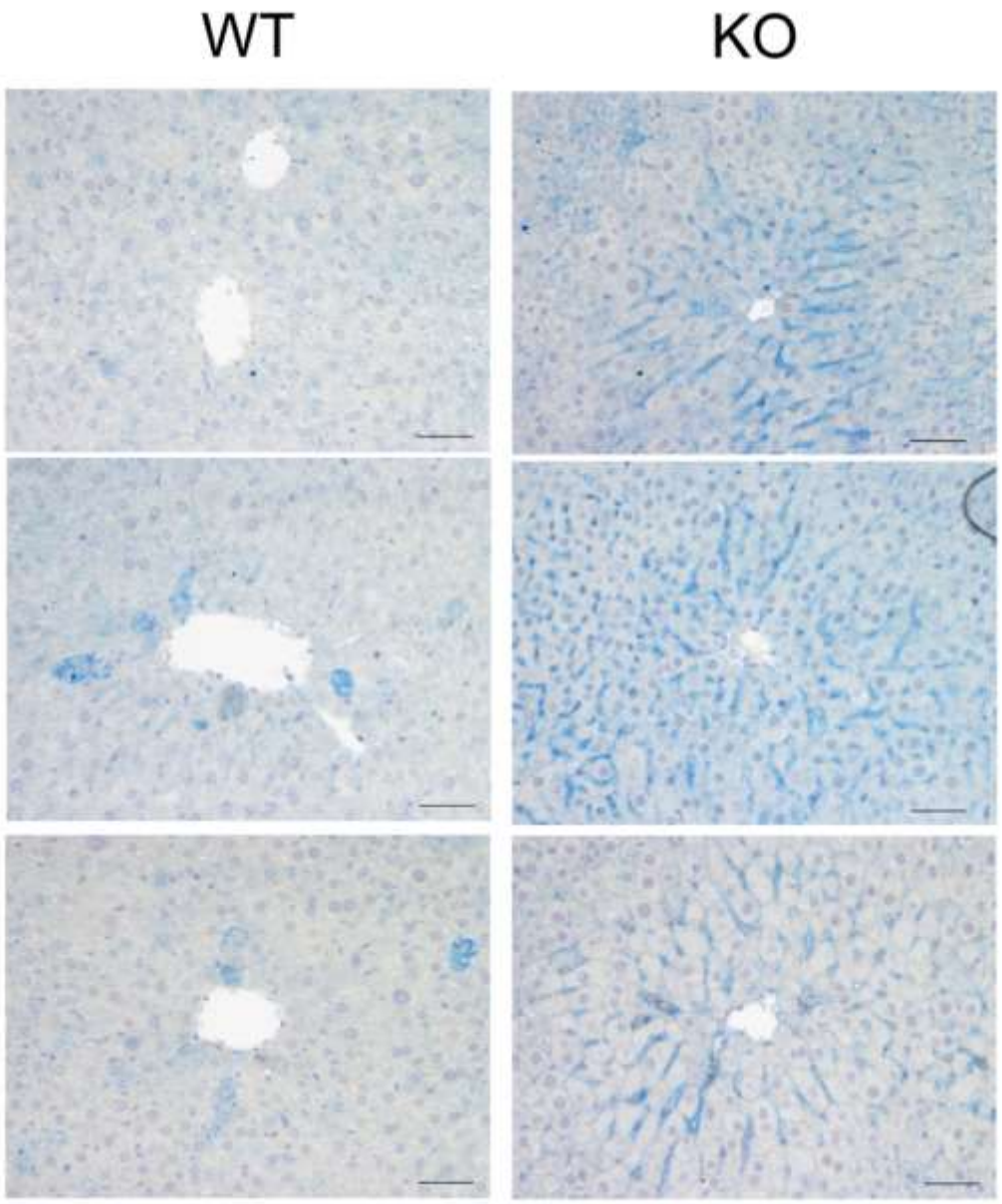

Figure 14. Immunohistochemistry of CD36 expression and cellular localization in mice liver. The antibody-CD36 interaction is visualized using chromogenic detection with the appropriate alkaline phosphatase conjugated secondary antibody, sections were counterstained with Carazzi's hematoxylin. (Scalebar 50μm).

As Parkin has been already reported to control lipid uptake by regulating CD36 (Kim et al., 2011), we next studied this protein in livers' lysates, and observed a protein level lower in KO than in control WT mice, suggesting parkin-mediated reduction of CD36 degradation (**figure 15**). Overall, our data therefore suggest that MAPK15, through the activation of Parkin, regulates CD36 amount inside the cell, whereby more experimental data confirming parkin-mediate contribution in CD36 levels is needed and are currently under investigation. As in the same proteomic analysis we also observed reduced levels of the SIRT1 protein in siMAPK15 transfected samples (**Figure 9**), additional experiments will be also addressed to establishing the role of this protein in MAPK15 dependent regulation of CD36 lipid uptake in liver cells.

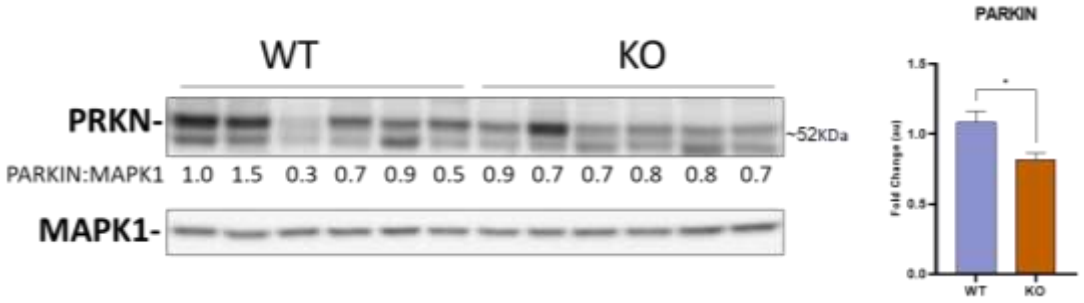

Figure 15. Parkin protein level western blot evaluation of total mice liver lysates (*p < 0.05).

3.5. Discussion

Altogether, our preliminary results uncovered new regulatory mechanism of lipid homeostasis regulation, *in vivo* and *in vitro.* We report that a reduction/depletion of atypical MAP kinase 15 overall increases lipid storage and leads to liver steatosis in C57BL/6J MAPK15 KO mice. Specifically, MAPK15 is involved in localization, upregulation, and stabilization of CD36, causing a gaining of an increased uptake of FAs to cells.

Mechanistically, downregulation (*in vitro*) or deletion (*in vivo*) of MAPK15: i) increases the level of ZDHHC5 protein, which has been already involved in CD36 plasma membrane localization (Wang et al., 2019), ii) reduces the level of PRKN, already involved in CD36 degradation under fatty acid stimuli (Kim et al., 2011), iii) reduces the level of SIRT1 (Niu et al., 2018), which is known to inhibit CD36 expression. In addition, in MAPK15 downregulated cells, we observed an upregulation of DGAT1 protein levels, involved in FAs storage, whose upregulation has been associated to cellular LDs increase.

Despite several functions have been assigned to MAPK15 *in vivo* and *in vitro,* (Iavarone et al., 2006; Xu et al., 2010b; Colecchia et al., 2015; Jin et al., 2015; Rossi et al., 2016; Groehler & Lannigan, 2010; Cerone et al., 2011; Rossi et al., 2016; Hasygar & Hietakangas, 2014; Colecchia et al., 2012a; Franci et al., 2022; Hasygar et al., 2021), its physiological role is not entirely clear. Importantly, MAPK15, through a genome-wide association studies, has been associated with obesity (Li et al., 2012) (https://www.ebi.ac.uk/gwas/genes/MAPK15): still, the role of MAPK15 in lipid metabolism in mammalians has not been previously addressed.

Here, we observed that MAPK15 KO mice on standard diet showed accumulation of more abundant subcutaneous and abdominal visceral fat compared to WT, exhibiting an “overweight” phenotype. Our hypothesis is that, upon feeding with a high content of lipids such as the Western diet, this tendency may switch to frank obesity phenotypes, with pathological alteration of the energetic metabolism of the organism. Our results indeed demonstrate an increased propensity of MAPK15 KO male mice to develop hepatic steatosis, the typical starting point for fatty liver diseases. In line with this findings, MAPK15 KO also had significantly higher levels of insulin and glucose, resulting in insulin resistance when compared to WT mice. Insulin resistance is defined clinically as the inability of a known quantity of exogenous or endogenous insulin to increase glucose uptake and utilization in an individual, as much as it does in a normal population. Among the causes of developing insulin resistance syndrome, such as genetic abnormality or reduced physical activity, there is an increase in visceral adiposity (Lebovitz,

2001). Whereby, the alteration observed in MAPK15 KO mice could be the cause of insulin resistance. Altogether, our findings therefore suggest an increased risk of developing obesity and NAFLD when reducing the MAPK15 protein.

In vitro, MAPK15 downregulation leads to an increased lipid storage, and a reduced lipid *de-novo* biosynthesis on HEPG2 cells. Moreover, CPT1a downregulation suggests a reduced FAO, worsening the FAs accumulation. To better understand MAPK15 mechanical role in controlling these pathways, it would be interesting to perform an experiment of MAPK15 WT rescue, on MAPK15 downregulated HepG2 cells. In addition, a rescue of MAPK15 mutant of kinase domain could help to evaluate whether the kinase domain is required to regulate these pathways.

Ultimately, a potential contribution of an increased level of cellular lipid uptake was associated to MAPK15. Indeed, our data suggest that MAPK15 is involved in a negative regulation of FAs uptake through CD36 activity regulation. Firstly, MAPK15 downregulation leads to reduce SIRT1 level, promoting CD36 expression (Niu et al., 2018). Secondly, downregulation of MAPK15, already proven to be involved in controlling PRKN activity (Franci et al., 2022), indirectly inhibit CD36 polyubiquitination-degradation PRKN-mediated. Moreover, we demonstrate an increased level of ZDHHC5 in mice liver, that leads to CD36 palmitoylation and stabilization on hepatocyte plasma-membrane. Moreover, it would be interesting to also check for a possible upregulation of the other lipid transporters, allowing us to evaluate whether the metabolic condition of the KO mice could be due to an excessive intake of lipids from the various uptake pathways, and not only CD36-mediated. In addition, the condition of increased lipid uptake may be worsened by the DGAT1 level upregulation on MAPK15 downregulation condition.

All our findings suggest a role of MAPK15 in positive control on degradation and localization of CD36 regulating lipid homeostasis, and in condition of downregulation/depletion of MAPK15, miss-regulated FAs uptake leads to a rise of fat depot and liver injury increasing the risk of developing NAFLD. Moreover, supported by these data, we are studying a possible arise of liver inflammation due to FAs accumulation, that may lead to a progression of NAFLD to NASH, and a worsening of its consequences.

3.6. Conclusion

Our studies show that differences in the storage of the unburnt energy in hepatocytes of MAPK15 KO mice cause lipids accumulation and tissue damage to the liver, which are associated to insulin resistance and obesity. Indeed, liver plays a central role in whole body energy homeostasis, by its ability to metabolize glucose and fatty acids, converting surplus glucose to fat storage. Hepatic steatosis and NAFLD progression may occur when the rate of hepatic fatty acid uptake mediated by CD36 and de novo fatty acid synthesis is greater than the rate of FAO. The evidences observed in mice livers and in human hepatocarcinoma HepG2 cell line start to shed some light about the molecular processes behind these findings, although they need a deeper investigation, e.g. also in primary hepatocyte cell lines and in human pathological samples.

In conclusion, our data suggest that MAPK15 may protect liver tissue from NAFLD, by controlling lipid metabolism and uptake, through Parkin- and Sirt1-dependent increased protein levels and ZDHHC5-dependent plasma membrane localization of CD36. All our findings, supported by Hasygar and colleague's data in drosophila (Hasygar et al., 2021), ultimately, address a new role to MAPK15 in mammalian lipid homeostasis, by controlling cellular lipid content, upgrading with new details our knowledge about the physiological role of MAPK15.

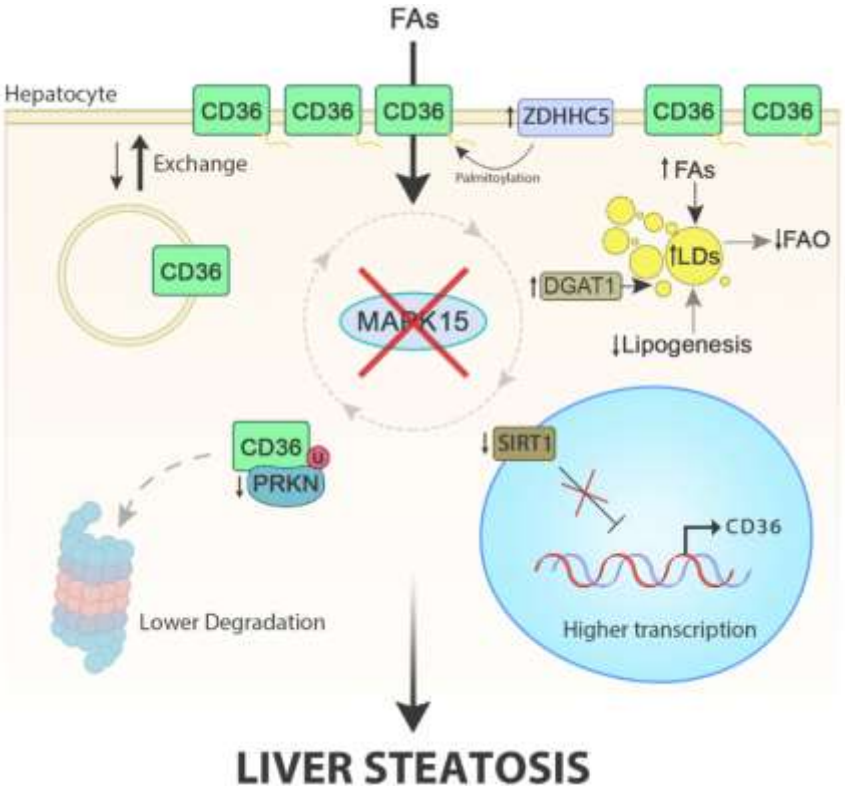

4. Future perspectives

The work presented in the thesis opens new perspectives for the exploitation of DDX3X and MAPK15 as biomarkers in treatment and cancer research development. Indeed, in the first section, we demonstrated a potent antiproliferative and cytotoxic effects of FHP01, a DDX3X helicase inhibitor, against diverse breast cancer cell types. Moreover, its robust inhibitory impact on tumour growth in xenograft models reinforces the notion that targeting DDX3X helicase activity holds promise for improving the prognosis of breast cancer. Noteworthy, the molecule was selected as a result of a in silico screening underlining the importance of working together with an interdisciplinary group where different expertise and skills can be employed to develop a more effective inhibitor for the helicase domain. As well, there is space for new preclinical studies with in vivo orthotropic models, to better characterize DDX3X in breast cancer. Moreover, it would be interesting to verify the possibility of increasing the anticancer effect using FHP01 in combination with other current targeted therapies, that may synergize the efficacy of the treatment in affect breast cancer patients.

At the same time, the role of MAPK15 can open newer exiting scenarios. Obesity is in fact a factor of risk of 20% of total new cancer (Santos & Schulze, 2012), and since our data suggests that MAPK15 may protect from obesity and deeply liver tissue from NAFLD by controlling lipid homeostasis and lipids uptake, it's important to better investigate the physiological role of MAPK15. In the near future, I am committed to continue with my investigation for highlighting the molecular processes behind these preliminary findings as I will carry out in vitro research using primary hepatocyte cell lines, as well as human derived pathological samples. Specifically, I am going to explore the mechanism behind the uptake MAPK15-mediated:

1. In controlling CD36 degradation through PRKN.
2. In regulating SIRT1 level leading to controls CD36 transcription.
3. In the expression of ZDHHC5, and its role in CD36-stabilization on plasma membrane.

With this in mind, a multi-omics approach such as tissue-specific proteomics and metabolomics could benefit the knowledge on the role of the atypical MAPK15. Furthermore, we will develop relevant preclinical models to verify the role of MAPK15 in obesity, e.g. treating mice with a High Fat Diet, in order to explore new unrevealed MAPK15 physiological roles in lipid homeostasis.

5. Acknowledgement

I would like to express my deepest gratitude to my tutor Mario Chiariello for supporting me and for his invaluable patience and constructive suggestions in the planning and development of this research during my PhD studies. His immense knowledge and plentiful experience have encouraged me in all the time of my researcher career.

Many thanks to my supervisor Laura Poliseno for enthusiastic encouragement and logistic support during the in vivo studies.

Special thanks to all the Laboratory staff that I'm worked with and contributed to obtain these data: Sara Gargiulo from Institute of Clinical Physiology at Italian National Research Council, Virginia Barone, Denise Bonente from Department of Molecular and Developmental Medicine at University of Siena, for the in vivo studies and Histology analysis. I express my gratitude to the Toscana Life Sciences Foundation in Siena for providing both infrastructure and instrumentation and their Mass Spectrometry Unit Laura Salvini, Laura Tinti and Vittoria Cicaloni for the proteomics data; Many thanks to First Health Pharmaceuticals B.V. (FHPBV) for providing the inhibitors and for giving the opportunity to publish the data obtained.

My special thanks are extended to all my colleagues Lorenzo Franci and Monia Taranta from Institute of Clinical Physiology at Italian National Research Council, Sara Panepinto of Istituto per lo Studio, la Prevenzione e la Rete Oncologica, Giulia Vallini and Franca Maria Bertolino from University of Siena and Veronica Vetri Buratti from University of Bologna for all scientific support and cherished time spent together in the lab.

I'm grateful to Andrea Morandi as associate professor from Dipartimento di Scienze Biomediche, Sperimentali e Cliniche "Mario Serio" at Università degli Studi di Firenze, and Lisa Gherardini as researcher from Institute of Clinical Physiology at Italian National Research Council for their critical reading and reviewing of this thesis.

6. Bibliography

Abumrad, N. A., & Moore, D. J. (2011). Parkin reinvents itself to regulate fatty acid metabolism by tagging CD36. *J Clin Invest*, *121*(9), 3389-3392. https://doi.org/10.1172/JCI59219

Ali, M. A., & Kravitz, A. V. (2018). Challenges in quantifying food intake in rodents. *Brain Res*, *1693*(Pt B), 188-191. https://doi.org/10.1016/j.brainres.2018.02.040

Altschul, S. F., Madden, T. L., Schäffer, A. A., Zhang, J., Zhang, Z., Miller, W., & Lipman, D. J. (1997). Gapped BLAST and PSI-BLAST: a new generation of protein database search programs. *Nucleic Acids Res*, *25*(17), 3389-3402. https://doi.org/10.1093/nar/25.17.3389

Alves-Bezerra, M., & Cohen, D. E. (2017). Triglyceride Metabolism in the Liver. *Compr Physiol*, *8*(1), 1-8. https://doi.org/10.1002/cphy.c170012

Amaro, R. E., Baudry, J., Chodera, J., Demir, Ö., McCammon, J. A., Miao, Y., & Smith, J. C. (2018). Ensemble Docking in Drug Discovery. *Biophys J*, *114*(10), 2271-2278. https://doi.org/10.1016/j.bpj.2018.02.038

Bartlett, K., & Eaton, S. (2004). Mitochondrial beta-oxidation. *Eur J Biochem*, *271*(3), 462-469. https://doi.org/10.1046/j.1432-1033.2003.03947.x

Benkert, P., Biasini, M., & Schwede, T. (2011). Toward the estimation of the absolute quality of individual protein structure models. *Bioinformatics*, *27*(3), 343-350. https://doi.org/10.1093/bioinformatics/btq662

Biasini, M., Schmidt, T., Bienert, S., Mariani, V., Studer, G., Haas, J., Johner, N., Schenk, A. D., Philippsen, A., & Schwede, T. (2013). OpenStructure: an integrated software framework for computational structural biology. *Acta Crystallogr D Biol Crystallogr*, *69*(Pt 5), 701-709. https://doi.org/10.1107/S0907444913007051

Bol, G. M., Vesuna, F., Xie, M., Zeng, J., Aziz, K., Gandhi, N., Levine, A., Irving, A., Korz, D., Tantravedi, S., Heerma van Voss, M. R., Gabrielson, K., Bordt, E. A., Polster, B. M., Cope, L., van der Groep, P., Kondaskar, A., Rudek, M. A., Hosmane, R. S., . . . Raman, V. (2015). Targeting DDX3 with a small molecule inhibitor for lung cancer therapy. *EMBO Mol Med*, *7*(5), 648-669. https://doi.org/10.15252/emmm.201404368

Botlagunta, M., Vesuna, F., Mironchik, Y., Raman, A., Lisok, A., Winnard, P., Mukadam, S., Van Diest, P., Chen, J. H., Farabaugh, P., Patel, A. H., & Raman, V. (2008). Oncogenic role of DDX3 in breast cancer biogenesis. *Oncogene*, *27*(28), 3912-3922. https://doi.org/10.1038/onc.2008.33

Brai, A., Fazi, R., Tintori, C., Zamperini, C., Bugli, F., Sanguinetti, M., Stigliano, E., Esté, J., Badia, R., Franco, S., Martinez, M. A., Martinez, J. P., Meyerhans, A., Saladini, F., Zazzi, M., Garbelli, A., Maga, G., & Botta, M. (2016). Human DDX3 protein is a valuable target to develop broad spectrum antiviral agents. *Proc Natl Acad Sci U S A*, *113*(19), 5388-5393. https://doi.org/10.1073/pnas.1522987113

Britton, K. A., & Fox, C. S. (2011). Ectopic fat depots and cardiovascular disease. *Circulation*, *124*(24), e837-41. https://doi.org/10.1161/CIRCULATIONAHA.111.077602

Carper, D., Coué, M., Laurens, C., Langin, D., & Moro, C. (2020). Reappraisal of the optimal fasting time for insulin tolerance tests in mice. *Mol Metab*, *42*, 101058. https://doi.org/10.1016/j.molmet.2020.101058

Cerone, M. A., Burgess, D. J., Naceur-Lombardelli, C., Lord, C. J., & Ashworth, A. (2011). High-throughput RNAi screening reveals novel regulators of telomerase. *Cancer Res*, *71*(9), 3328-3340. https://doi.org/10.1158/0008-5472.CAN-10-2734

Chalasani, N., Younossi, Z., Lavine, J. E., Charlton, M., Cusi, K., Rinella, M., Harrison, S. A., Brunt, E. M., & Sanyal, A. J. (2018). The diagnosis and management of nonalcoholic fatty liver disease: Practice guidance from the American Association for the Study of Liver Diseases. *Hepatology*, *67*(1), 328-357. https://doi.org/10.1002/hep.29367

Chaudhary, N., & Pfluger, P. T. (2009). Metabolic benefits from Sirt1 and Sirt1 activators. *Current Opinion in Clinical Nutrition & …*. https://journals.lww.com/co-clinicalnutrition/Fulltext/2009/07000/Short_bowel_syndrome_and_intestinal.17.aspx

Chen, H. C., & Farese, R. V. (2005a). Inhibition of triglyceride synthesis as a treatment strategy for obesity: lessons from DGAT1-deficient mice. *Arterioscler Thromb Vasc Biol*, *25*(3), 482-486. https://doi.org/10.1161/01.ATV.0000151874.81059.ad

Chen, H. C., & Farese, R. V. (2005b). Inhibition of triglyceride synthesis as a treatment strategy for obesity: lessons from DGAT1-deficient mice. *Arterioscler Thromb Vasc Biol*, *25*(3), 482-486. https://doi.org/10.1161/01.ATV.0000151874.81059.ad

Chen, H. H., Yu, H. I., Cho, W. C., & Tarn, W. Y. (2015a). DDX3 modulates cell adhesion and motility and cancer cell metastasis via Rac1-mediated signaling pathway. *Oncogene*, *34*(21), 2790-2800. https://doi.org/10.1038/onc.2014.190

Chen, H. H., Yu, H. I., Cho, W. C., & Tarn, W. Y. (2015b). DDX3 modulates cell adhesion and motility and cancer cell metastasis via Rac1-mediated signaling pathway. *Oncogene*, *34*(21), 2790-2800. https://doi.org/10.1038/onc.2014.190

Colak, Y., Ozturk, O., Senates, E., & Tuncer…, I. (2011). SIRT1 as a potential therapeutic target for treatment of nonalcoholic fatty liver disease. *… medical journal of …*. https://www.ncbi.nlm.nih.gov/pmc/articles/PMC3539588

Colak, Y., Yesil, A., Mutlu, H. H., & Caklili…, O. T. (2014). A potential treatment of non-alcoholic fatty liver disease with SIRT1 activators. *J Gastrointestin Liver …*.

Colecchia, D., Rossi, M., Sasdelli, F., Sanzone, S., Strambi, A., & Chiariello, M. (2015). MAPK15 mediates BCR-ABL1-induced autophagy and regulates oncogene-dependent cell proliferation and tumor formation. *Autophagy*, *11*(10), 1790-1802. https://doi.org/10.1080/15548627.2015.1084454

Colecchia, D., Strambi, A., Sanzone, S., Iavarone, C., Rossi, M., Dall'Armi, C., Piccioni, F., Verrotti di Pianella, A., & Chiariello, M. (2012a). MAPK15/ERK8 stimulates autophagy by interacting with LC3 and GABARAP proteins. *Autophagy*, *8*(12), 1724-1740. https://doi.org/10.4161/auto.21857

Constantinides, C., Mean, R., & Janssen, B. J. (2011). Effects of isoflurane anesthesia on the cardiovascular function of the C57BL/6 mouse. *ILAR J*, *52*(3), e21-31. https://pubmed.ncbi.nlm.nih.gov/21677360

Cowley, P. M., Roberts, C. R., & Baker, A. J. (2019). Monitoring the Health Status of Mice with Bleomycin-induced Lung Injury by Using Body Condition Scoring. *Comp Med*, *69*(2), 95-102. https://doi.org/10.30802/AALAS-CM-18-000060

Crimini, E., Repetto, M., Aftimos, P., Botticelli, A., Marchetti, P., & Curigliano, G. (2021). Precision medicine in breast cancer: From clinical trials to clinical practice. *Cancer Treatment Reviews*, *98*, 102223. https://www.sciencedirect.com/science/article/pii/S0305737221000712

Cruciat, C. M., Dolde, C., de Groot, R. E., Ohkawara, B., Reinhard, C., Korswagen, H. C., & Niehrs, C. (2013). RNA helicase DDX3 is a regulatory subunit of casein kinase 1 in Wnt-β-catenin signaling. *Science*, *339*(6126), 1436-1441. https://doi.org/10.1126/science.1231499

De Oliveira, M. P., & Liesa, M. (2020). The Role of Mitochondrial Fat Oxidation in Cancer Cell Proliferation and Survival. *Cells*, *9*(12), 2600. https://doi.org/10.3390/cells9122600

Deniz, O., Hasygar, K., & Hietakangas, V. (2023). Cellular and physiological roles of the conserved atypical MAP kinase ERK7. *FEBS Lett*, *597*(5), 601-607. https://doi.org/10.1002/1873-3468.14521

Ding, R. B., Bao, J., & Deng, C. X. (2017). Emerging roles of SIRT1 in fatty liver diseases. *Int J Biol Sci*, *13*(7), 852-867. https://doi.org/10.7150/ijbs.19370

DiStefano, J. K. (2020). NAFLD and NASH in Postmenopausal Women: Implications for Diagnosis and Treatment. *Endocrinology*, *161*(10), bqaa134. https://doi.org/10.1210/endocr/bqaa134

Dolinsky, T. J., Czodrowski, P., Li, H., Nielsen, J. E., Jensen, J. H., Klebe, G., & Baker, N. A. (2007). PDB2PQR: expanding and upgrading automated preparation of biomolecular structures for molecular simulations. *Nucleic Acids Res*, *35*(Web Server issue), W522-5. https://doi.org/10.1093/nar/gkm276

Dolinsky, T. J., Nielsen, J. E., McCammon, J. A., & Baker, N. A. (2004). PDB2PQR: an automated pipeline for the setup of Poisson-Boltzmann electrostatics calculations. *Nucleic Acids Res*, *32*(Web Server issue), W665-7. https://doi.org/10.1093/nar/gkh381

Eliyatkın, N., Yalçın, E., Zengel, B., Aktaş, S., & Vardar, E. (2015). Molecular Classification of Breast Carcinoma: From Traditional, Old-Fashioned Way to A New Age, and A New Way. *J Breast Health*, *11*(2), 59-66. https://doi.org/10.5152/tjbh.2015.1669

Ellacott, K. L., Morton, G. J., Woods, S. C., Tso, P., & Schwartz, M. W. (2010). Assessment of feeding behavior in laboratory mice. *Cell Metab*, *12*(1), 10-17. https://doi.org/10.1016/j.cmet.2010.06.001

Fader Kaiser, C. M., Romano, P. S., Vanrell, M. C., Pocognoni, C. A., Jacob, J., Caruso, B., & Delgui, L. R. (2021). Biogenesis and Breakdown of Lipid Droplets in Pathological Conditions. *Front Cell Dev Biol*, *9*, 826248. https://doi.org/10.3389/fcell.2021.826248

Fasola, G., Barducci, M. C., Pelizzari, G., Grossi, F., Pinto, C., Daniele, B., Giordano, M., Ortega, C., Silva, R. R., Tozzi, V. D., Cavanna, L., & Aprile, G. (2023). Implementation of Precision Oncology in Clinical Practice: Results of a National Survey for Health Care Professionals. *Oncologist*, *28*(6), e324-e330. https://doi.org/10.1093/oncolo/oyad020

Franci, L., Tubita, A., Bertolino, F. M., Palma, A., Cannino, G., Settembre, C., Rasola, A., Rovida, E., & Chiariello, M. (2022). MAPK15 protects from oxidative stress-dependent cellular

senescence by inducing the mitophagic process. *Aging Cell*, *21*(7), e13620. https://doi.org/10.1111/acel.13620

Friedman, S. L., Neuschwander-Tetri, B. A., Rinella, M., & Sanyal, A. J. (2018). Mechanisms of NAFLD development and therapeutic strategies. *Nat Med*, *24*(7), 908-922. https://doi.org/10.1038/s41591-018-0104-9

Fu, Y., Zou, T., Shen, X., Nelson, P. J., Li, J., Wu, C., Yang, J., Zheng, Y., Bruns, C., Zhao, Y., Qin, L., & Dong, Q. (2021). Lipid metabolism in cancer progression and therapeutic strategies. *MedComm (2020)*, *2*(1), 27-59. https://doi.org/10.1002/mco2.27

Fuller-Pace, F. V. (2013). DEAD box RNA helicase functions in cancer. *RNA biology*, *10*(1), 121-132. https://www.tandfonline.com/doi/pdf/10.4161/rna.23312

Garbelli, A., Beermann, S., Di Cicco, G., Dietrich, U., & Maga, G. (2011). A motif unique to the human DEAD-box protein DDX3 is important for nucleic acid binding, ATP hydrolysis, RNA/DNA unwinding and HIV-1 replication. *PLoS One*, *6*(5), e19810. https://doi.org/10.1371/journal.pone.0019810

Gherardini, L., Inzalaco, G., Imperatore, F., D'Aurizio, R., Franci, L., Miragliotta, V., Boccuto, A., Calandro, P., Andreini, M., Tarditi, A., & Chiariello, M. (2021). The FHP01 DDX3X Helicase Inhibitor Exerts Potent Anti-Tumor Activity In Vivo in Breast Cancer Pre-Clinical Models. *Cancers (Basel)*, *13*(19), 4830. https://doi.org/10.3390/cancers13194830

Gimeno, R. E., Ortegon, A. M., Patel, S., Punreddy, S., Ge, P., Sun, Y., Lodish, H. F., & Stahl, A. (2003). Characterization of a heart-specific fatty acid transport protein. *J Biol Chem*, *278*(18), 16039-16044. https://doi.org/10.1074/jbc.M211412200

Githaka, J. M., Vega, A. R., Baird, M. A., Davidson, M. W., Jaqaman, K., & Touret, N. (2016). Ligand-induced growth and compaction of CD36 nanoclusters enriched in Fyn induces Fyn signaling. *J Cell Sci*, *129*(22), 4175-4189. https://doi.org/10.1242/jcs.188946

Greenberg, A. S., Coleman, R. A., Kraemer, F. B., McManaman, J. L., Obin, M. S., Puri, V., Yan, Q. W., Miyoshi, H., & Mashek, D. G. (2011). The role of lipid droplets in metabolic disease in rodents and humans. *J Clin Invest*, *121*(6), 2102-2110. https://doi.org/10.1172/JCI46069

Greenberg, A. S., & Coleman…, R. A. (2011). The role of lipid droplets in metabolic disease in rodents and humans. *The Journal of …*. https://www.jci.org/articles/view/46069

Groehler, A. L., & Lannigan, D. A. (2010). A chromatin-bound kinase, ERK8, protects genomic integrity by inhibiting HDM2-mediated degradation of the DNA clamp PCNA. *J Cell Biol*, *190*(4), 575-586. https://doi.org/10.1083/jcb.201002124

Guerra, I. M. S., Ferreira, H. B., Melo, T., Rocha, H., Moreira, S., Diogo, L., Domingues, M. R., & Moreira, A. S. P. (2022). Mitochondrial Fatty Acid β-Oxidation Disorders: From Disease to Lipidomic Studies-A Critical Review. *Int J Mol Sci*, *23*(22), 13933. https://doi.org/10.3390/ijms232213933

Gustafson, E. A., & Wessel, G. M. (2010). DEAD-box helicases: posttranslational regulation and function. *Biochem Biophys Res Commun*, *395*(1), 1-6. https://doi.org/10.1016/j.bbrc.2010.02.172

Hames, K. C., Vella, A., Kemp, B. J., & Jensen, M. D. (2014). Free fatty acid uptake in humans with CD36 deficiency. *Diabetes*, *63*(11), 3606-3614. https://doi.org/10.2337/db14-0369

Hasygar, K., Deniz, O., Liu, Y., Gullmets, J., Hynynen, R., Ruhanen, H., Kokki, K., Käkelä, R., & Hietakangas, V. (2021). Coordinated control of adiposity and growth by anti-anabolic kinase ERK7. *EMBO Rep*, *22*(2), e49602. https://doi.org/10.15252/embr.201949602

Hasygar, K., & Hietakangas, V. (2014). p53- and ERK7-dependent ribosome surveillance response regulates Drosophila insulin-like peptide secretion. *PLoS Genet*, *10*(11), e1004764. https://doi.org/10.1371/journal.pgen.1004764

He, T. Y., Wu, D. W., Lin, P. L., Wang, L., Huang, C. C., Chou, M. C., & Lee, H. (2016). DDX3 promotes tumor invasion in colorectal cancer via the CK1ε/Dvl2 axis. *Sci Rep*, *6*, 21483. https://doi.org/10.1038/srep21483

He, Y., Zhang, D., Yang, Y., Wang, X., Zhao, X., Zhang, P., Zhu, H., Xu, N., & Liang, S. (2018). A double-edged function of DDX3, as an oncogene or tumor suppressor, in cancer progression (Review). *Oncol Rep*, *39*(3), 883-892. https://doi.org/10.3892/or.2018.6203

Heerma van Voss, M. R., Schrijver, W. A., Ter Hoeve, N. D., Hoefnagel, L. D., Manson, Q. F., van der Wall, E., Raman, V., van Diest, P. J., & Dutch, D. B. C. M. C. (2017a). The prognostic effect of DDX3 upregulation in distant breast cancer metastases. *Clin Exp Metastasis*, *34*(1), 85-92. https://doi.org/10.1007/s10585-016-9832-8

Heerma van Voss, M. R., van Diest, P. J., & Raman, V. (2017b). Targeting RNA helicases in cancer: The translation trap. *Biochim Biophys Acta Rev Cancer*, *1868*(2), 510-520. https://doi.org/10.1016/j.bbcan.2017.09.006

Holliday, D. L., & Speirs, V. (2011). Choosing the right cell line for breast cancer research. *Breast cancer research*, *13*, 1-7. https://link.springer.com/article/10.1186/bcr2889

Houten, S. M., & Wanders, R. J. (2010). A general introduction to the biochemistry of mitochondrial fatty acid β-oxidation. *J Inherit Metab Dis*, *33*(5), 469-477. https://doi.org/10.1007/s10545-010-9061-2

Huang, M. M., Bolen, J. B., Barnwell, J. W., Shattil, S. J., & Brugge, J. S. (1991). Membrane glycoprotein IV (CD36) is physically associated with the Fyn, Lyn, and Yes protein-tyrosine kinases in human platelets. *Proc Natl Acad Sci U S A*, *88*(17), 7844-7848. https://doi.org/10.1073/pnas.88.17.7844

Humphrey, W., Dalke, A., & Schulten, K. (1996). VMD: visual molecular dynamics. *J Mol Graph*, *14*(1), 33-8, 27. https://doi.org/10.1016/0263-7855(96)00018-5

Iavarone, C., Acunzo, M., Carlomagno, F., Catania, A., Melillo, R. M., Carlomagno, S. M., Santoro, M., & Chiariello, M. (2006). Activation of the Erk8 mitogen-activated protein (MAP) kinase by RET/PTC3, a constitutively active form of the RET proto-oncogene. *J Biol Chem*, *281*(15), 10567-10576. https://doi.org/10.1074/jbc.M513397200

Jiang, L., Gu, Z. H., Yan, Z. X., Zhao, X., Xie, Y. Y., Zhang, Z. G., Pan, C. M., Hu, Y., Cai, C. P., Dong, Y., Huang, J. Y., Wang, L., Shen, Y., Meng, G., Zhou, J. F., Hu, J. D., Wang, J. F., Liu, Y. H., Yang, L. H., . . . Chen, S. J. (2015). Exome sequencing identifies somatic mutations of DDX3X in natural killer/T-cell lymphoma. *Nat Genet*, *47*(9), 1061-1066. https://doi.org/10.1038/ng.3358

Jiménez, B., Volpert, O. V., Crawford, S. E., Febbraio, M., Silverstein, R. L., & Bouck, N. (2000). Signals leading to apoptosis-dependent inhibition of neovascularization by thrombospondin-1. *Nat Med*, *6*(1), 41-48. https://doi.org/10.1038/71517

Jin, D. H., Lee, J., Kim, K. M., Kim, S., Kim, D. H., & Park, J. (2015). Overexpression of MAPK15 in gastric cancer is associated with copy number gain and contributes to the stability of c-Jun. *Oncotarget*, *6*(24), 20190-20203. https://doi.org/10.18632/oncotarget.4171

Kamińska, M., Ciszewski, T., Łopacka-Szatan, K., Miotła, P., & Starosławska, E. (2015). Breast cancer risk factors. *Prz Menopauzalny*, *14*(3), 196-202. https://doi.org/10.5114/pm.2015.54346

Kennedy, D. J., Kuchibhotla, S., Westfall, K. M., Silverstein, R. L., Morton, R. E., & Febbraio, M. (2011). A CD36-dependent pathway enhances macrophage and adipose tissue inflammation and impairs insulin signalling. *Cardiovasc Res*, *89*(3), 604-613. https://doi.org/10.1093/cvr/cvq360

Kim, K. Y., Stevens, M. V., Akter, M. H., Rusk, S. E., Huang, R. J., Cohen, A., Noguchi, A., Springer, D., Bocharov, A. V., Eggerman, T. L., Suen, D. F., Youle, R. J., Amar, M., Remaley, A. T., & Sack, M. N. (2011). Parkin is a lipid-responsive regulator of fat uptake in mice and mutant human cells. *J Clin Invest*, *121*(9), 3701-3712. https://doi.org/10.1172/JCI44736

Kohjima, M., Enjoji, M., Higuchi, N., Kato, M., Kotoh, K., Yoshimoto, T., Fujino, T., Yada, M., Yada, R., Harada, N., Takayanagi, R., & Nakamuta, M. (2007). Re-evaluation of fatty acid metabolism-related gene expression in nonalcoholic fatty liver disease. *Int J Mol Med*, *20*(3), 351-358. https://pubmed.ncbi.nlm.nih.gov/17671740

Kool, M., Jones, D. T., Jäger, N., Northcott, P. A., Pugh, T. J., Hovestadt, V., Piro, R. M., Esparza, L. A., Markant, S. L., Remke, M., Milde, T., Bourdeaut, F., Ryzhova, M., Sturm, D., Pfaff, E., Stark, S., Hutter, S., Seker-Cin, H., Johann, P., . . . ICGC, P. T. P. (2014). Genome sequencing of SHH medulloblastoma predicts genotype-related response to smoothened inhibition. *Cancer Cell*, *25*(3), 393-405. https://doi.org/10.1016/j.ccr.2014.02.004

Koundouros, N., & Poulogiannis, G. (2020). Reprogramming of fatty acid metabolism in cancer. *Br J Cancer*, *122*(1), 4-22. https://doi.org/10.1038/s41416-019-0650-z

Krahmer, N., Farese, R. V., & Walther, T. C. (2013a). Balancing the fat: lipid droplets and human disease. *EMBO Mol Med*, *5*(7), 973-983. https://doi.org/10.1002/emmm.201100671

Krahmer, N., Jr, R. V. F., & Walther, T. C. (2013b). Balancing the fat: lipid droplets and human disease. *EMBO molecular medicine*. https://www.embopress.org/doi/full/10.1002/emmm.201100671

Kukhanova, M. K., Karpenko, I. L., & Ivanov, A. V. (2020). DEAD-box RNA Helicase DDX3: Functional Properties and Development of DDX3 Inhibitors as Antiviral and Anticancer Drugs. *Molecules*, *25*(4), 1015. https://doi.org/10.3390/molecules25041015

Lebovitz, H. E. (2001). Insulin resistance: definition and consequences. *Exp Clin Endocrinol Diabetes*, *109 Suppl 2*, S135-48. https://doi.org/10.1055/s-2001-18576

Lee, C. S., Dias, A. P., Jedrychowski, M., Patel, A. H., Hsu, J. L., & Reed, R. (2008). Human DDX3 functions in translation and interacts with the translation initiation factor eIF3. *Nucleic Acids Res*, *36*(14), 4708-4718. https://doi.org/10.1093/nar/gkn454

Lefere, S., & Tacke, F. (2019). Macrophages in obesity and non-alcoholic fatty liver disease: Crosstalk with metabolism. *JHEP Rep*, *1*(1), 30-43. https://doi.org/10.1016/j.jhepr.2019.02.004

Lessa, A. S., Paredes, B. D., Dias, J. V., Carvalho, A. B., Quintanilha, L. F., Takiya, C. M., Tura, B. R., Rezende, G. F., Campos de Carvalho, A. C., Resende, C. M., & Goldenberg, R. C. (2010). Ultrasound imaging in an experimental model of fatty liver disease and cirrhosis in rats. *BMC Vet Res*, *6*, 6. https://doi.org/10.1186/1746-6148-6-6

Li, M. J., Wang, P., Liu, X., Lim, E. L., Wang, Z., Yeager, M., Wong, M. P., Sham, P. C., Chanock, S. J., & Wang, J. (2012). GWASdb: a database for human genetic variants identified by genome-wide association studies. *Nucleic Acids Res*, *40*(Database issue), D1047-54. https://doi.org/10.1093/nar/gkr1182

Longo, N., Frigeni, M., & Pasquali, M. (2016). Carnitine transport and fatty acid oxidation. *Biochim Biophys Acta*, *1863*(10), 2422-2435. https://doi.org/10.1016/j.bbamcr.2016.01.023

López-Terrada, D., Cheung, S. W., Finegold, M. J., & Knowles, B. B. (2009). Hep G2 is a hepatoblastoma-derived cell line. *Hum Pathol*, *40*(10), 1512-1515. https://doi.org/10.1016/j.humpath.2009.07.003

MacDonald, B. T., Hien, A., Zhang, X., Iranloye, O., Virshup, D. M., Waterman, M. L., & He, X. (2014). Disulfide bond requirements for active Wnt ligands. *J Biol Chem*, *289*(26), 18122-18136. https://doi.org/10.1074/jbc.M114.575027

Mancini, M., Prinster, A., Annuzzi, G., Liuzzi, R., Giacco, R., Medagli, C., Cremone, M., Clemente, G., Maurea, S., Riccardi, G., Rivellese, A. A., & Salvatore, M. (2009). Sonographic hepatic-renal ratio as indicator of hepatic steatosis: comparison with (1)H magnetic resonance spectroscopy. *Metabolism*, *58*(12), 1724-1730. https://doi.org/10.1016/j.metabol.2009.05.032

Matthews, D. R., Hosker, J. P., Rudenski, A. S., Naylor, B. A., Treacher, D. F., & Turner, R. C. (1985). Homeostasis model assessment: insulin resistance and beta-cell function from fasting plasma glucose and insulin concentrations in man. *Diabetologia*, *28*(7), 412-419. https://doi.org/10.1007/BF00280883

Meagher, K. L., Redman, L. T., & Carlson, H. A. (2003). Development of polyphosphate parameters for use with the AMBER force field. *J Comput Chem*, *24*(9), 1016-1025. https://doi.org/10.1002/jcc.10262

Mo, J., Liang, H., Su, C., Li, P., Chen, J., & Zhang, B. (2021). DDX3X: structure, physiologic functions and cancer. *Molecular cancer*, *20*(1), 1-20. https://molecular-cancer.biomedcentral.com/articles/10.1186/s12943-021-01325-7

Moore, D. J. (2006). Parkin: a multifaceted ubiquitin ligase. *Biochem Soc Trans*, *34*(Pt 5), 749-753. https://doi.org/10.1042/BST0340749

Moore, D. J., West, A. B., Dikeman, D. A., Dawson, V. L., & Dawson, T. M. (2008). Parkin mediates the degradation-independent ubiquitination of Hsp70. *J Neurochem*, *105*(5), 1806-1819. https://doi.org/10.1111/j.1471-4159.2008.05261.x

Morley, S. D., & Afshar, M. (2004). Validation of an empirical RNA-ligand scoring function for fast flexible docking using Ribodock. *J Comput Aided Mol Des*, *18*(3), 189-208. https://doi.org/10.1023/b:jcam.0000035199.48747.1e

Musselman, L. P., Fink, J. L., Ramachandran, P. V., Patterson, B. W., Okunade, A. L., Maier, E., Brent, M. R., Turk, J., & Baranski, T. J. (2013). Role of fat body lipogenesis in protection against the effects of caloric overload in Drosophila. *J Biol Chem*, *288*(12), 8028-8042. https://doi.org/10.1074/jbc.M112.371047

Nassir, F., & Ibdah, J. A. (2016). Sirtuins and nonalcoholic fatty liver disease. *World Journal of Gastroenterology*. https://www.ncbi.nlm.nih.gov/pmc/articles/PMC5155167

Niu, B., He, K., Li, P., Gong, J., Zhu, X., Ye, S., Ou, Z., & Ren, G. (2018). SIRT1 upregulation protects against liver injury induced by a HFD through inhibiting CD36 and the NF-κB pathway in mouse kupffer cells. *Mol Med Rep*, *18*(2), 1609-1615. https://doi.org/10.3892/mmr.2018.9088

Nusse, R., & Clevers, H. (2017). Wnt/β-Catenin Signaling, Disease, and Emerging Therapeutic Modalities. *Cell*, *169*(6), 985-999. https://doi.org/10.1016/j.cell.2017.05.016

Olzmann, J. A., & Carvalho, P. (2019). Dynamics and functions of lipid droplets. *Nat Rev Mol Cell Biol*, *20*(3), 137-155. https://doi.org/10.1038/s41580-018-0085-z

Pagliuca, C., Cicatiello, A. G., Colicchio, R., Greco, A., Cerciello, R., Auletta, L., Albanese, S., Scaglione, E., Pagliarulo, C., Pastore, G., Mansueto, G., Brunetti, A., Avallone, B., & Salvatore, P. (2016). Novel Approach for Evaluation of Bacteroides fragilis Protective Role against Bartonella henselae Liver Damage in Immunocompromised Murine Model. *Front Microbiol*, *7*, 1750. https://doi.org/10.3389/fmicb.2016.01750

Palumbo, M. O., Kavan, P., Miller, W. H., Panasci, L., Assouline, S., Johnson, N., Cohen, V., Patenaude, F., Pollak, M., Jagoe, R. T., & Batist, G. (2013). Systemic cancer therapy: achievements and challenges that lie ahead. *Front Pharmacol*, *4*, 57. https://doi.org/10.3389/fphar.2013.00057

Patel, V. B. (2018). *The Molecular Nutrition of Fats*. Academic Press. https://play.google.com/store/books/details?id=SrF1DwAAQBAJ&source=gbs_api

Patmore, D. M., Jassim, A., Nathan, E., Gilbertson, R. J., Tahan, D., Hoffmann, N., Tong, Y., Smith, K. S., Kanneganti, T. D., Suzuki, H., Taylor, M. D., Northcott, P., & Gilbertson, R. J. (2020). DDX3X Suppresses the Susceptibility of Hindbrain Lineages to Medulloblastoma. *Dev Cell*, *54*(4), 455-470.e5. https://doi.org/10.1016/j.devcel.2020.05.027

Phillips, J. C., Braun, R., Wang, W., Gumbart, J., Tajkhorshid, E., Villa, E., Chipot, C., Skeel, R. D., Kalé, L., & Schulten, K. (2005). Scalable molecular dynamics with NAMD. *J Comput Chem*, *26*(16), 1781-1802. https://doi.org/10.1002/jcc.20289

Pinter, M., Pinato, D. J., Ramadori, P., & Heikenwalder, M. (2023). NASH and Hepatocellular Carcinoma: Immunology and Immunotherapy. *Clin Cancer Res*, *29*(3), 513-520. https://doi.org/10.1158/1078-0432.CCR-21-1258

Ponugoti, B., Kim, D. H., Xiao, Z., Smith, Z., Miao, J., Zang, M., Wu, S. Y., Chiang, C. M., Veenstra, T. D., & Kemper, J. K. (2010). SIRT1 deacetylates and inhibits SREBP-1C activity in regulation

of hepatic lipid metabolism. *J Biol Chem*, *285*(44), 33959-33970. https://doi.org/10.1074/jbc.M110.122978

Postic, C., & Girard, J. (2008). Contribution of de novo fatty acid synthesis to hepatic steatosis and insulin resistance: lessons from genetically engineered mice. *J Clin Invest*, *118*(3), 829-838. https://doi.org/10.1172/JCI34275

Powell, E. E., Wong, V. W., & Rinella, M. (2021). Non-alcoholic fatty liver disease. *Lancet*, *397*(10290), 2212-2224. https://doi.org/10.1016/S0140-6736(20)32511-3

Prinz, W. A. (2014). Bridging the gap: membrane contact sites in signaling, metabolism, and organelle dynamics. *Journal of Cell Biology*. https://rupress.org/jcb/article/205/6/759/37583

Purushotham, A., Schug, T. T., Xu, Q., Surapureddi, S., & Guo…, X. (2009). Hepatocyte-specific deletion of SIRT1 alters fatty acid metabolism and results in hepatic steatosis and inflammation. *Cell metabolism*.

Rada, P., González-Rodríguez, Á., García-Monzón, C., & Valverde, Á. M. (2020). Understanding lipotoxicity in NAFLD pathogenesis: is CD36 a key driver. *Cell Death Dis*, *11*(9), 802. https://doi.org/10.1038/s41419-020-03003-w

Radi, M., Falchi, F., Garbelli, A., Samuele, A., Bernardo, V., Paolucci, S., Baldanti, F., Schenone, S., Manetti, F., Maga, G., & Botta, M. (2012). Discovery of the first small molecule inhibitor of human DDX3 specifically designed to target the RNA binding site: towards the next generation HIV-1 inhibitors. *Bioorg Med Chem Lett*, *22*(5), 2094-2098. https://doi.org/10.1016/j.bmcl.2011.12.135

Remmert, M., Biegert, A., Hauser, A., & Söding, J. (2011). HHblits: lightning-fast iterative protein sequence searching by HMM-HMM alignment. *Nat Methods*, *9*(2), 173-175. https://doi.org/10.1038/nmeth.1818

Riazi, K., Azhari, H., Charette, J. H., Underwood, F. E., King, J. A., Afshar, E. E., Swain, M. G., Congly, S. E., Kaplan, G. G., & Shaheen, A. A. (2022). The prevalence and incidence of NAFLD worldwide: a systematic review and meta-analysis. *Lancet Gastroenterol Hepatol*, *7*(9), 851-861. https://doi.org/10.1016/S2468-1253(22)00165-0

Rocks, O., Gerauer, M., Vartak, N., Koch, S., Huang, Z. P., Pechlivanis, M., Kuhlmann, J., Brunsveld, L., Chandra, A., Ellinger, B., Waldmann, H., & Bastiaens, P. I. (2010). The palmitoylation machinery is a spatially organizing system for peripheral membrane proteins. *Cell*, *141*(3), 458-471. https://doi.org/10.1016/j.cell.2010.04.007

Rody, A., Karn, T., Liedtke, C., Pusztai, L., Ruckhaeberle, E., Hanker, L., Gaetje, R., Solbach, C., Ahr, A., Metzler, D., Schmidt, M., Müller, V., Holtrich, U., & Kaufmann, M. (2011). A clinically relevant gene signature in triple negative and basal-like breast cancer. *Breast Cancer Res*, *13*(5), R97. https://doi.org/10.1186/bcr3035

Rossi, M., Colecchia, D., Ilardi, G., Acunzo, M., Nigita, G., Sasdelli, F., Celetti, A., Strambi, A., Staibano, S., Croce, C. M., & Chiariello, M. (2016). MAPK15 upregulation promotes cell proliferation and prevents DNA damage in male germ cell tumors. *Oncotarget*, *7*(15), 20981-20998. https://doi.org/10.18632/oncotarget.8044

Samovski, D., Sun, J., Pietka, T., Gross, R. W., Eckel, R. H., Su, X., Stahl, P. D., & Abumrad, N. A. (2015). Regulation of AMPK activation by CD36 links fatty acid uptake to β-oxidation. *Diabetes*, *64*(2), 353-359. https://doi.org/10.2337/db14-0582

Santos, C. R., & Schulze, A. (2012). Lipid metabolism in cancer. *FEBS J*, *279*(15), 2610-2623. https://doi.org/10.1111/j.1742-4658.2012.08644.x

Sanyal, A. J. (2019). Past, present and future perspectives in nonalcoholic fatty liver disease. *Nat Rev Gastroenterol Hepatol*, *16*(6), 377-386. https://doi.org/10.1038/s41575-019-0144-8

Sheka, A. C., Adeyi, O., Thompson, J., Hameed, B., Crawford, P. A., & Ikramuddin, S. (2020). Nonalcoholic Steatohepatitis: A Review. *JAMA*, *323*(12), 1175-1183. https://doi.org/10.1001/jama.2020.2298

Smiriglia, A., Lorito, N., Serra, M., Perra, A., Morandi, A., & Kowalik, M. A. (2023). Sex difference in liver diseases: How preclinical models help to dissect the sex-related mechanisms sustaining NAFLD and hepatocellular carcinoma. *iScience*, *26*(12), 108363. https://doi.org/10.1016/j.isci.2023.108363

Stine, J. G., Wentworth, B. J., Zimmet, A., Rinella, M. E., Loomba, R., Caldwell, S. H., & Argo, C. K. (2018). Systematic review with meta-analysis: risk of hepatocellular carcinoma in non-alcoholic steatohepatitis without cirrhosis compared to other liver diseases. *Aliment Pharmacol Ther*, *48*(7), 696-703. https://doi.org/10.1111/apt.14937

Strable, M. S., & Ntambi, J. M. (2010). Genetic control of de novo lipogenesis: role in diet-induced obesity. *Crit Rev Biochem Mol Biol*, *45*(3), 199-214. https://doi.org/10.3109/10409231003667500

Sun, Y. S., Zhao, Z., Yang, Z. N., Xu, F., Lu, H. J., Zhu, Z. Y., Shi, W., Jiang, J., Yao, P. P., & Zhu, H. P. (2017). Risk Factors and Preventions of Breast Cancer. *Int J Biol Sci*, *13*(11), 1387-1397. https://doi.org/10.7150/ijbs.21635

Szrok-Jurga, S., Czumaj, A., Turyn, J., Hebanowska, A., Swierczynski, J., Sledzinski, T., & Stelmanska, E. (2023a). The Physiological and Pathological Role of Acyl-CoA Oxidation. *Int J Mol Sci*, *24*(19), 14857. https://doi.org/10.3390/ijms241914857

Szrok-Jurga, S., Turyn, J., Hebanowska, A., Swierczynski, J., Czumaj, A., Sledzinski, T., & Stelmanska, E. (2023b). The Role of Acyl-CoA β-Oxidation in Brain Metabolism and Neurodegenerative Diseases. *Int J Mol Sci*, *24*(18), 13977. https://doi.org/10.3390/ijms241813977

Tauchi-Sato, K., Ozeki, S., Houjou, T., & Taguchi…, R. (2002). The surface of lipid droplets is a phospholipid monolayer with a unique fatty acid composition. *Journal of Biological …*. https://www.jbc.org/article/S0021-9258(19)71806-7/abstract

Teixeira, L., Pereira-Dutra, F. S., & Reis…, P. A. (2023). Prevention of lipid droplet accumulation by DGAT1 inhibition ameliorates sepsis-induced liver injury and inflammation. *JHEP Reports*. https://www.sciencedirect.com/science/article/pii/S2589555923003154

Thorne, R. F., Law, E. G., Elith, C. A., Ralston, K. J., Bates, R. C., & Burns, G. F. (2006). The association between CD36 and Lyn protein tyrosine kinase is mediated by lipid. *Biochem Biophys Res Commun*, *351*(1), 51-56. https://doi.org/10.1016/j.bbrc.2006.09.156

Trott, O., & Olson, A. J. (2010). AutoDock Vina: improving the speed and accuracy of docking with a new scoring function, efficient optimization, and multithreading. *J Comput Chem*, *31*(2), 455-461. https://doi.org/10.1002/jcc.21334

Veeman, M. T., Slusarski, D. C., Kaykas, A., Louie, S. H., & Moon, R. T. (2003). Zebrafish prickle, a modulator of noncanonical Wnt/Fz signaling, regulates gastrulation movements. *Curr Biol*, *13*(8), 680-685. https://doi.org/10.1016/s0960-9822(03)00240-9

Villanueva, C. J., Monetti, M., Shih, M., Zhou, P., Watkins, S. M., Bhanot, S., & Farese, R. V. (2009a). Specific role for acyl CoA:Diacylglycerol acyltransferase 1 (Dgat1) in hepatic steatosis due to exogenous fatty acids. *Hepatology*, *50*(2), 434-442. https://doi.org/10.1002/hep.22980

Villanueva, C. J., Monetti, M., Shih, M., Zhou, P., Watkins, S. M., Bhanot, S., & Farese, R. V. (2009b). Specific role for acyl CoA:Diacylglycerol acyltransferase 1 (Dgat1) in hepatic steatosis due to exogenous fatty acids. *Hepatology*, *50*(2), 434-442. https://doi.org/10.1002/hep.22980

Voet, D., Voet, J. G., & Pratt, C. W. (2006). *Fundamentals of Biochemistry: Life at the Molecular Level*. John Wiley & Sons. http://books.google.it/books?id=h0FCAQAAIAAJ&hl=&source=gbs_api

Voss, M. R. H. V., Diest, P. J. V., & Raman, V. (2017). Targeting RNA helicases in cancer: The translation trap. *Biochimica et Biophysica Acta …*. https://www.ncbi.nlm.nih.gov/pmc/articles/PMC5675762

Wang, J., Hao, J. W., Wang, X., Guo, H., Sun, H. H., Lai, X. Y., Liu, L. Y., Zhu, M., Wang, H. Y., Li, Y. F., Yu, L. Y., Xie, C., Wang, H. R., Mo, W., Zhou, H. M., Chen, S., Liang, G., & Zhao, T. J. (2019). DHHC4 and DHHC5 Facilitate Fatty Acid Uptake by Palmitoylating and Targeting CD36 to the Plasma Membrane. *Cell Rep*, *26*(1), 209-221.e5. https://doi.org/10.1016/j.celrep.2018.12.022

Wang, R. H., Li, C., & Deng, C. X. (2010). Liver steatosis and increased ChREBP expression in mice carrying a liver specific SIRT1 null mutation under a normal feeding condition. *International journal of biological …*. https://www.ncbi.nlm.nih.gov/pmc/articles/PMC2990071

Waterhouse, A., Bertoni, M., Bienert, S., Studer, G., Tauriello, G., Gumienny, R., Heer, F. T., de Beer, T. A. P., Rempfer, C., Bordoli, L., Lepore, R., & Schwede, T. (2018). SWISS-MODEL: homology modelling of protein structures and complexes. *Nucleic Acids Res*, *46*(W1), W296-W303. https://doi.org/10.1093/nar/gky427

Wilson, K., & Walker, J. (2006). *Biochimica e biologia molecolare. Principi e tecniche*. http://books.google.it/books?id=o3rHPAAACAAJ&hl=&source=gbs_api

Wójcikowski, M., Ballester, P. J., & Siedlecki, P. (2017). Performance of machine-learning scoring functions in structure-based virtual screening. *Sci Rep*, *7*, 46710. https://doi.org/10.1038/srep46710

Wong, R. J., Cheung, R., & Ahmed, A. (2014). Nonalcoholic steatohepatitis is the most rapidly growing indication for liver transplantation in patients with hepatocellular carcinoma in the U.S. *Hepatology*, *59*(6), 2188-2195. https://doi.org/10.1002/hep.26986

Xie, M., Vesuna, F., Botlagunta, M., Bol, G. M., Irving, A., Bergman, Y., Hosmane, R. S., Kato, Y., Winnard, P. T., & Raman, V. (2015). NZ51, a ring-expanded nucleoside analog, inhibits motility and viability of breast cancer cells by targeting the RNA helicase DDX3. *Oncotarget*, *6*(30), 29901-29913. https://doi.org/10.18632/oncotarget.4898

Xu, F., Gao, Z., Zhang, J., Rivera, C. A., Yin, J., & Weng…, J. (2010a). Lack of SIRT1 (Mammalian Sirtuin 1) Activity Leads to Liver Steatosis in the SIRT1^{+/−} Mice: A Role of Lipid Mobilization and Inflammation. …. https://academic.oup.com/endo/article/151/6/2504/2456785

Xu, Y. M., Zhu, F., Cho, Y. Y., Carper, A., Peng, C., Zheng, D., Yao, K., Lau, A. T., Zykova, T. A., Kim, H. G., Bode, A. M., & Dong, Z. (2010b). Extracellular signal-regulated kinase 8-mediated c-Jun phosphorylation increases tumorigenesis of human colon cancer. *Cancer Res*, *70*(8), 3218-3227. https://doi.org/10.1158/0008-5472.CAN-09-4306

Yoon, H., Shaw, J. L., Haigis, M. C., & Greka, A. (2021). Lipid metabolism in sickness and in health: Emerging regulators of lipotoxicity. *Mol Cell*, *81*(18), 3708-3730. https://doi.org/10.1016/j.molcel.2021.08.027

Younossi, Z. M., Koenig, A. B., Abdelatif, D., Fazel, Y., Henry, L., & Wymer, M. (2016). Global epidemiology of nonalcoholic fatty liver disease-Meta-analytic assessment of prevalence, incidence, and outcomes. *Hepatology*, *64*(1), 73-84. https://doi.org/10.1002/hep.28431

Zacharogianni, M., Kondylis, V., Tang, Y., Farhan, H., Xanthakis, D., Fuchs, F., Boutros, M., & Rabouille, C. (2011). ERK7 is a negative regulator of protein secretion in response to amino-acid starvation by modulating Sec16 membrane association. *EMBO J*, *30*(18), 3684-3700. https://doi.org/10.1038/emboj.2011.253

Zhang, M., Fang, L., Zhou, L., Molino, A., Valentino, M. R., Yang, S., Zhang, J., Li, Y., & Roth, M. (2021). MAPK15-ULK1 signaling regulates mitophagy of airway epithelial cell in chronic obstructive pulmonary disease. *Free Radic Biol Med*, *172*, 541-549. https://doi.org/10.1016/j.freeradbiomed.2021.07.004

Zhao, L., Zhang, C., Luo, X., Wang, P., Zhou, W., Zhong, S., Xie, Y., Jiang, Y., Yang, P., Tang, R., Pan, Q., Hall, A. R., Luong, T. V., Fan, J., Varghese, Z., Moorhead, J. F., Pinzani, M., Chen, Y., & Ruan, X. Z. (2018). CD36 palmitoylation disrupts free fatty acid metabolism and promotes tissue inflammation in non-alcoholic steatohepatitis. *J Hepatol*, *69*(3), 705-717. https://doi.org/10.1016/j.jhep.2018.04.006